Sezione di Bologna
Sezione di Napoli
Sezione di Roma Tor Vergata
Sezione di Torino
TIFPA Trento

Geophysics from space: using particles and electromagnetic waves for precision physics in the ionosphere

Roberto Battiston
Università e TIFPA
Trento

Near-Earth space is a coupled system

The space near Earth is a chain of interfaces.

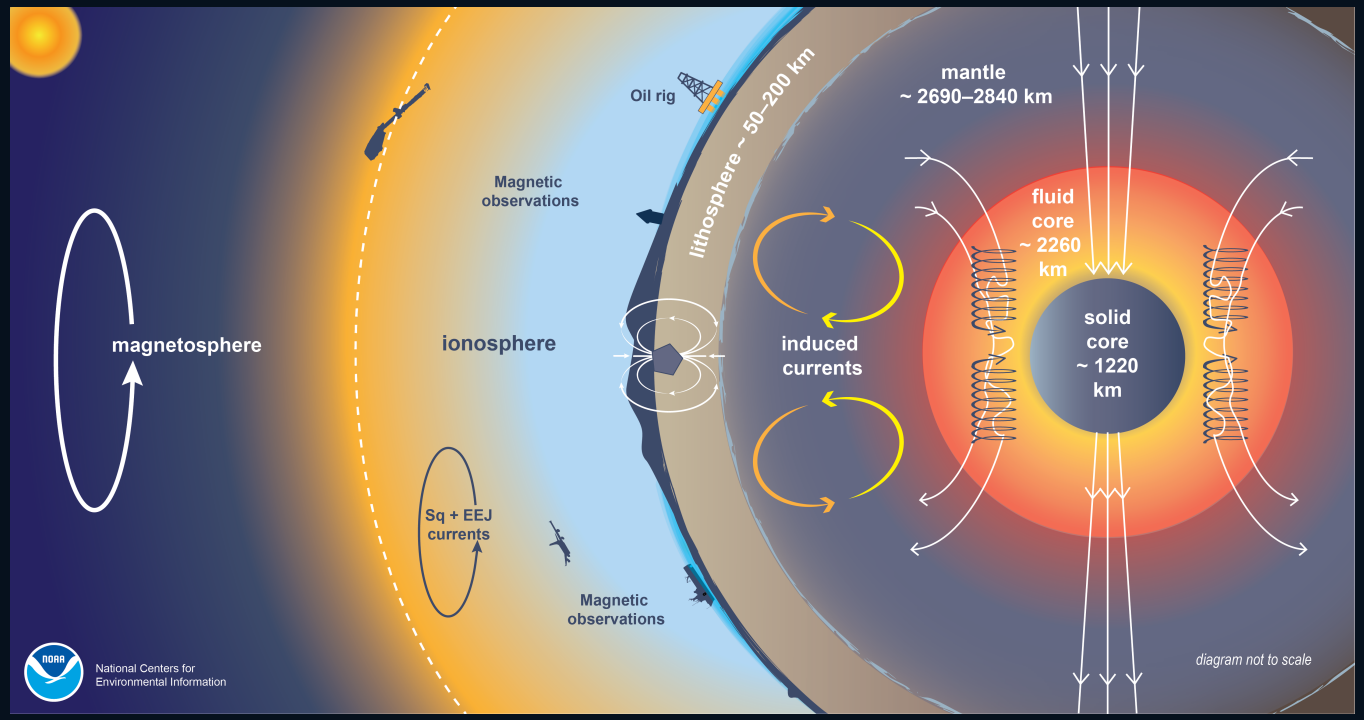

- The lithosphere, atmosphere, ionosphere, and magnetosphere exchange energy, momentum, particles, and currents.
- Disturbances can propagate from bottom to top and from top to bottom: both directions matter.
- From a satellite, the entire system can be observed with global coverage, orbital repetition, and multiple parameters simultaneously.

INTRODUCTION

Lithosphere: where the source originates

The observational problem starts in the crust, but the useful signal often emerges above it.

- The lithosphere is the rigid shell formed by the crust and cold upper mantle, broken into plates that slide over a more ductile mantle.
- Earthquakes, eruptions, and tsunamis release mechanical, thermal, and chemical energy over very different timescales.
- In space geophysics, the source is not observed directly: its signatures are sought in the atmosphere and ionosphere above.

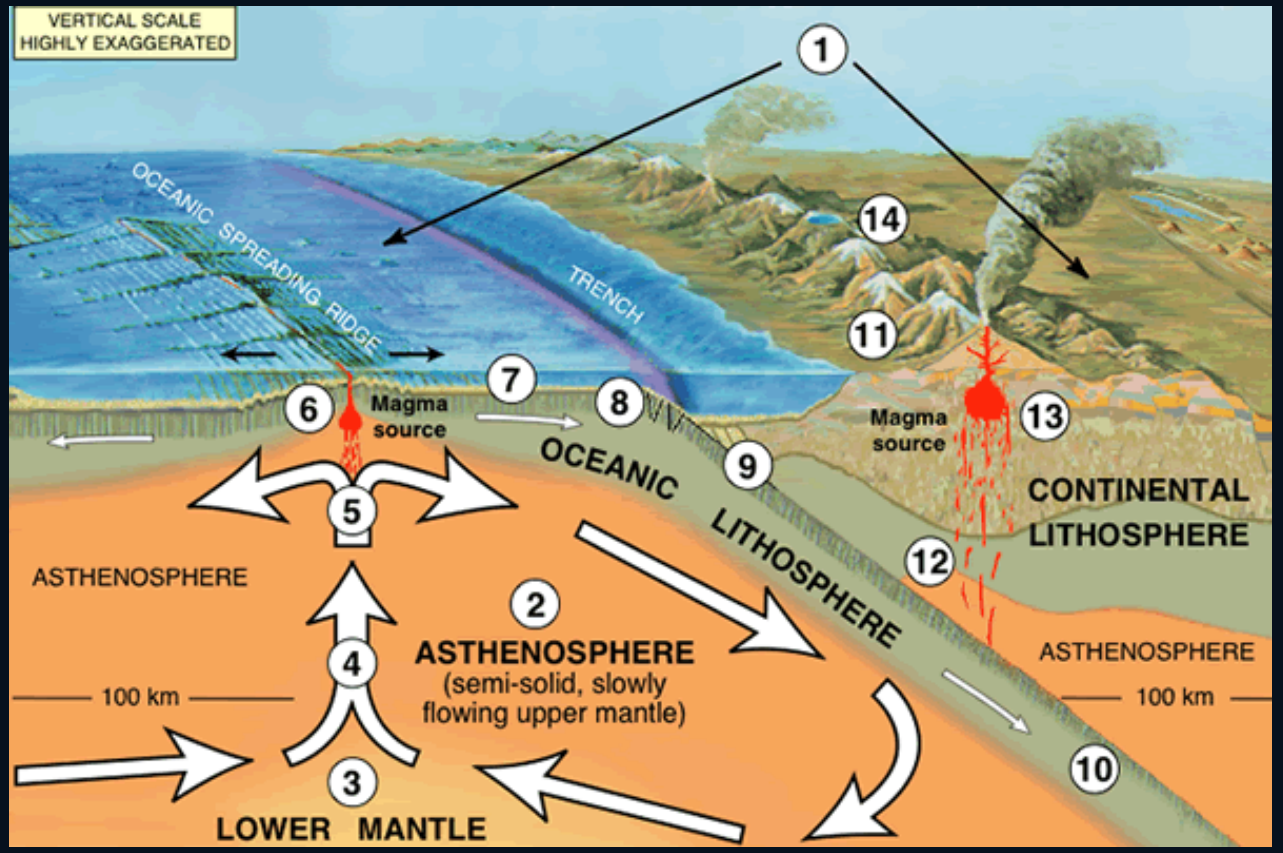

INTRODUCTION

Atmosphere: the medium of propagation

In a neutral medium, waves are transformed, filtered, and often amplified with altitude.

- The five main layers are the troposphere, stratosphere, mesosphere, thermosphere, and exosphere.
- Air density decreases rapidly with altitude: this is why many dynamic disturbances increase in amplitude as they rise.
- The thermosphere is the bridge to the ionized upper atmosphere, where neutral dynamics intertwine with those of plasma.

In the lithosphere → atmosphere → ionosphere chain, the atmosphere is not a "passive filter": it is a dynamic transformer.

Ionosphere: tenuous plasma, strong signals

Here, the upper atmosphere begins to behave like a plasma sensitive to both the Sun and the dynamics below.

- It is a region of the upper atmosphere roughly between ~80 and ~600 km, but the ionosphere-thermosphere-mesosphere system extends higher depending on the physical context.

- EUV and X solar radiation produces the D, E, and F layers, with very strong diurnal, seasonal, and geomagnetic variability.

- The ionosphere is crucial for radio and GNSS: it reflects, delays, distorts, or scintillates signals, and is therefore also an excellent detector of disturbances.

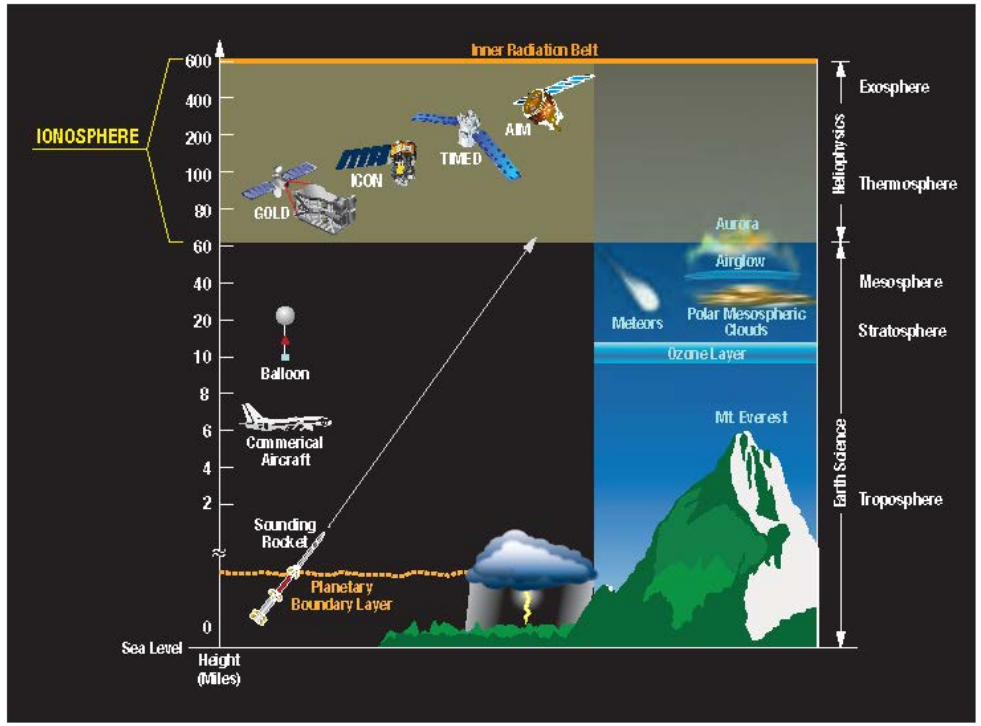

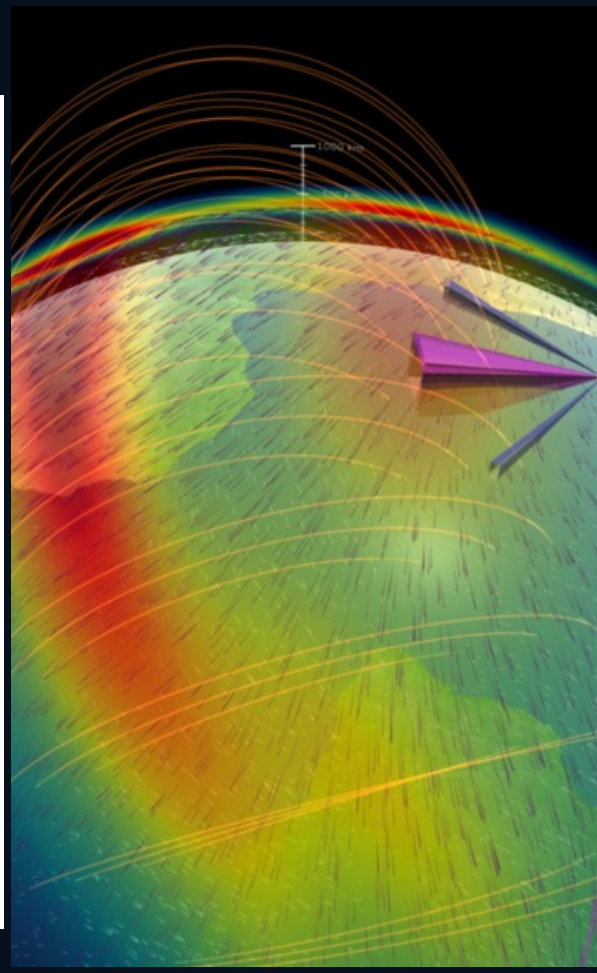

neutral atmosphere → ionized plasma

Magnetosphere: the dynamic boundary with space

The Sun's "background noise" is real physics: it must be measured and subtracted, not simply ignored.

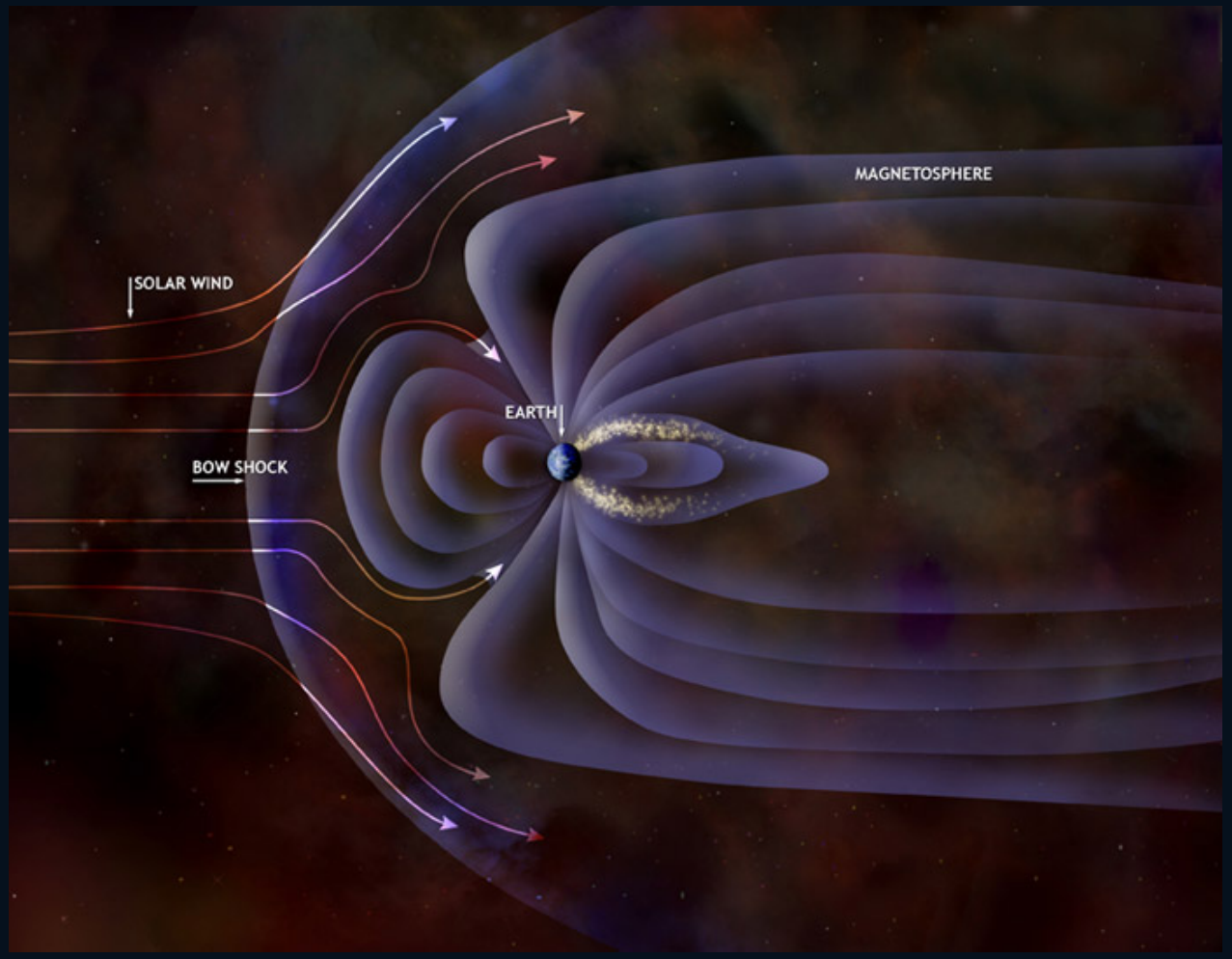

- The geomagnetic field deflects most of the solar wind, but the magnetospheric cavity remains continuously compressed, stretched, and reconnected.

- Electric currents, trapped particles, and auroras are part of the same Sun-Earth circuit.

- For those looking for lithospheric signals in the ionosphere, the magnetosphere is the dominant dynamic context.

Top-down coupling: Sun → magnetosphere → ionosphere

Space weather continuously modulates density, fields, currents, and radio propagation.

Sun / CME / flare
↓
solar wind + IMF
↓
magnetosphere: reconnection, FACs, ring current
↓
ionosphere-thermosphere: heating, density, conductivity
↓
GPS, radio, drag, observational background

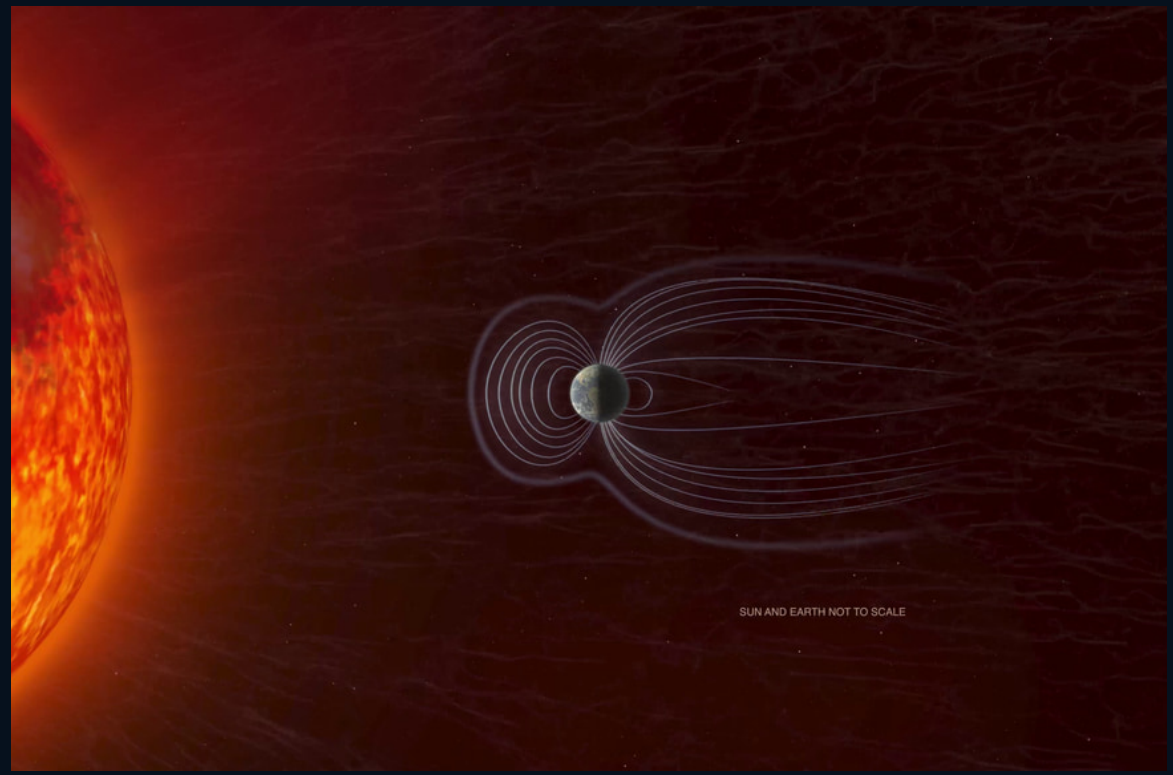

In seismo-ionospheric studies, the first step is always to estimate and remove solar and geomagnetic forcing.

Bottom-up coupling: lithosphere → atmosphere → ionosphere

This is where the most delicate scientific challenge lies: separating physical signals from statistical coincidences.

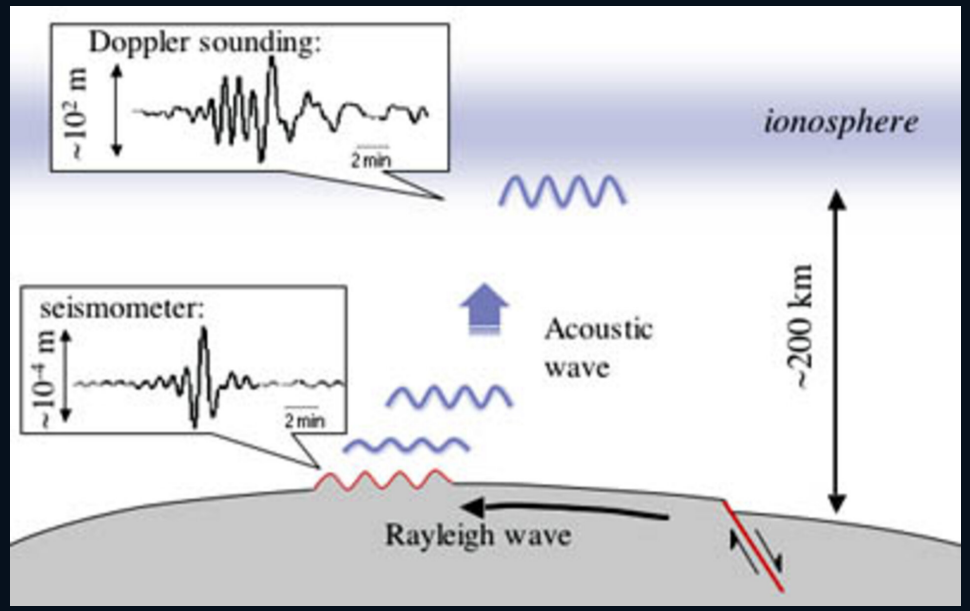

- Earthquakes, tsunamis, and eruptions can launch acoustic-gravitational waves that reach the F region and disturb the electron density.
- Co-seismic and post-seismic disturbances are now well observed in TEC, density, and waves; possible pre-seismic signals remain the most debated frontier.
- The strong criterion is multi-instrument consistency: space, ground, control statistics, and comparison with space weather.

How to truly measure the observable

The observable is not a single number: it is a constellation of physical proxies.

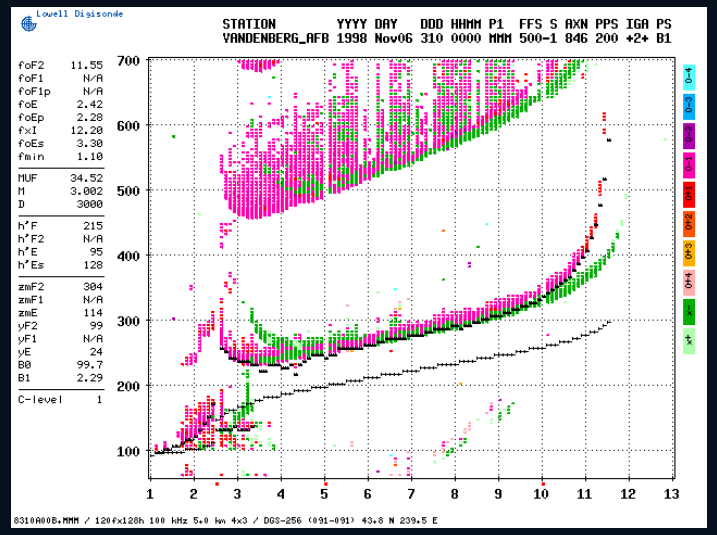

From the ground

GNSS-TEC · ionosondes · magnetometers · VLF/LF

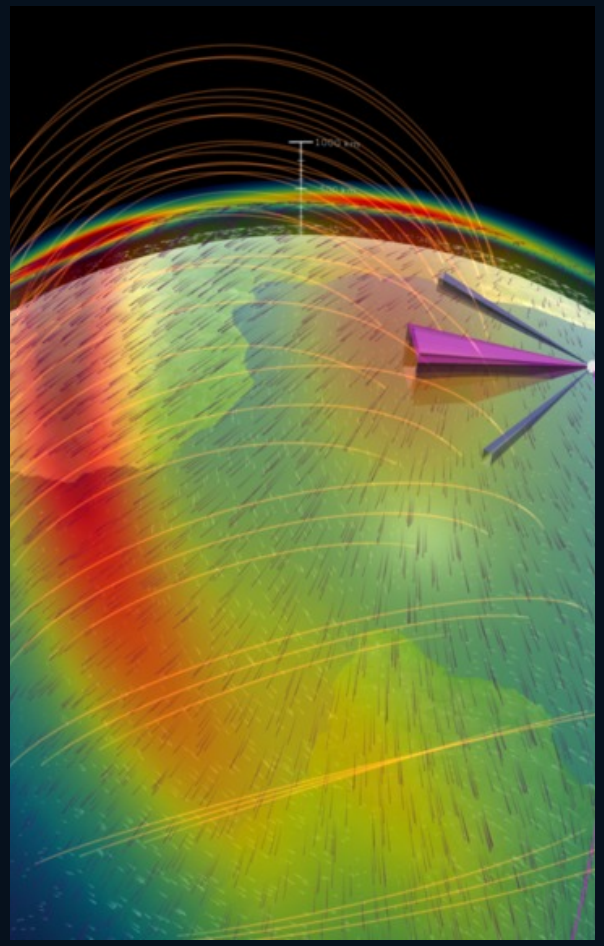

In orbit

- electric and magnetic fields
- in situ plasma and density
- electromagnetic waves
- energetic particles
- occultations / radio science

> *The most credible signature is the one that appears on different instruments, at different altitudes, and on consistent time scales.*

Lightning: an impulsive electromagnetic source

In the Earth–ionosphere system, lightning is not just weather: it is a broadband injector of ELF/VLF waves.

- The return stroke launches impulsive electric and magnetic fields that populate the Earth–ionosphere waveguide.
- Part of the energy stays near the ground as a sferic; part of it can leak through the ionosphere and access the plasma around Earth.
- For satellite EM studies, lightning is both a science target and a background that must be recognized.

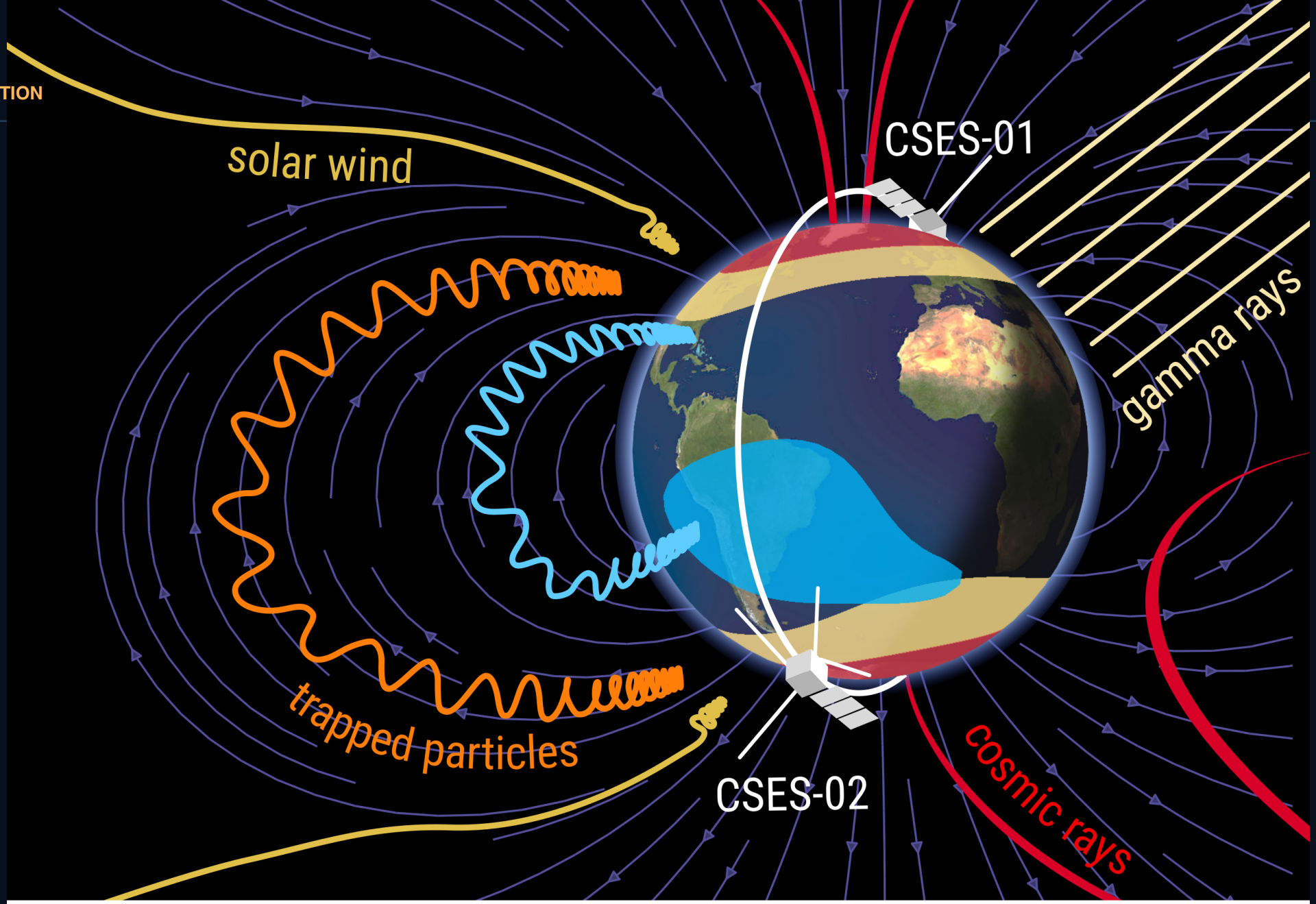
solar wind
CSES-01
gamma rays
trapped particles
CSES-02
cosmic rays
South Atlantic Anomaly, B < 21 uT
Van Allen belts footprint, 2 < L < 4
Polar regions, L > 4

Why CSES is a decisive orbiting laboratory

The mission shifts the focus from "anecdotal anomalies" to multi-parametric and multipoint physics.

- CSES is a China–Italy collaboration dedicated to monitoring electromagnetic fields, plasma, and particles in the topside ionosphere.
- Objectives include: signals associated with major geophysical events, topside ionosphere dynamics, geomagnetic variability, and Sun–Earth interactions.
- With CSES-01 (2018) and CSES-02 (2025), temporal coverage increases and it becomes more realistic to distinguish structure, noise, and causality.

HEPD · EFD · plasma · waves · particles

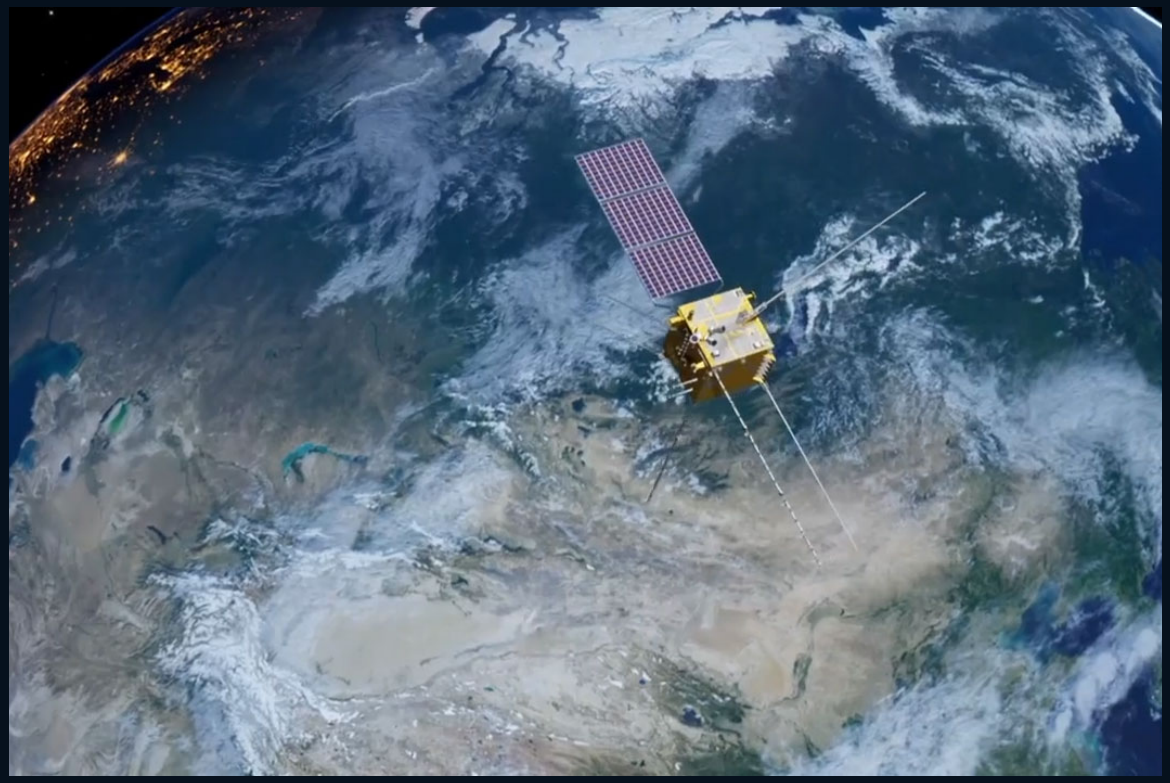

> *For "precision physics" in the ionosphere, instrumentation, orbital coverage, and control of the space environment all matter.*

PRESS RELEASE 2025

ITALIAN SCIENCE IN SPACE WITH CSES-02: A NEW EARTH OBSERVATION MISSION IS LAUNCHED

14 June 2025

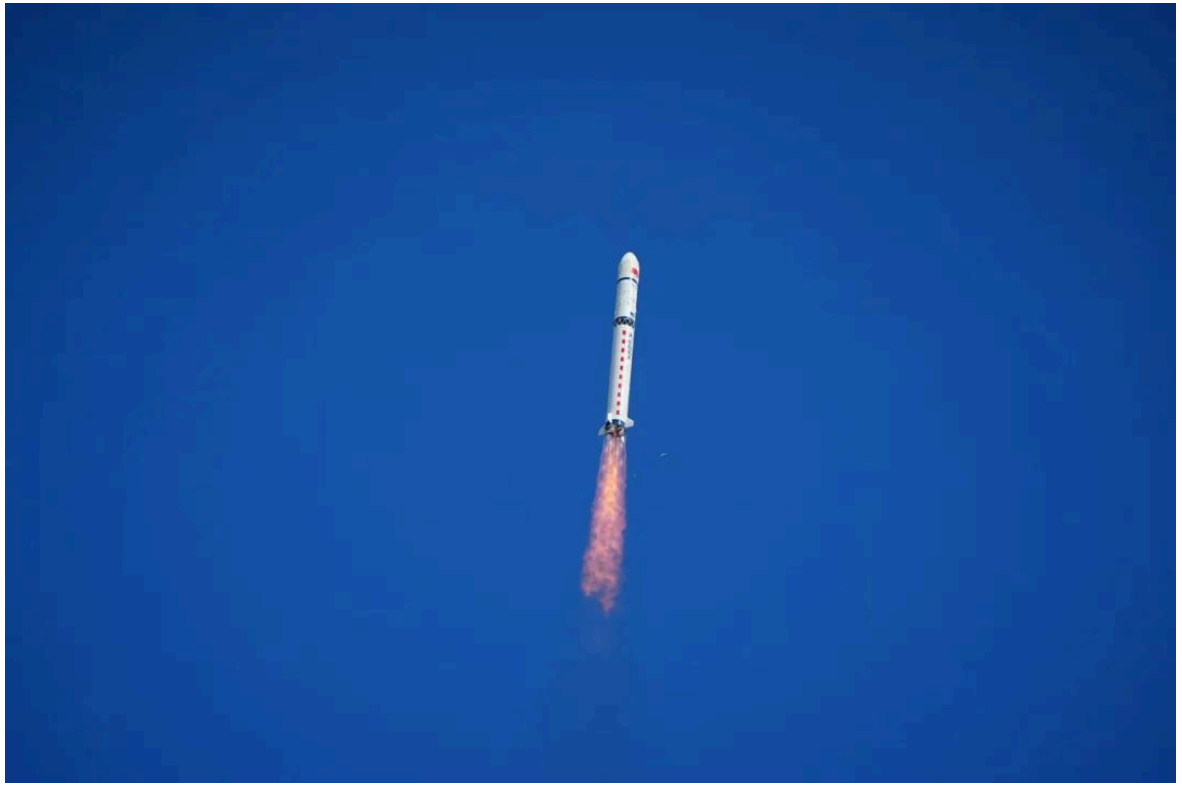

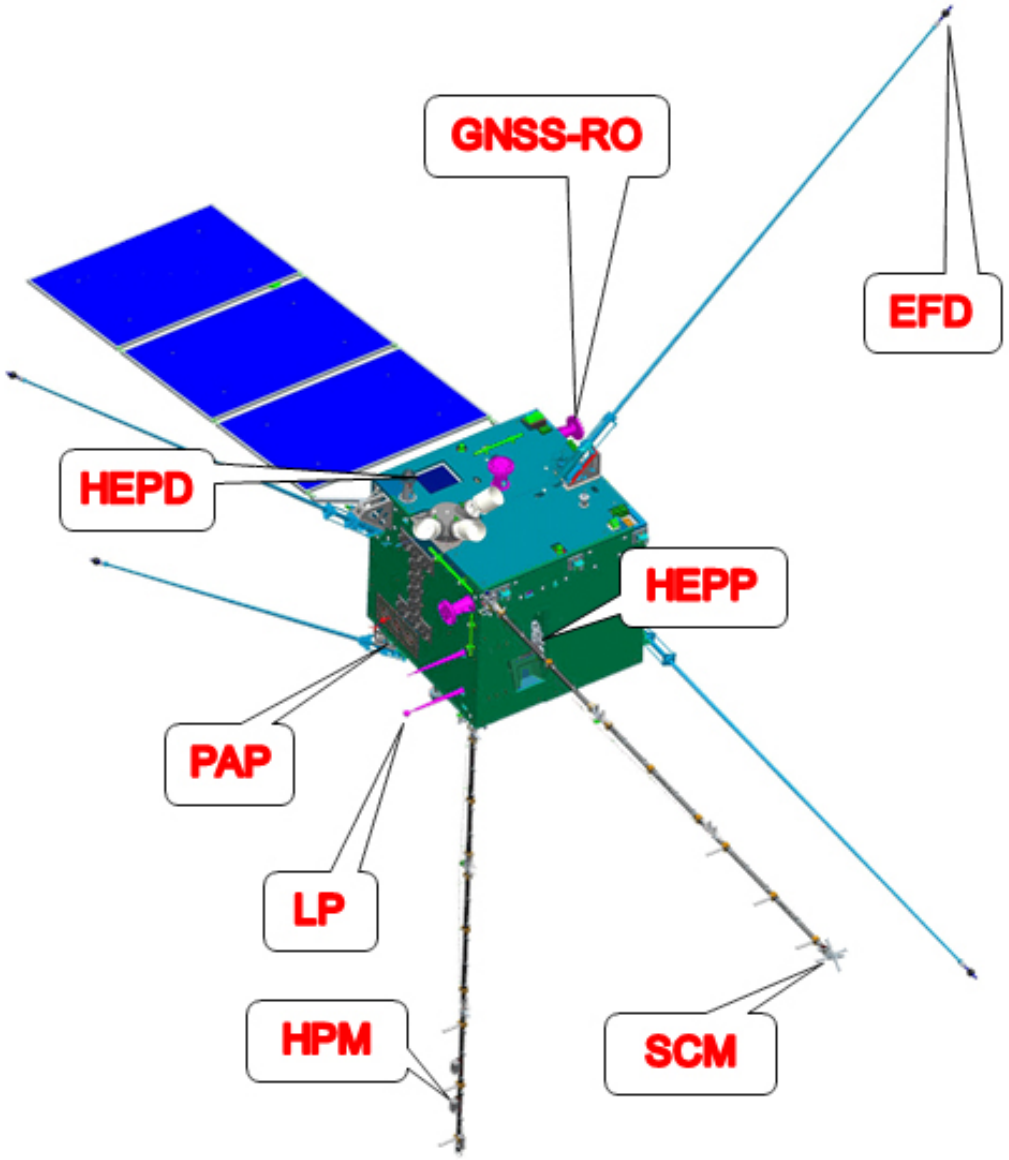

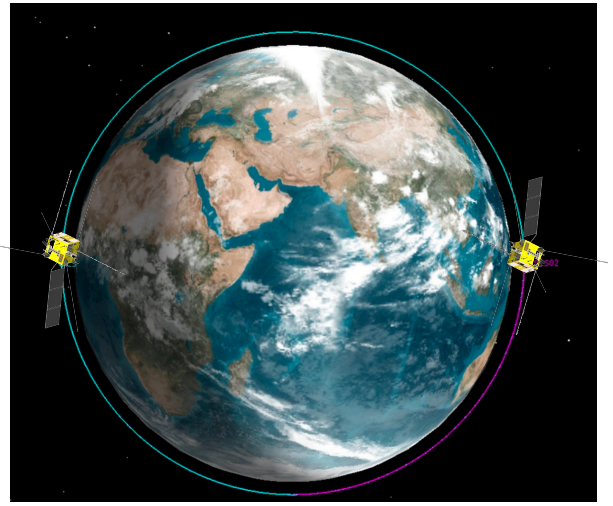

The CSES mission is the most advanced space program ever conceived for the study of the lithosphere-atmosphere-ionosphere-magnetosphere coupling.
*It is a **China-led initiative** and **Italy contributes** with two instruments: HEPD and EFD.*

CSES-02 uses the same platform of CSES-01, but upgraded.

Platform	Mass	$\simeq$ 700 kg
Orbit	**Type**	**Sun-Synchronous**
	Altitude	**507 km**
	Inclination	**97°**
	Period	94 minutes
	Revisit period	5 days
Mission	Life Span	$\geq$ 5 years

Major change: full-orbit data acquisition

Limadou HEPD-02 expected performance

HEPD-02 is designed to measure fluxes **electrons, protons, light-nuclei and GRB** in a wide energy range.

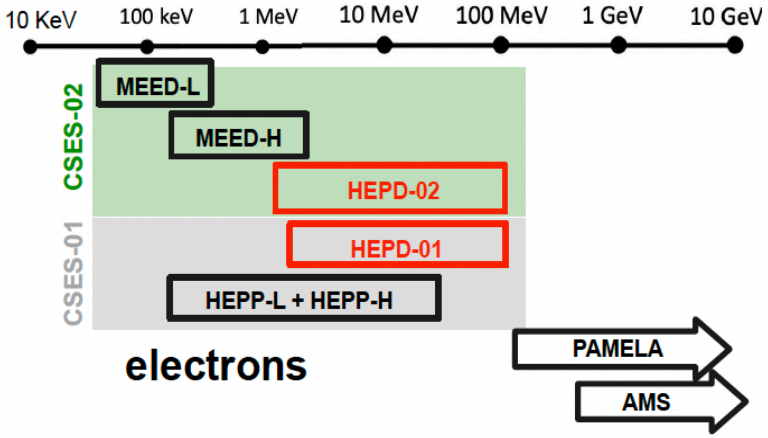

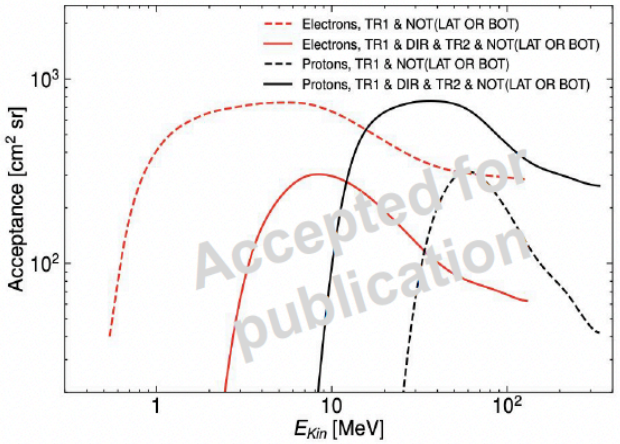

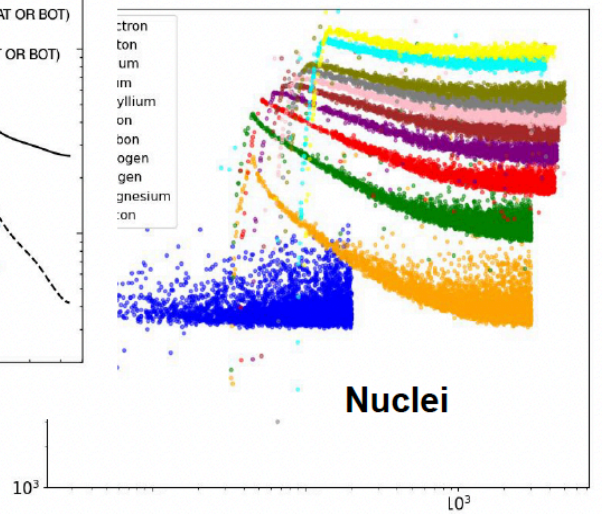

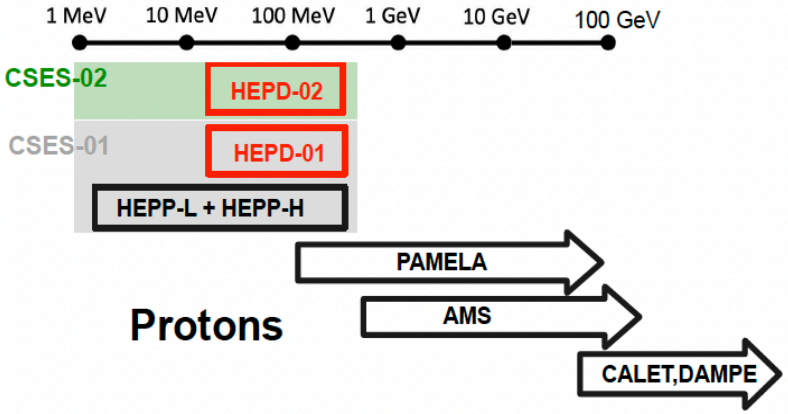

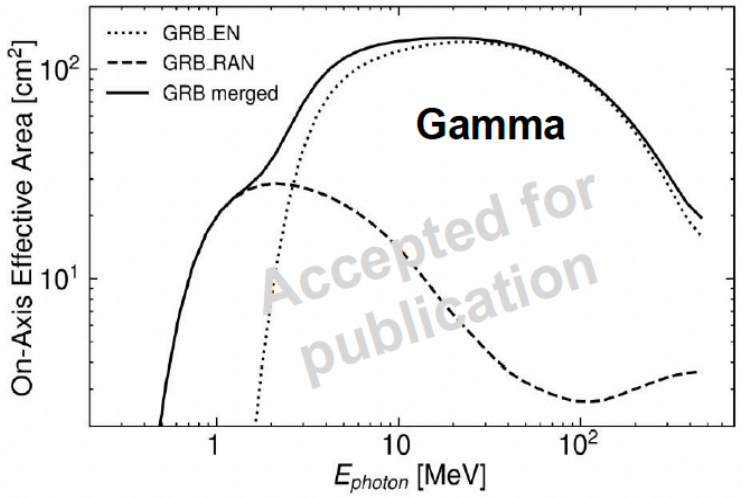

HEPD-02 system requirements

Kin. energy range (e^-)	3 MeV to 100 MeV
Kin. energy range (p)	30 MeV to 200 MeV
Angular resolution	≤10° for E_{kin} > 3 MeV (e^-)
Energy resolution	≤10% for E_{kin} > 5 MeV (e^-)
PID efficiency	> 90%
Detectable flux	up to 10^7 $m^{-2}s^{-1}sr^{-1}$
Op. temperature	-10 °C to +35 °C
Op. pressure	≤ $6.65 \cdot 10^{-3}$ Pa ("vacuum")
Mass budget	50 kg
Power Budget	45 W
Data budget	≤ 100 Gb/day

HEPD-02

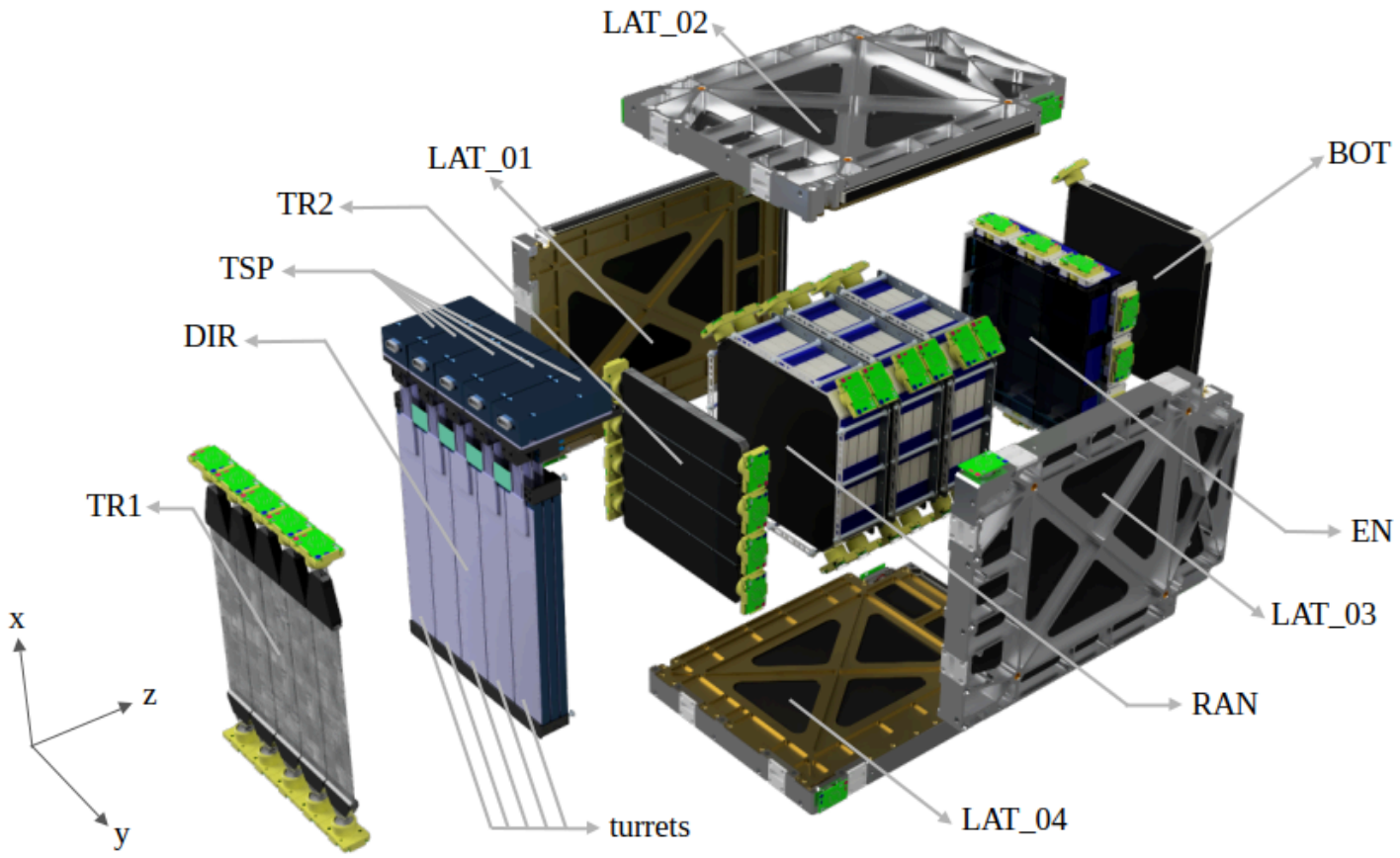

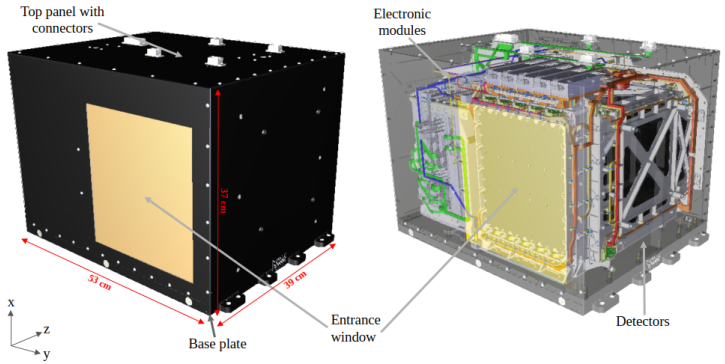

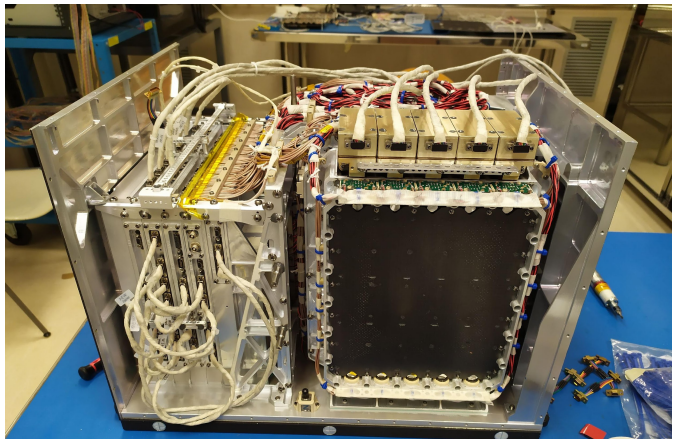

Energy range (e^-)	**3-100 MeV**
Energy range (p)	**30-250 MeV**
Energy range (nuclei)	**30-250 MeV/n**
Angular resolution	$< 8^\circ$ @ 5 MeV
Energy resolution	$< 10\%$ @ 5 MeV
Acceptance	~ 400 cm^{2}sr
Mass	~ 44 kg

- First space particle tracker based on Monolithic Active Pixel Sensors
- DAQ configuration adjusted and optimized according to the satellite position: 128 different configurations
- Dedicated acquisition mode for 0.1-100 MeV photon transients: HEPD-02 sensitive to GRBs

besides overall improvement of sensitivity (e.g. nuclei) w.r.t. HEPD-01

HEPD-02 event topology and energy range

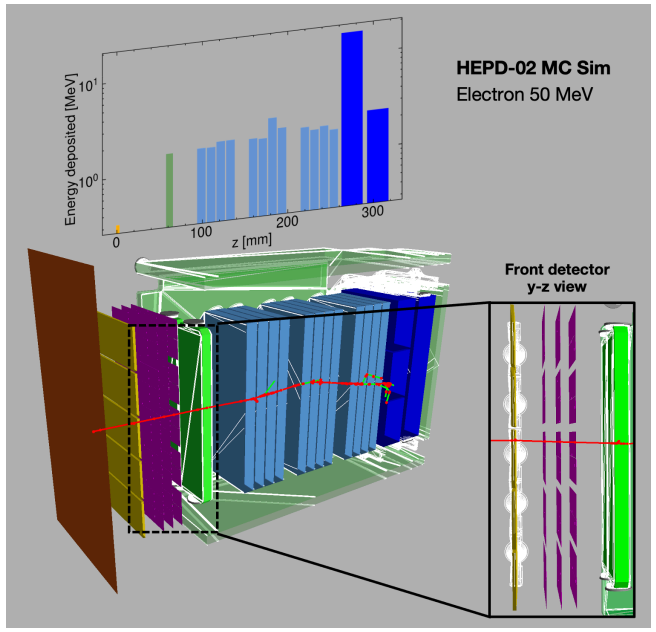

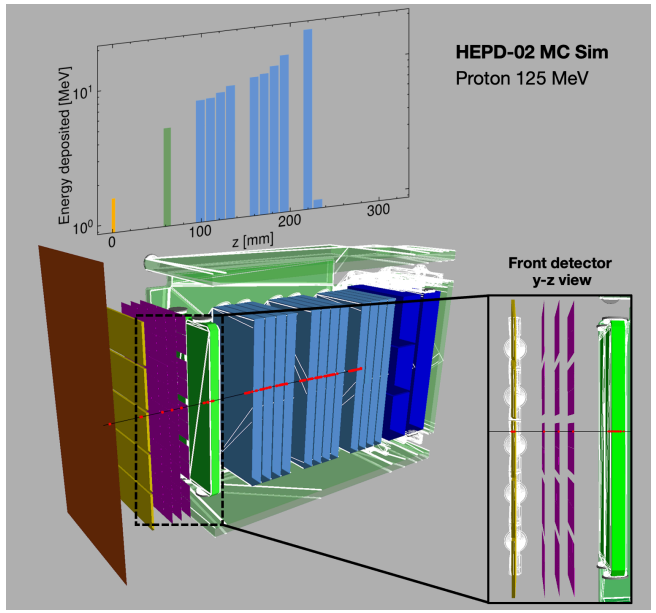

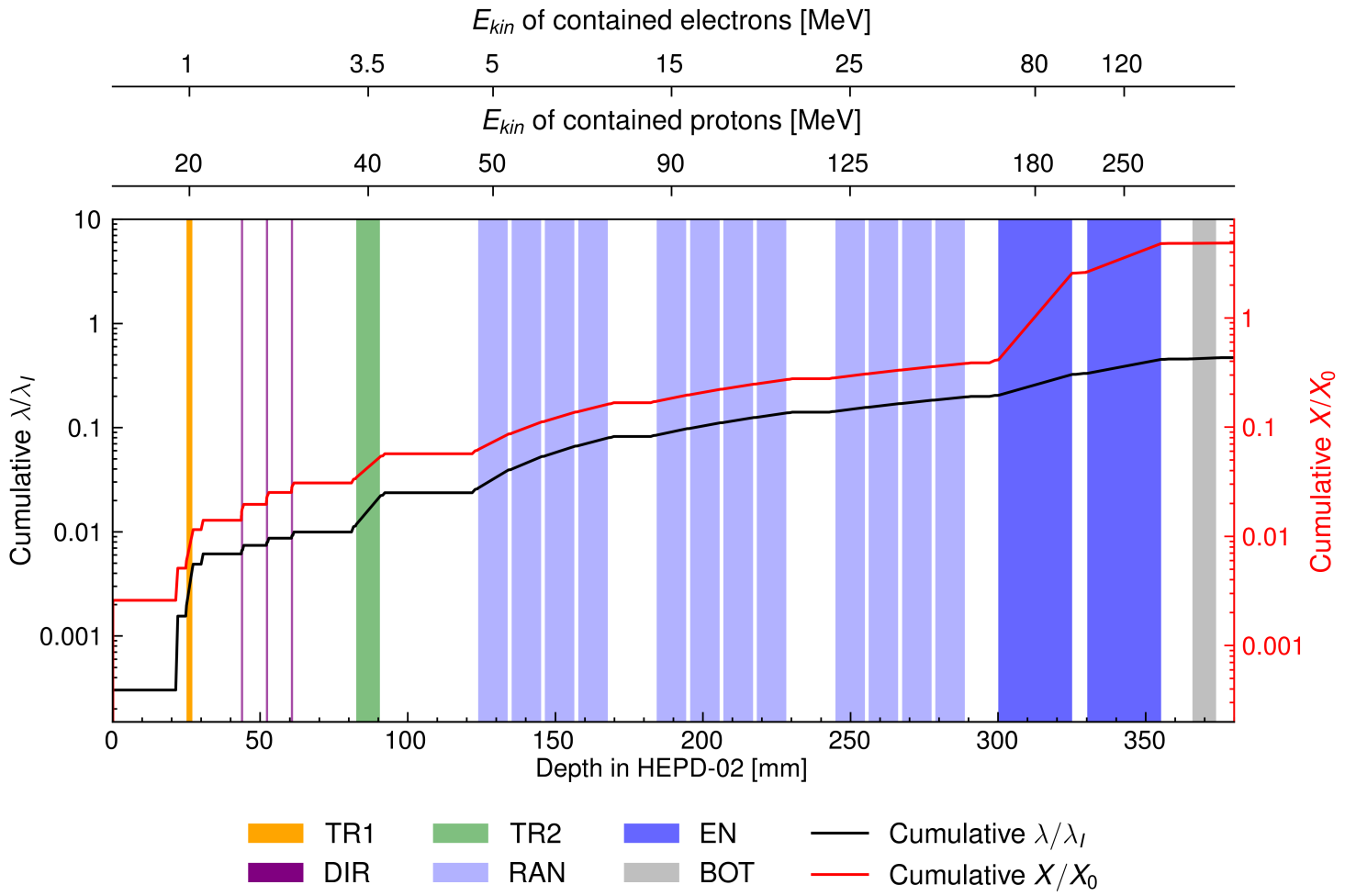

HEPD-02 pixel tracker

IEEE Aer.and Electronics Syst. Mag. 10.1109/MAES.2025.3568361 (2025)

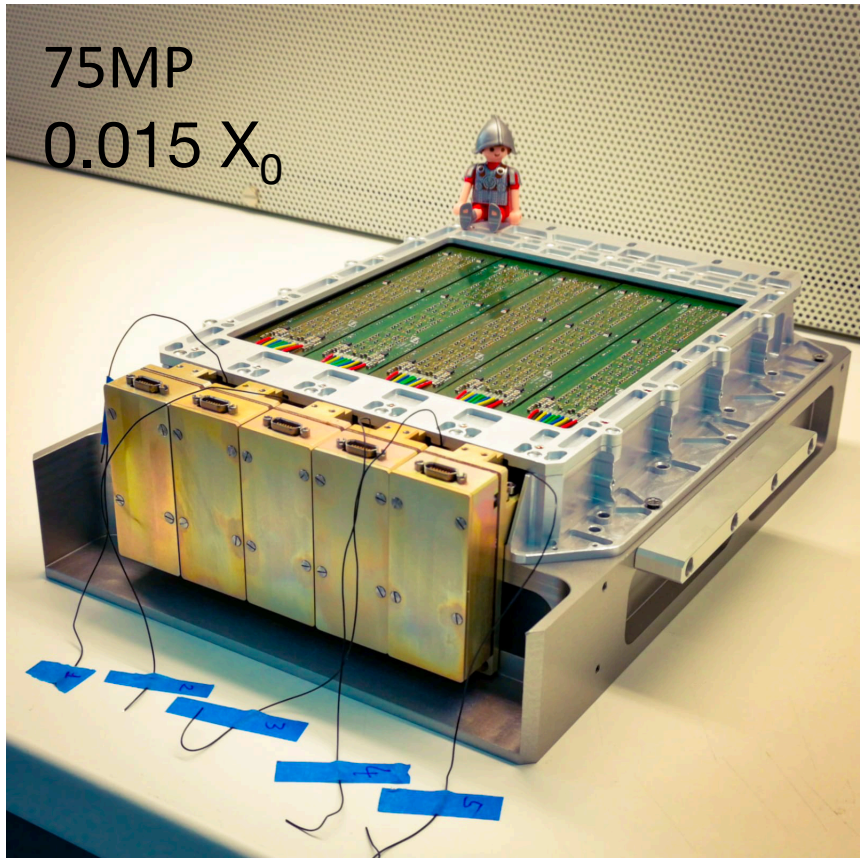

first ever use of MAPS in space

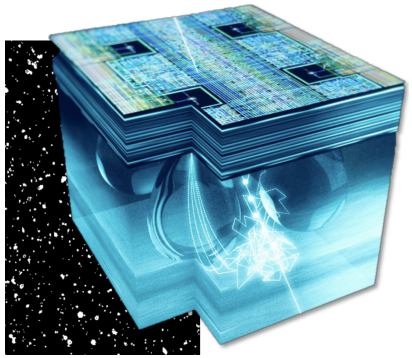

a Monolithic Active Pixel (artist impression) courtesy of CERN

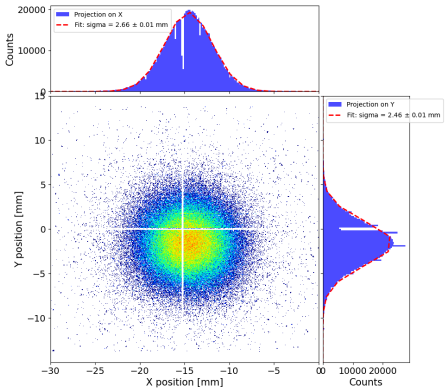

beam-spot measured @ APSS proton-therapy center

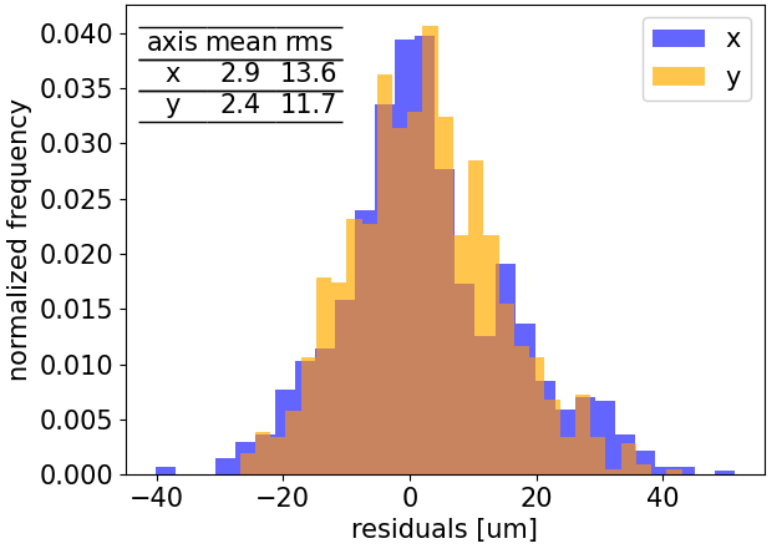

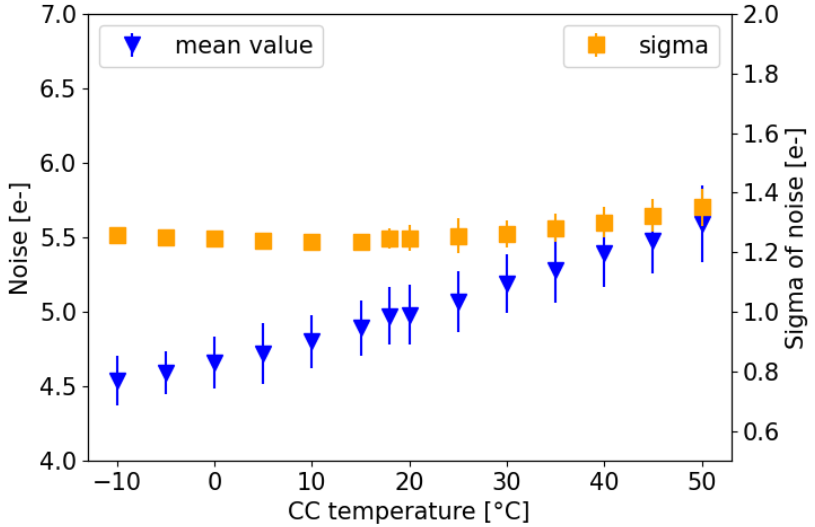

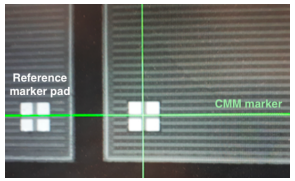

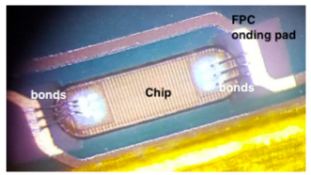

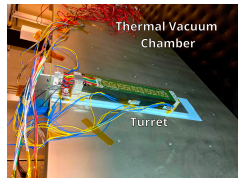

GRB 221009A: why it was the BOAT

A cosmic event outside the Galaxy bright enough to leave a measurable imprint on the near-Earth environment.

- GRB 221009A was likely the brightest gamma-ray burst to appear in Earth’s skies in roughly 10,000 years.
- The 9 October 2022 event saturated many detectors in orbit, forcing reconstruction of the most intense part of the flash.
- The standard picture is core collapse plus relativistic jets aimed almost directly toward Earth.

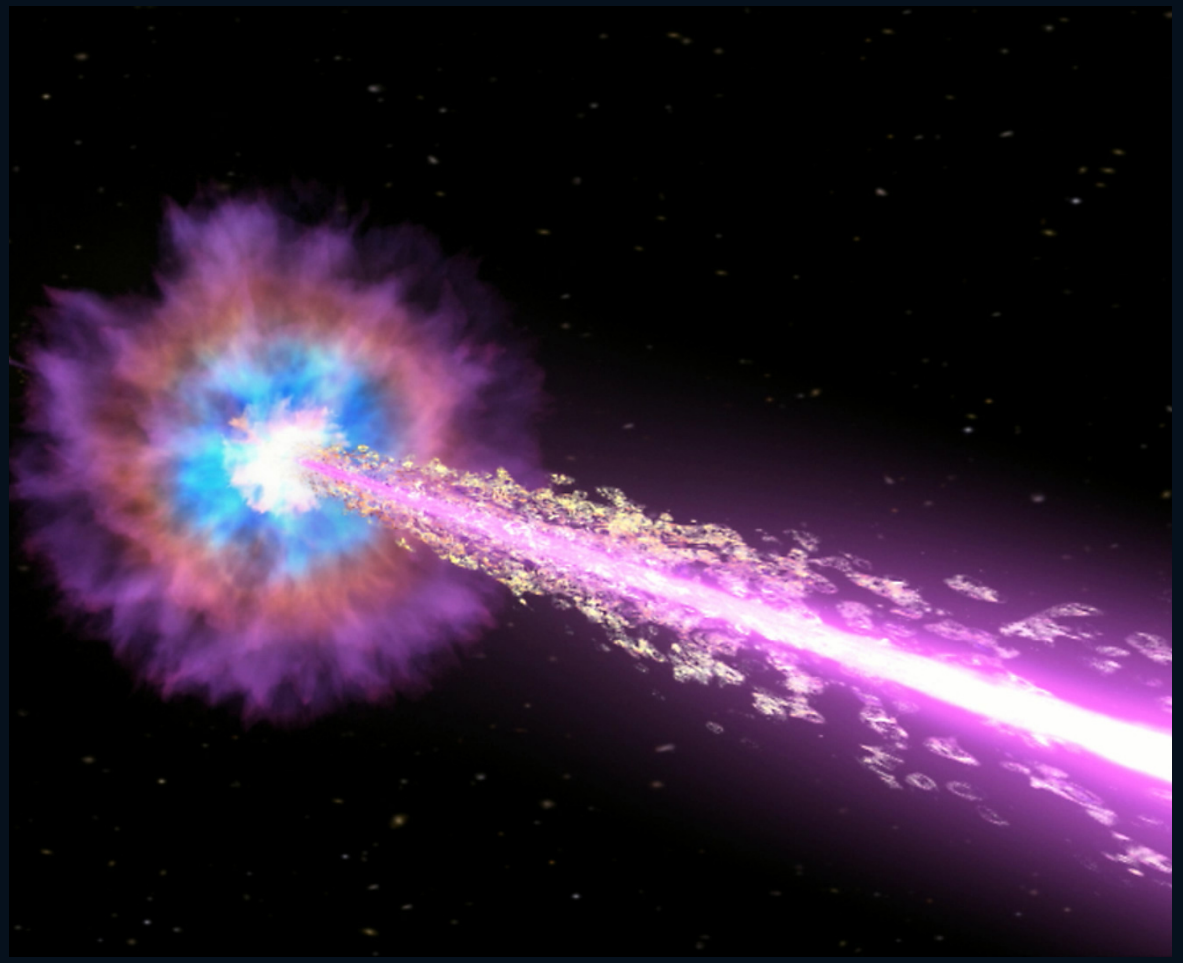

NASA/Swift/Cruz deWilde jet concept

Where it was and how we saw it

The line of sight is part of the story: the burst sat close to the dusty plane of the Milky Way.

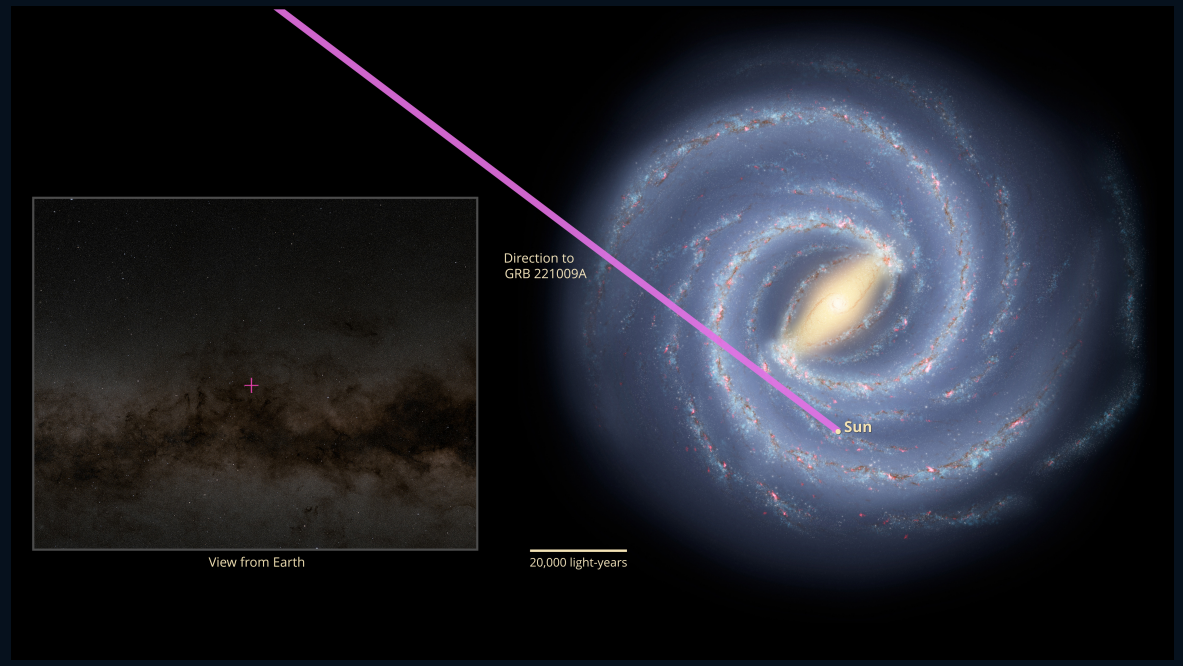

- The radiation arrived from the direction of Sagitta after traveling about 1.9 billion years.
- That sightline crosses dust-rich Galactic regions — crucial for understanding the later X-ray echoes and rings.
- Fermi, Swift, INTEGRAL, and many follow-up observatories measured prompt and afterglow emission across bands.
- CSES observed **GRB 221009A “BOAT”** from the conversions of X/gamma into the particle detector sensitive elements

When a GRB perturbs Earth’s atmosphere

An extragalactic flash with a measurable geophysical response.

- The burst was so intense that even Earth’s atmosphere showed a measurable response.

- European VLF transmitter paths showed ionospheric changes, while no associated broadband ELF/VLF burst was detected.

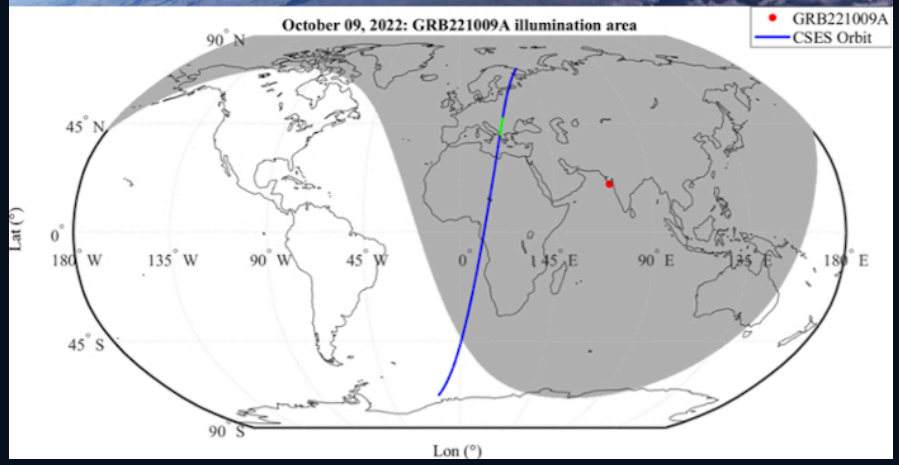

Observation of Anomalous Electron Fluxes Induced by GRB221009A on CSES-01 Low-energy Charged Particle Detector

R. Battiston[1], C. Neubüser[2], F. M. Follega[1,2], R. Iuppa[1], V. Vitale[3], R. Ammendola[4], D. Badoni[4], S. Bartocci[4], A. Bazzano[5], S. Beolè[6], I. Bertello[5], W. J. Burger[2], D. Campana[7], A. Cicone[8], P. Cipollone[4], S. Coli[9], L. Conti[4,10], A. Contin[11], M. Cristoforetti[12], G. D'Angelo[5], F. De Angelis[5], C. De Donato[4], C. De Santis[4], P. Diego[5], A. Di Luca[1], E. Fiorenza[5], G. Gebbia[1,2], A. Lega[1,2], M. Lolli[13], B. Martino[14], M. Martucci[4], G. Masciantonio[4], M. Mergè[15], M. Mese[7,16], A. Morbidini[5], F. Nuccilli[5], F. Nozzoli[2], A. Oliva[11], G. Osteria[7], E. Papini[5], F. Palma[4], F. Palmonari[11], A. Parmentier[5], B. Panico[7,16], S. Perciballi[6], F. Perfetto[7], A. Perinelli[1], P. Picozza[3], M. Piersanti[8], M. Pozzato[13], G. Rebustini[4], D. Recchiuti[5], E. Ricci[1,2], M. Ricci[17], J. Rodi[5], A. Russi[5], S. B. Ricciarini[18], Z. Sahnoun[11,13], U. Savino[6], V. Scotti[7,16], X. Shen[19], A. Sotgiu[4], R. Sparvoli[3], S. Tofani[5], P. Ubertini[5], N. Vertolli[5], V. Vilona[2], U. Zannoni[5], Z. Zeren[20], S. Zoffoli[15], and P. Zuccon[1]

[1] University of Trento, Via Sommarive 14, I-38123 Trento, Italy
[2] TIFPA-INFN, Via Sommarive 14, I-38123 Trento, Italy; coralie.neubueser@tifpa.infn.it
[3] University of Rome, Tor Vergata, I-38123 Rome, Italy
[4] INFN—Sezione di Roma Tor Vergata, Via della Ricerca Scientifica 1, I-00133, Rome, Italy

The Astrophysical Journal Letters, 946:L29 (6pp), 2023 March 20

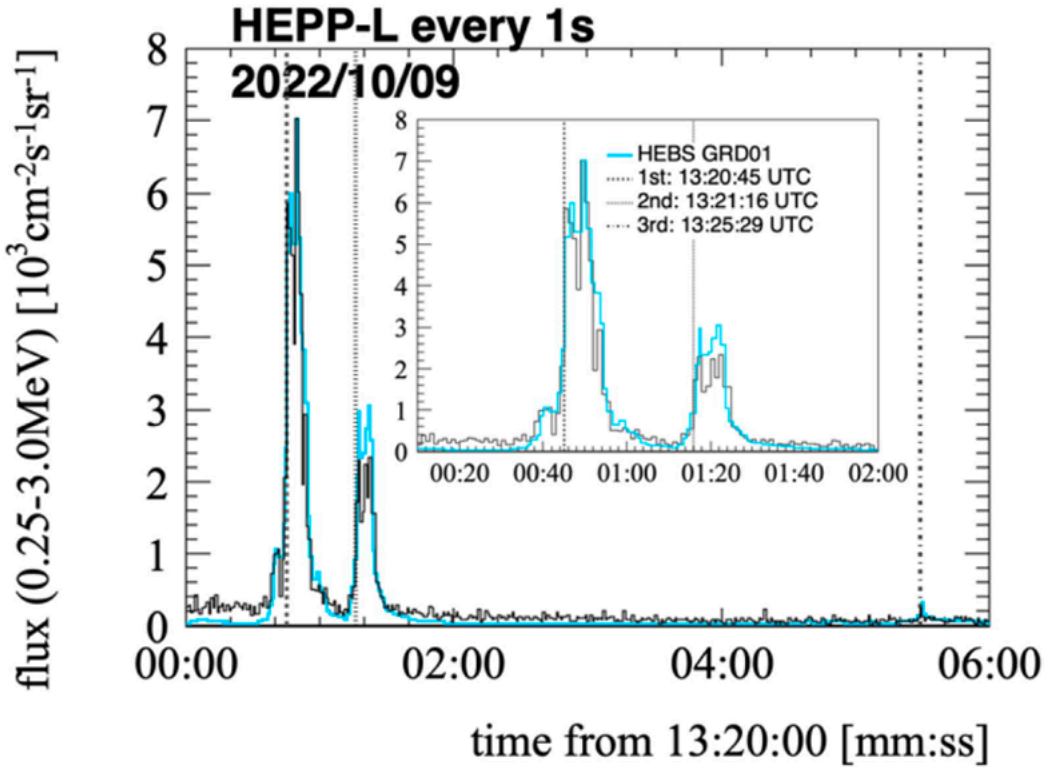

Figure 4. Electron flux of all HEPP-L channels summed over the energy range from 250 keV to 3 MeV on 2022 October 9 starting from 13:20:00 UTC. The blue curve shows the measured photon counts per second of the HEBS GRD01 instrument (Liu et al. 2022b), scaled to match the maximum of the first HEPP-L peak. The scaling factor is given in the legend. The vertical dashed lines mark the reference UTC times of the signals measured by other instruments; see Table 1. No corrections were applied to the timing provided by HEBS and HEPP-L instruments.

MeV GRB observation with the HEPD-01

Roberto Iuppa

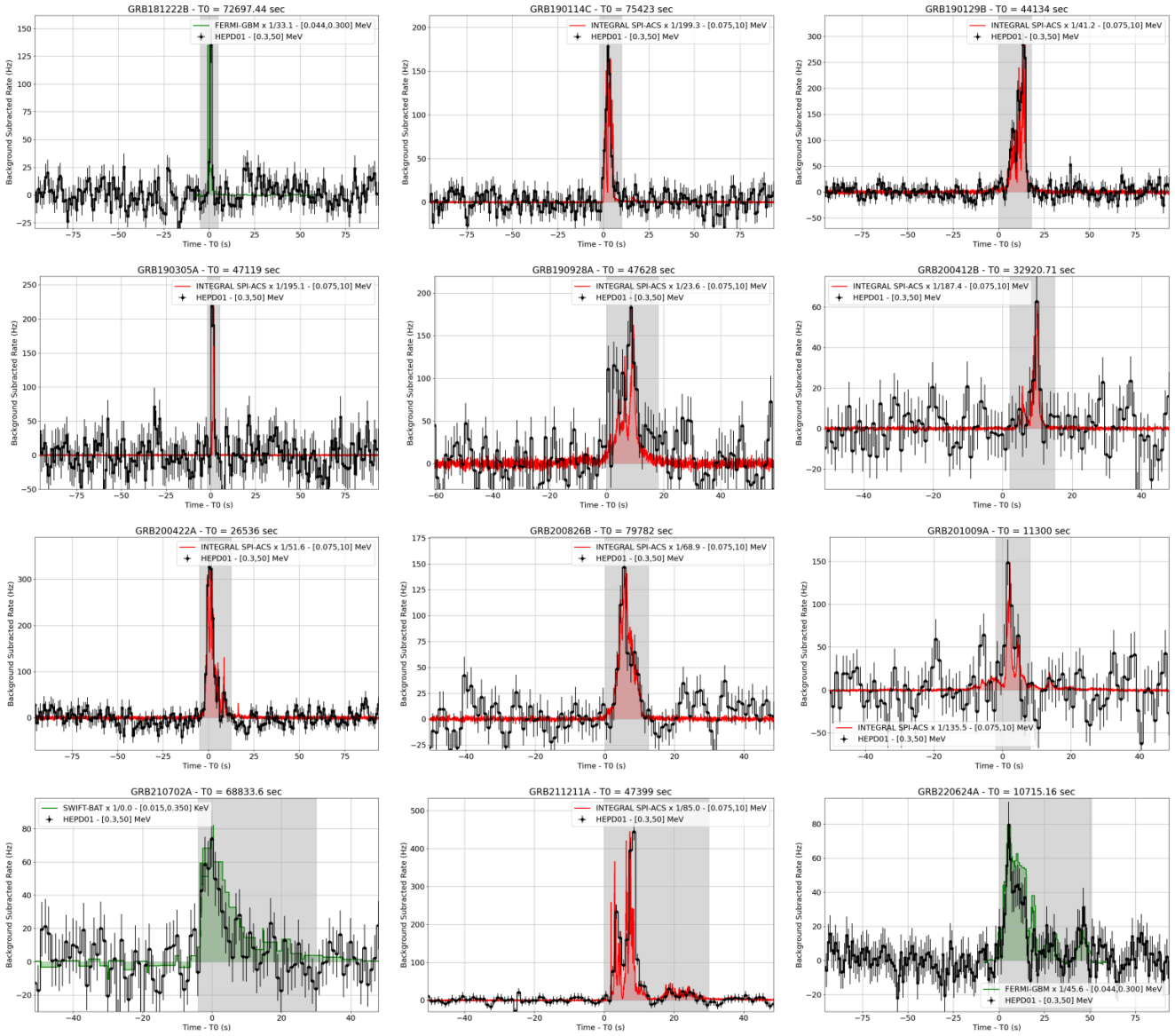

0.3-50 MeV measurement of duration, fluence and time-profile for 12 GRBs observed by INTEGRAL-SPI, Fermi-Lat and Konus Wind.

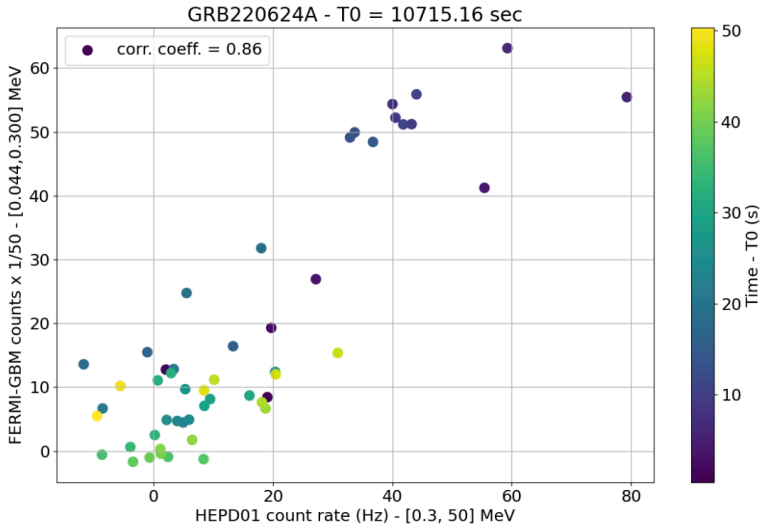

Important information retrieved from time-profile: comparison of tens of keV / tens of MeV emissions available for modelling

HEPD-02:
x200 improvement in time resolution
x10 improvement in energy resolution
x40 improvement in effective area

Limadou_CSN2 - stato dell'esperimento

Sept. 15, 2025

HEPD-02 GRB sensitivity

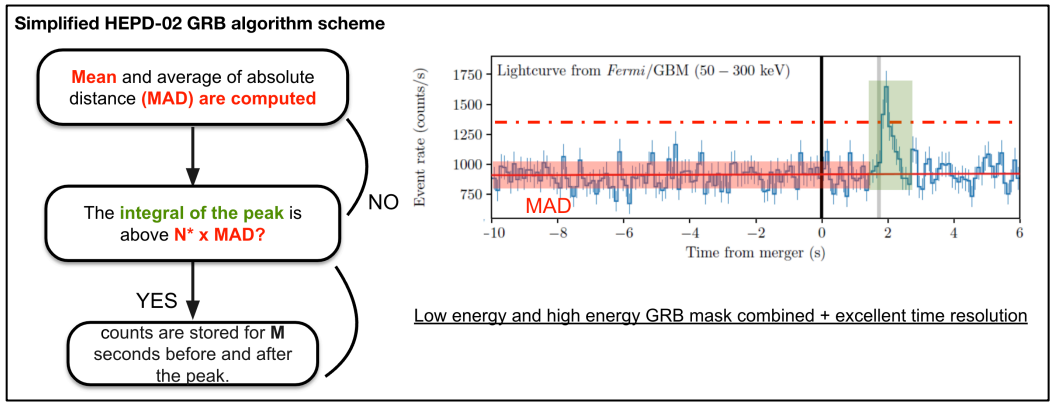

time-base: 5ms

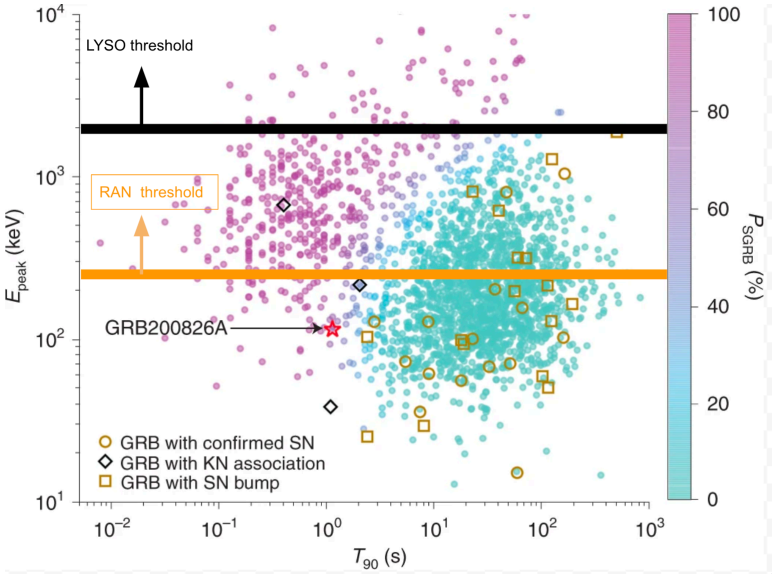

7 consecutive ~ 1 sec gamma pulses

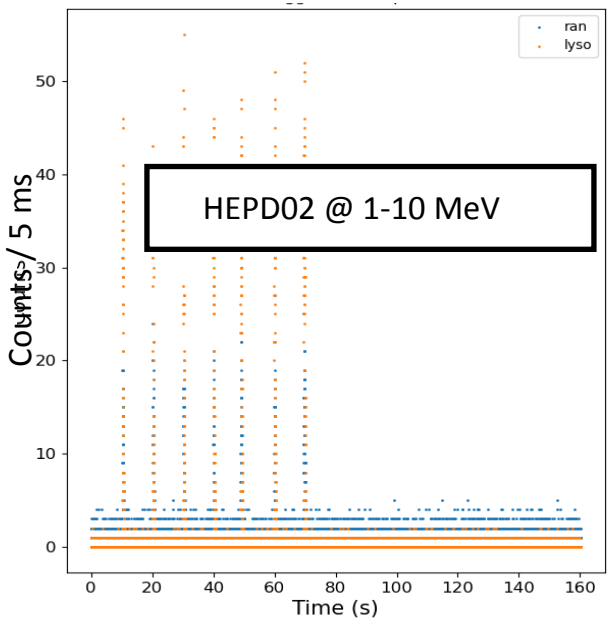

single ~10 sec pulse

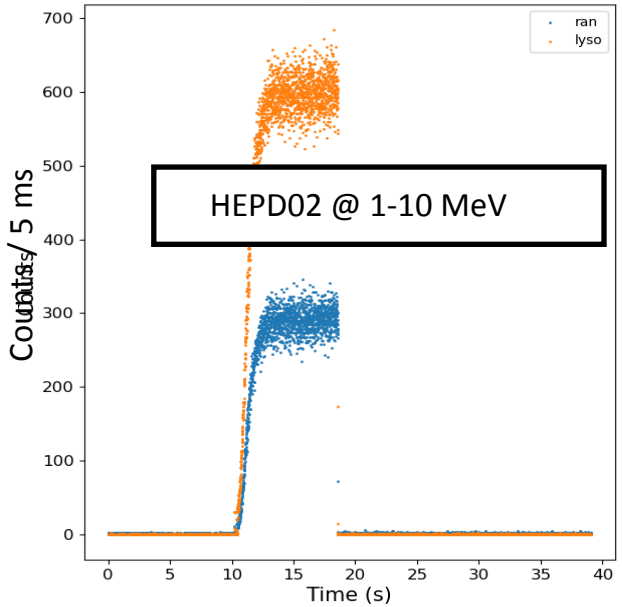

very good grasp at 3-30 MeV

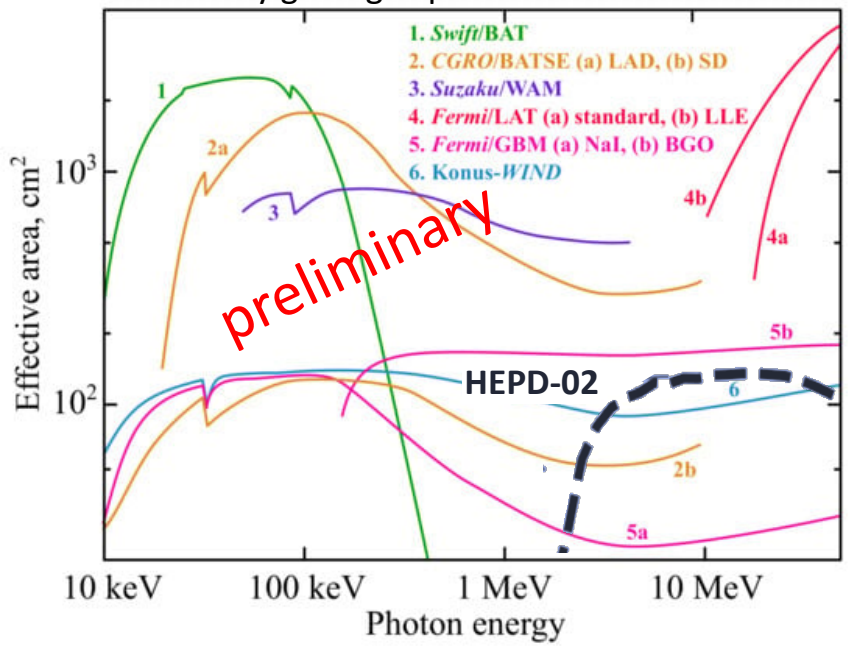

HEPD-02 GRB sensitivity

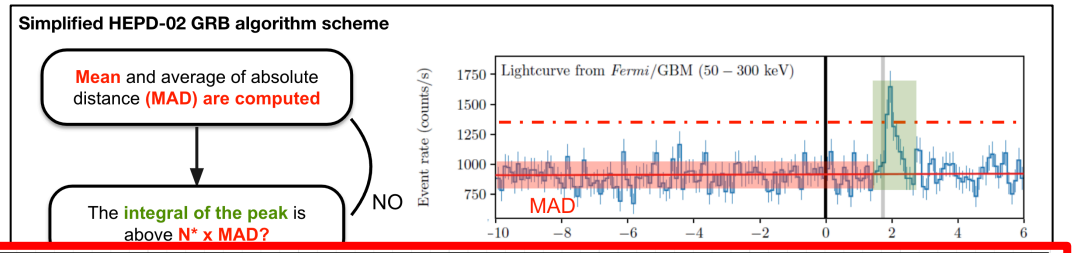

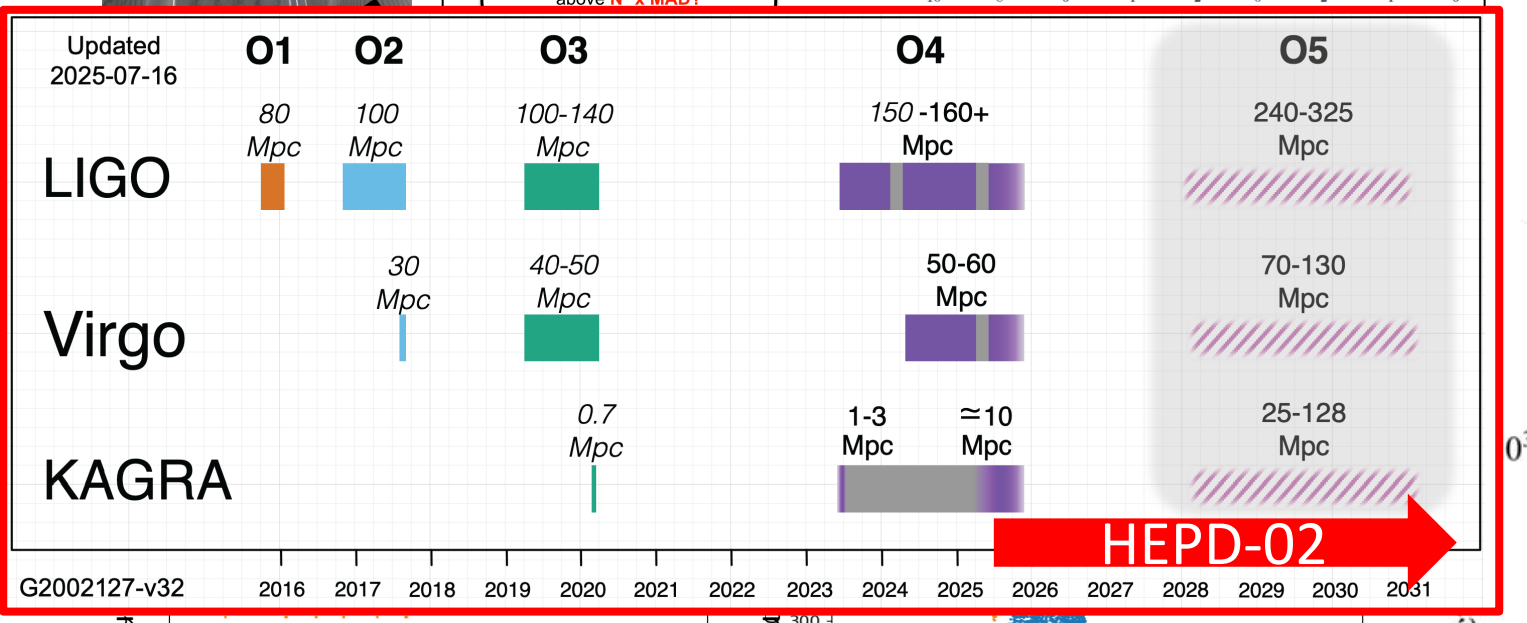

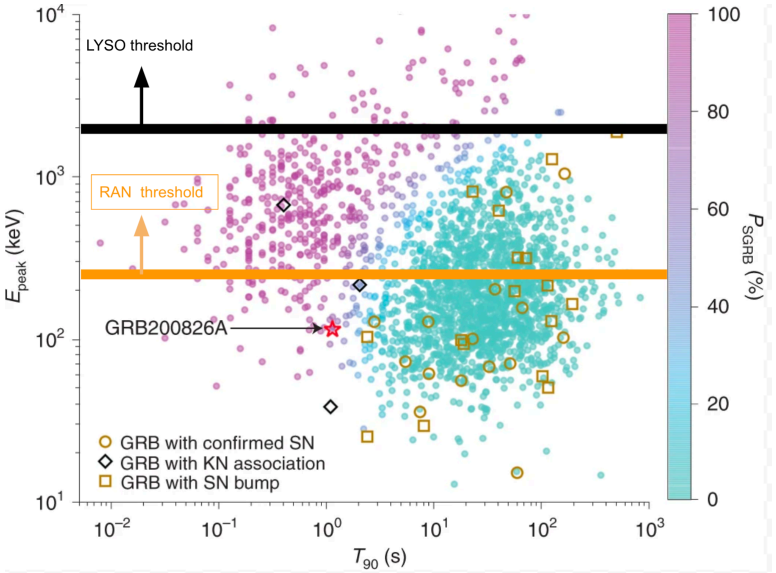

very good grasp at 3-30 MeV

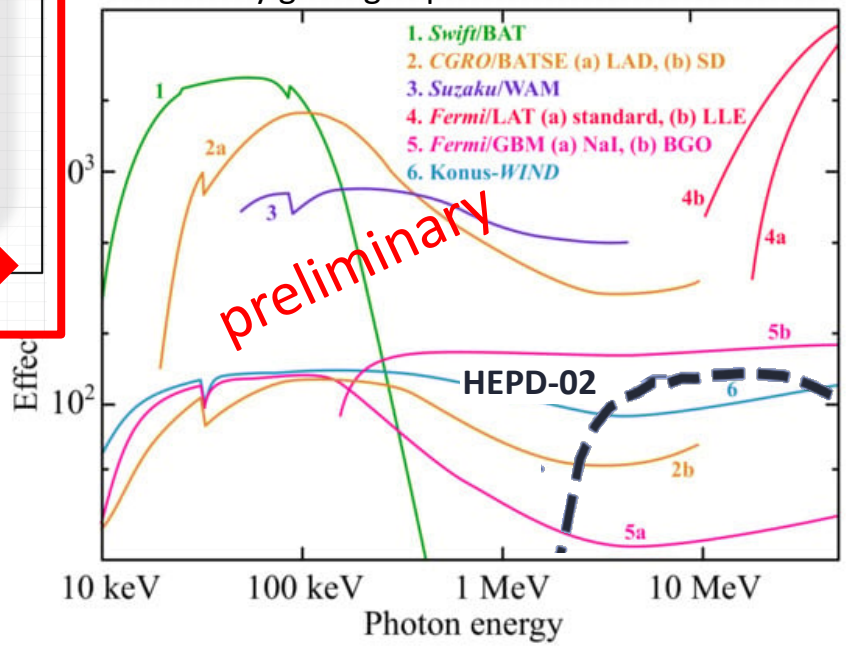

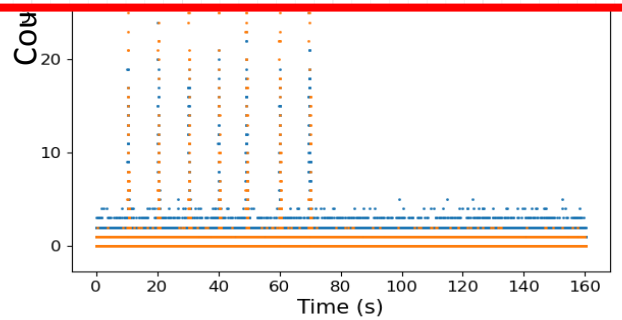

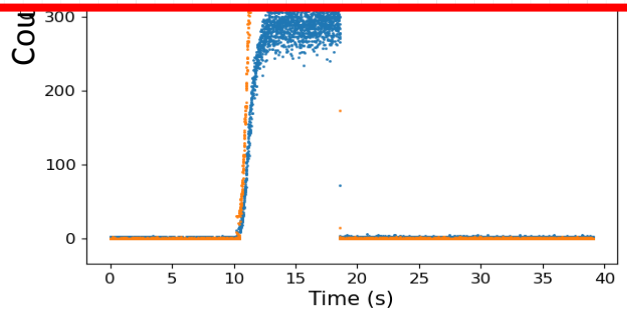

Remote Sens. **2024**, *16*, 3982. https://doi.org/10.3390/rs16213982

remote sensing

MDPI

Article

The Scintillation Counters of the High-Energy Particle Detector of the China Seismo-Electromagnetic (CSES-02) Satellite

Simona Bartocci [1], Roberto Battiston [2,3], Stefania Beolè [4,5], Franco Benotto [5], Piero Cipollone [6], Silvia Coli [5], Andrea Contin [7,8], Marco Cristoforetti [3,9], Cinzia De Donato [6], Cristian De Santis [6], Andrea Di Luca [3,9], Floarea Dumitrache [5], Francesco Maria Follega [2,3], Simone Garrafa Botta [5], Giuseppe Gebbia [2,3], Roberto Iuppa [2,3], Alessandro Lega [2,3], Mauro Lolli [8], Giuseppe Masciantonio [6], Matteo Mergè [10], Marco Mese [11,12], Riccardo Nicolaidis [2,3], Francesco Nozzoli [3], Alberto Oliva [8], Giuseppe Osteria [12], Francesco Palma [6], Federico Palmonari [7,8], Beatrice Panico [11,12], Stefania Perciballi [4,5], Francesco Perfetto [12], Piergiorgio Picozza [6,13], Michele Pozzato [8], Ester Ricci [2,3], Marco Ricci [14], Sergio Bruno Ricciarini [15], Zouleikha Sahnoun [7,8,*], Umberto Savino [4,5], Valentina Scotti [11,12], Enrico Serra [3], Alessandro Sotgiu [6], Roberta Sparvoli [6,13], Pietro Ubertini [16], Veronica Vilona [3], Simona Zoffoli [10] and Paolo Zuccon [2,3]

Remote Sensing

IEEE TRANSACTIONS ON INSTRUMENTATION AND MEASUREMENT, VOL. 74, 2025 2008413

Trigger and Calorimeter Data Acquisition of the High-Energy Particle Detector Onboard the CSES-02 Satellite

Antonio Anastasio, Simona Bartocci, Roberto Battiston, Stefania Beolè, Franco Benotto, Alfonso Boiano, Piero Cipollone, Silvia Coli, Andrea Contin, Marco Cristoforetti, Cinzia De Donato, Cristian De Santis, Andrea Di Luca, Flori Dumitrache, Francesco Maria Follega, Simone Garrafa Botta, Giuseppe Gebbia, Roberto Iuppa, Alessandro Lega, Mauro Lolli, Giuseppe Masciantonio, Vincenzo Masone, Matteo Mergè, Marco Mese, Riccardo Nicolaidis, Francesco Nozzoli, Alberto Oliva, Giuseppe Osteria, Francesco Palma, Federico Palmonari, Beatrice Panico, Stefania Perciballi, Francesco Perfetto, Piergiorgio Picozza, Michele Pozzato, Ester Ricci, Marco Ricci, Sergio Bruno Ricciarini, Zouleikha Sahnoun, Umberto Savino, Valentina Scotti, *Senior Member, IEEE*, Enrico Serra, Alessandro Sotgiu, Roberta Sparvoli, Veronica Vilona, Simona Zoffoli, and Paolo Zuccon

IEEE Trans. Instr. and Meas.

Journals & Magazines > IEEE Aerospace and Electronic... > Early Access

The Monolithic Active Pixel Sensors Tracker System of the High Energy Particle Detector aboard the Second Chinese Seismo-Electromagnetic Satellite

Publisher: IEEE

Cite This PDF

IEEE Aerospace and Electronics

Luca Barioglio ; Simona Bartocci ; Roberto Battiston ; Stefania Beolè ; Franco Benotto ; Stefania Bufalino

All Authors

inst

PUBLISHED BY IOP PUBLISHING FOR SISSA MEDIALAB

RECEIVED: *February 25, 2025*
REVISED: *April 15, 2025*
ACCEPTED: *April 16, 2025*
PUBLISHED: *June 6, 2025*

Development of the power supply of HEPD-02 instrument on board CSES-02 satellite

S. Bartocci [a], R. Battiston [b,c], S. Beolé [d,e], F. Benotto [e], G. Castellini [f], P. Cipollone [g], S. Coli [e], A. Contin [h,i], M. Cristoforetti [j,c], C. De Donato [g], C. De Santis [g], A. Di Luca [j,c], F. Dumitrache [e], F.M. Follega [b,c], S. Garrafa Botta [e], G. Gebbia [b,c], R. Iuppa [b,c], A. Lega [b,c], M. Lolli [i], G. Masciantonio [g,*], M. Mergè [k], M. Mese [l,m], R. Nicolaidis [b,c], F. Nozzoli [c], A. Oliva [i], G. Osteria [m], F. Palma [g], F. Palmonari [h,i], B. Panico [l,m], S. Perciballi [d,e], F. Perfetto [m], P. Picozza [n,g], M. Pozzato [i], E. Ricci [b,c], M. Ricci [g,o], S.B. Ricciarini [f], Z. Sahnoun [h,i], U. Savino [d,e], V. Scotti [l,m], E. Serra [c], A. Sotgiu [g], R. Sparvoli [n,g], P. Ubertini [p], V. Vilona [c], S. Zoffoli [k] and P. Zuccon [b,c]

Journal of Instrumentation

Methods in Physics Research A 1080 (2025) 170756

s lists available at ScienceDirect

Methods in Physics Research, A

page: www.elsevier.com/locate/nima

Full Length Article

TROPix: A parametric tool reproducing the output of the HEPD-02 pixel detector

Simona Bartocci [a], Roberto Battiston [b,c], Stefania Beolè [d,e], Franco Benotto [e], Piero Cipollone [f], Silvia Coli [e], Andrea Contin [g,h], Marco Cristoforetti [i,c], Cinzia De Donato [f], Cristian De Santis [f], Floarea Dumitrache [e], Andrea Di Luca [i,c,*], Francesco Maria Follega [b,c], Simone Garrafa Botta [e], Giuseppe Gebbia [b,c], Roberto Iuppa [b,c], Alessandro Lega [b,c], Mauro Lolli [h], Giuseppe Masciantonio [f], Matteo Mergè [j], Marco Mese [k,l], Riccardo Nicolaidis [b,c], Francesco Nozzoli [c], Alberto Oliva [h], Giuseppe Osteria [l], Francesco Palma [f], Federico Palmonari [g,h], Beatrice Panico [k,l], Stefania Perciballi [d,e], Francesco Perfetto [l], Piergiorgio Picozza [m,f], Michele Pozzato [h], Marco Ricci [n], Ester Ricci [b,c], Sergio Bruno Ricciarini [o], Zouleikha Sahnoun [g,h], Umberto Savino [d,e], Valentina Scotti [k,l], Enrico Serra [c], Alessandro Sotgiu [f], Roberta Sparvoli [m,f], Pietro Ubertini [p], Veronica Vilona [c], Simona Zoffoli [j], Paolo Zuccon [b,c]

Nuclear Instruments and Methods A

Control and read-out of the HEPD-02 tracking system onboard CSES-02 satellite

Simona Bartocci, Roberto Battiston, Stefania Beolè, Franco Benotto, Piero Cipollone, Silvia Coli, Andrea Conti Marco Cristoforetti, Cinzia De Donato, Cristian De Santis, Andrea Di Luca, Floarea Dumitrache, Francesco Maria Follega, Simone Garrafa Botta, Giuseppe Gebbia, Roberto Iuppa, Alessandro Lega, Mauro Lolli, Giusepp Masciantonio, Matteo Mergè, Marco Mese, Riccardo Nicolaidis, Francesco Nozzoli, Alberto Oliva, Giuseppe Osteria, Francesco Palma, Federico Palmonari, Beatrice Panico, Stefania Perciballi, Francesco Perfetto, Piergiorgio Picozza, Michele Pozzato, Ester Ricci, Marco Ricci, Sergio Bruno Ricciarini, Zouleikha Sahnoun, Umberto Savino, Valentina Scotti, Enrico Serra, Alessandro Sotgiu, Roberta Sparvoli, Pietro Ubertini, Veronic Vilona, Simona Zoffoli and Paolo Zuccon

submitted to IEEE Trans. Instr. and Meas.

GEANT4-based detector virtual model for an Astroparticle Physics experiment: the case of the High-Energy Particle Detector onboard the CSES-02 satellite

Simona Bartocci[a], Roberto Battiston[b,c], Stefania Beolè[d,e], Franco Benotto[e], Piero Cipollone[f], Silvia Coli[e], Andrea Contin[g,h], Marco Cristoforetti[i,c], Cinzia De Donato[f], Cristian De Santis[f], Andrea Di Luca[i,c], Floarea Dumitrache[e], Francesco Maria Follega[b,c], Simone Garrafa Botta[e], Giuseppe Gebbia[b,c], Roberto Iuppa[b,c], Alessandro Lega[b,c], Mauro Lolli[h], Giuseppe Masciantonio[f], Matteo Mergè[j], Marco Mese[k,l], Riccardo Nicolaidis[b,c], Francesco Nozzoli[c], Alberto Oliva[h], Giuseppe Osteria[l], Francesco Palma[f], Federico Palmonari[g,h], Beatrice Panico[k,l], Stefania Perciballi[d,e], Francesco Perfetto[l], Piergiorgio Picozza[m,f], Michele Pozzato[h], Marco Ricci[f,n], Ester Ricci[b,c], Sergio Bruno Ricciarini[o], Zouleikha Sahnoun[g,h], Umberto Savino[d,e], Valentina Scotti[k,l], Enrico Serra[c], Alessandro Sotgiu[f], Roberta Sparvoli[m,f], Pietro Ubertini[p], Veronica Vilona[c], Simona Zoffoli[j], Paolo Zuccon[b,c]

submitted to Nuclear Instruments and Methods A

Main paper on EFD-02 published on Space Science Reviews

Space Science Reviews (2025) 221:39
https://doi.org/10.1007/s11214-025-01167-5

SPECIAL COMMUNICATION

Check for updates

Electric Field Detector on Board the CSES-02 Satellite for Characterization of Ionospheric Plasma Dynamics

Piero Diego[1] · Davide Badoni[2] · Cristian De Santis[2] · Emanuele Papini[1] · Alexandra Parmentier[1] · Mirko Piersanti[3,1,2] · Livio Conti[4,1,2] · Gianmaria Rebustini[2] · Roberto Ammendola[2] · Simona Bartocci[2] · Roberto Battiston[5] · Igor Bertello[1] · Piero Cipollone[2] · Giulia D'Angelo[3,1] · Fabrizio De Angelis[1] · Emiliano Fiorenza[1] · Giuseppe Masciantonio[2] · Alfredo Morbidini[1] · Fabrizio Nuccilli[1] · Piergiorgio Picozza[2,6] · Andrea Russi[1] · Alessandro Sotgiu[2] · Roberta Sparvoli[2,6] · Silvia Tofani[7] · Pietro Ubertini[1] · Nello Vertolli[1] · Ugo Zannoni[1] · Simona Zoffoli[8]

Main paper on HEPD-02 in review by Space Science Reviews

The High-Energy Particle Detector on board the CSES-02 satellite

Simona Bartocci[1], Roberto Battiston[2,3], Stefania Beolè[4,5], Franco Benotto[5], Piero Cipollone[6], Silvia Coli[5], Andrea Contin[7,8], Marco Cristoforetti[9,3], Cinzia De Donato[6], Cristian De Santis[6*], Andrea Di Luca[9,3], Flori Dumitrache[5], Francesco Maria Follega[2,3], Simone Garrafa Botta[5], Giuseppe Gebbia[3], Roberto Iuppa[2,3*], Alessandro Lega[9,3], Mauro Lolli[8], Matteo Martucci[6], Giuseppe Masciantonio[6], Matteo Mergè[10], Marco Mese[11,12], Riccardo Nicolaidis[2,3], Francesco Nozzoli[3], Alberto Oliva[8], Giuseppe Osteria[12], Francesco Palma[6], Federico Palmonari[7,8], Beatrice Panico[11,12], Stefania Perciballi[4,5], Francesco Perfetto[12], Alessio Perinelli[2,3], Piergiorgio Picozza[13,6], Michele Pozzato[8], Ester Ricci[2,3], Leonardo Ricci[2,3], Marco Ricci[6,14], Sergio Bruno Ricciarini[15], Zouleikha Sahnoun[7,8], Umberto Savino[4,5], Valentina Scotti[11,12], Enrico Serra[3], Matteo Sorbara[13,6], Alessandro Sotgiu[6], Roberta Sparvoli[13,6], Pietro Ubertini[16], Veronica Vilona[9,3], Simona Zoffoli[10], Paolo Zuccon[2,3]

HEPD-02 tracker in-flight performance

data taken after 08/07/2025 (first reconfiguration)

tuning ALTAI thresholds to optimize module efficiencies

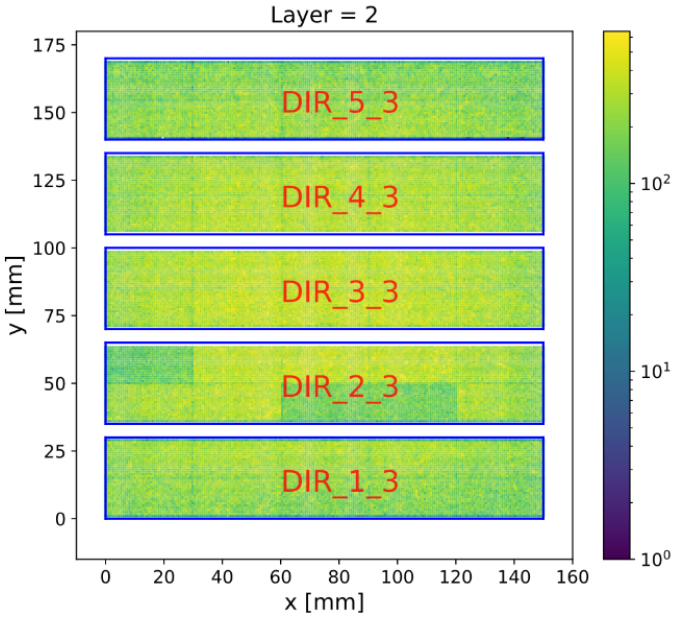

Targeting design performances

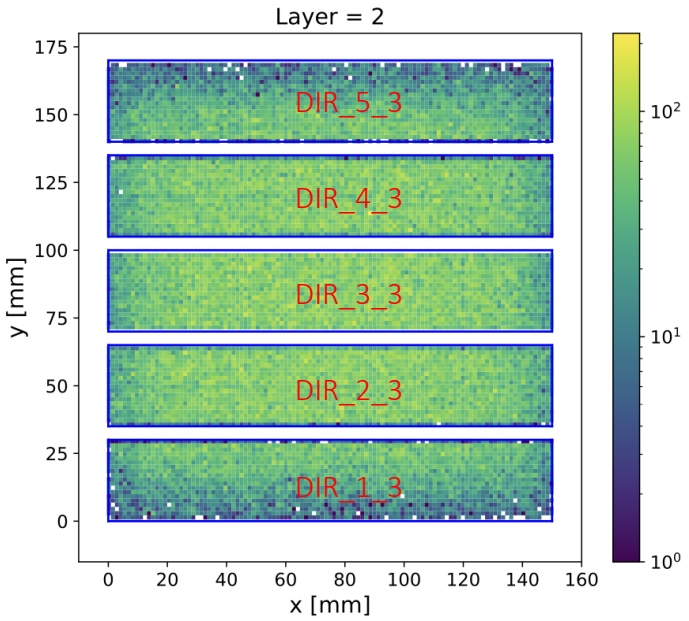

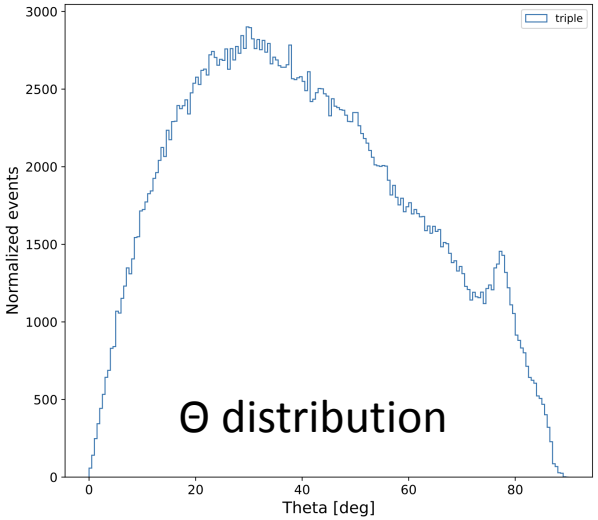

structures due to passive materials, as expected

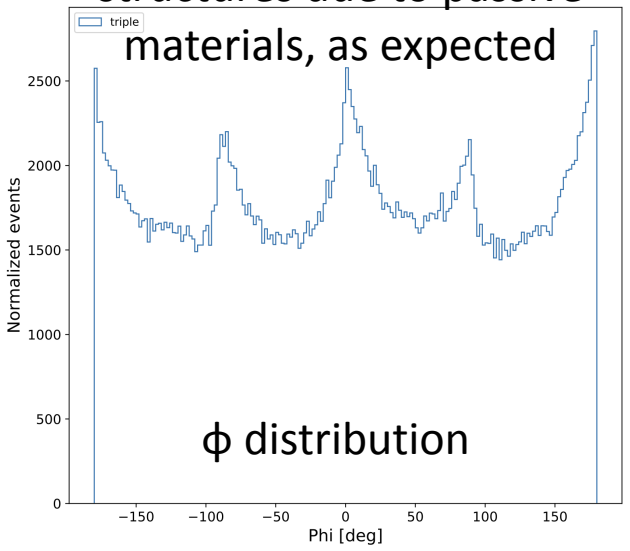

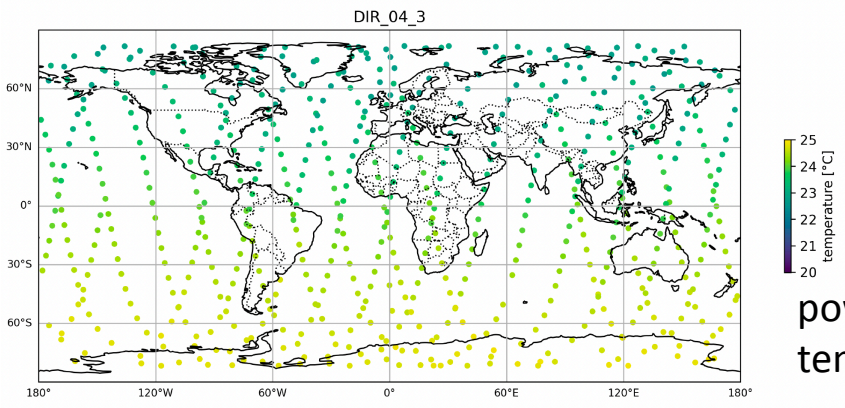

power consumption and operation temperature well under control

HEPD-02 rate maps

Counting rates for all trigger masks are as large as expected or already measured with HEPD-01.
Signatures very sensitive to space weather phenomena.

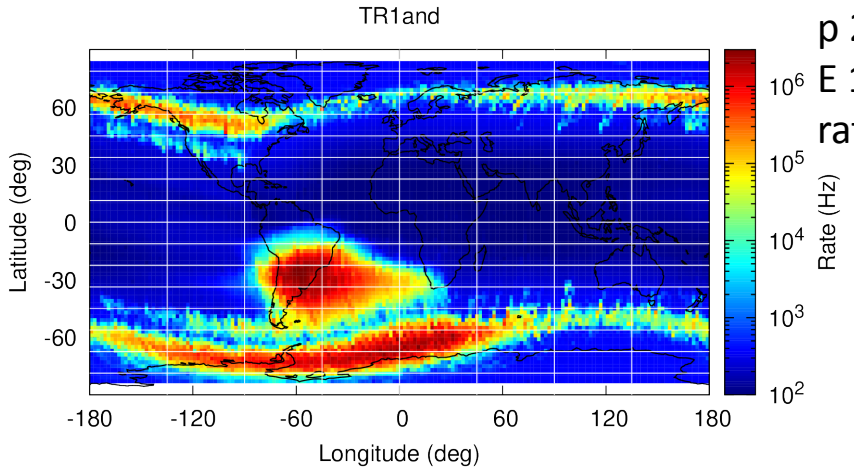

p 20MeV+
E 1MeV+
$rate_{MAX}$=3.2MHz

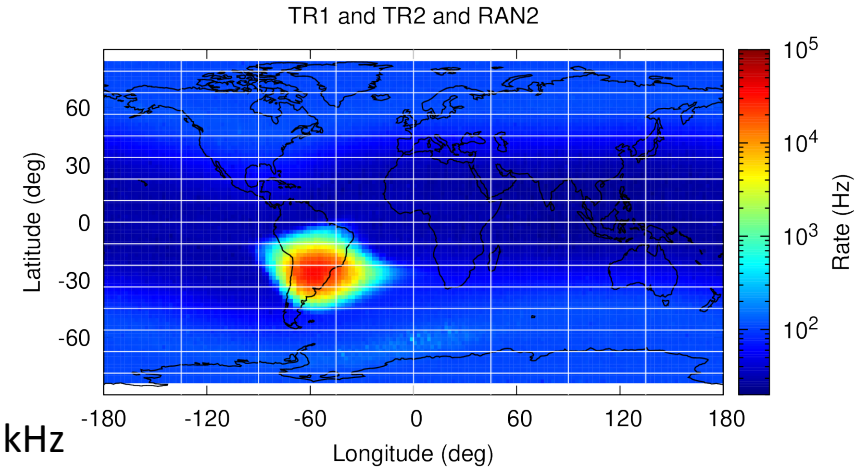

p 80MeV+
E 7.5MeV+
$rate_{MAX}$=33kHz

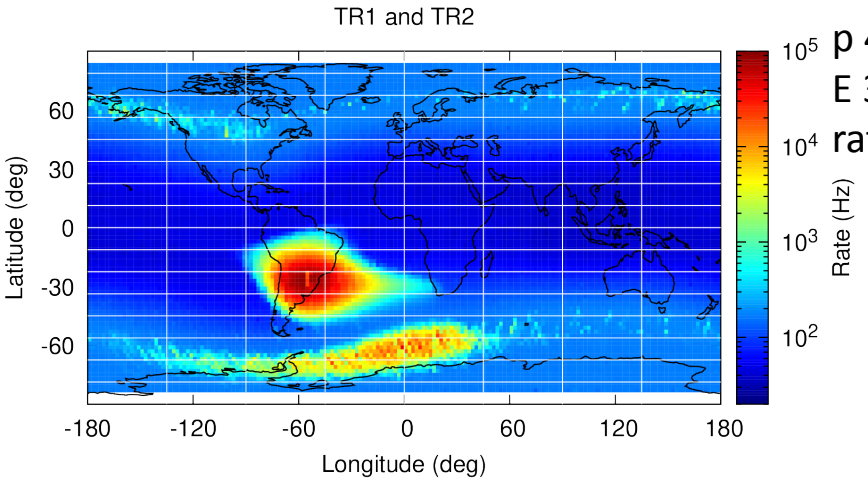

p 40MeV+
E 3.5MeV+
$rate_{MAX}$=100kHz

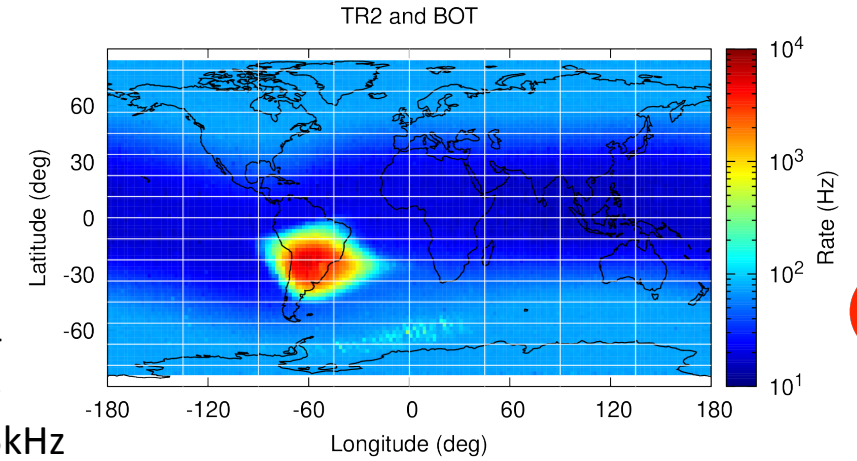

p 250MeV+
E 120MeV+
$rate_{MAX}$=5.5kHz

consistent with HEPD-01 findings

400 asc semi-orbits, from June 20 to July 27

HEPD-02 data: sensitivity to light nuclei

All data collected from June 20th to September 2nd (1,602,652,499 evts)

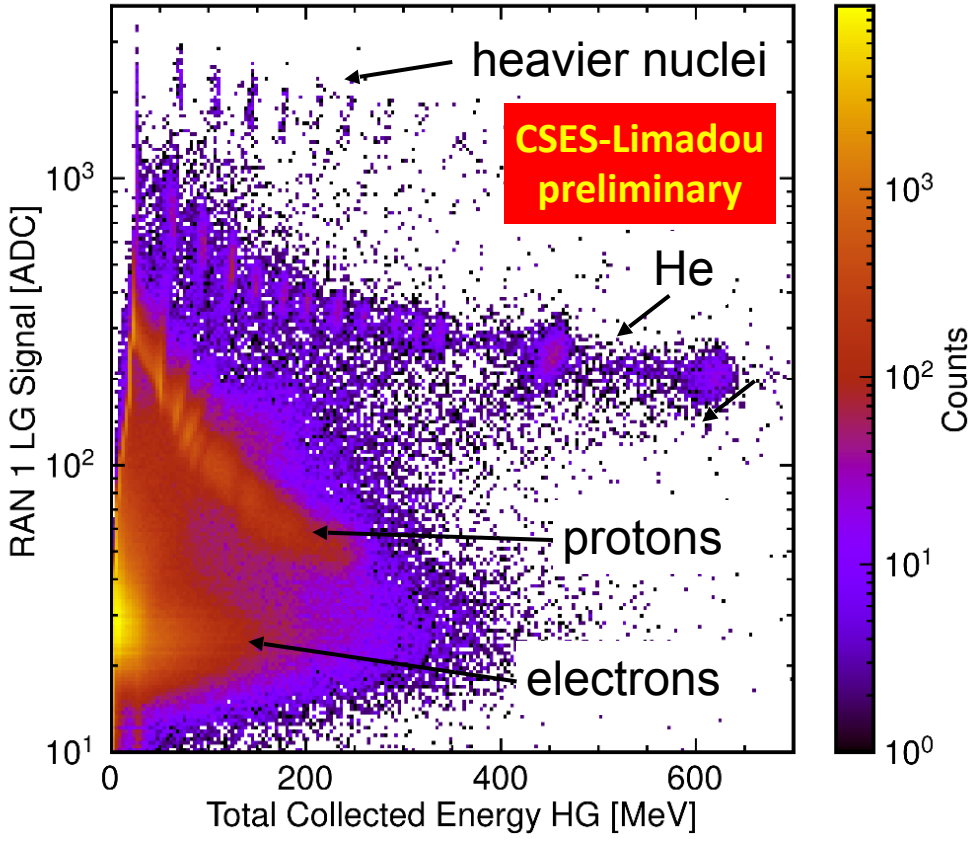

dE/dx representations clearly show e-, p, He and heavier **nuclei**

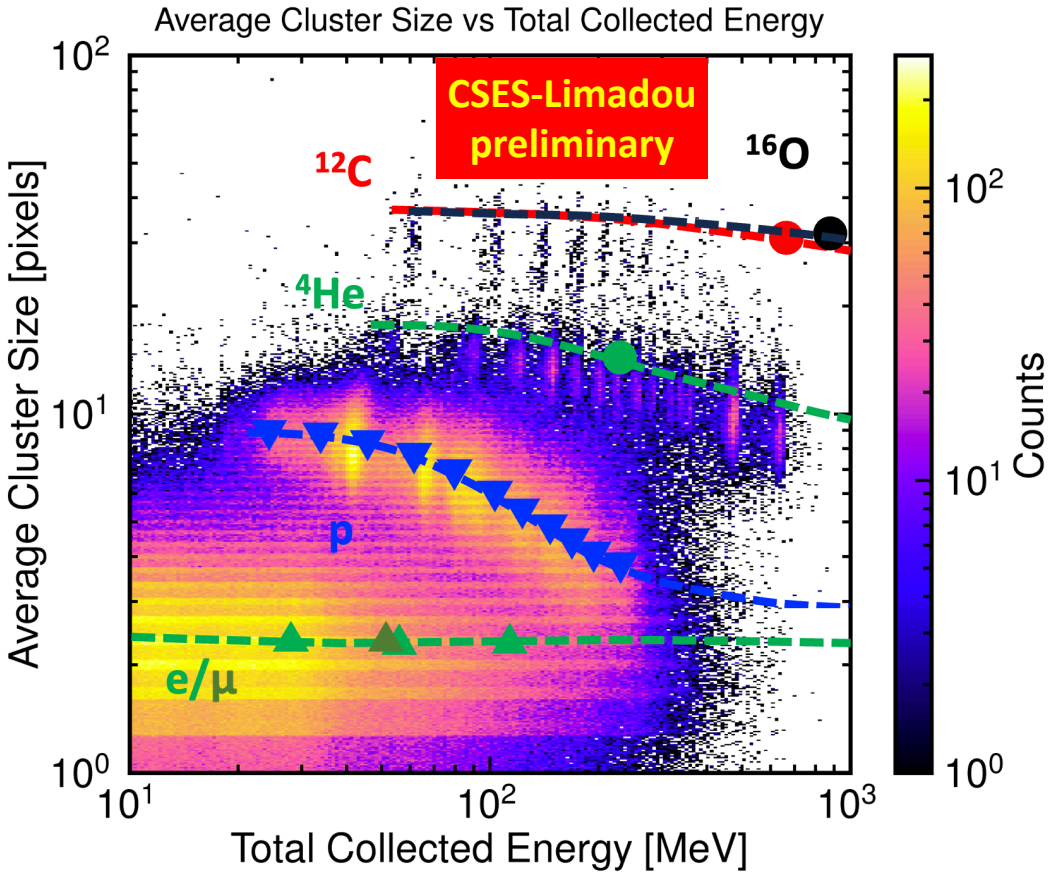

average cluster sizes, calibrated at beam tests, provide **independent information for P.ID.**

Some results in 2024-2025 from CSES-01

A systematic study of SEPs during solar cycle 25

ApJ 974 (October 2024), 2

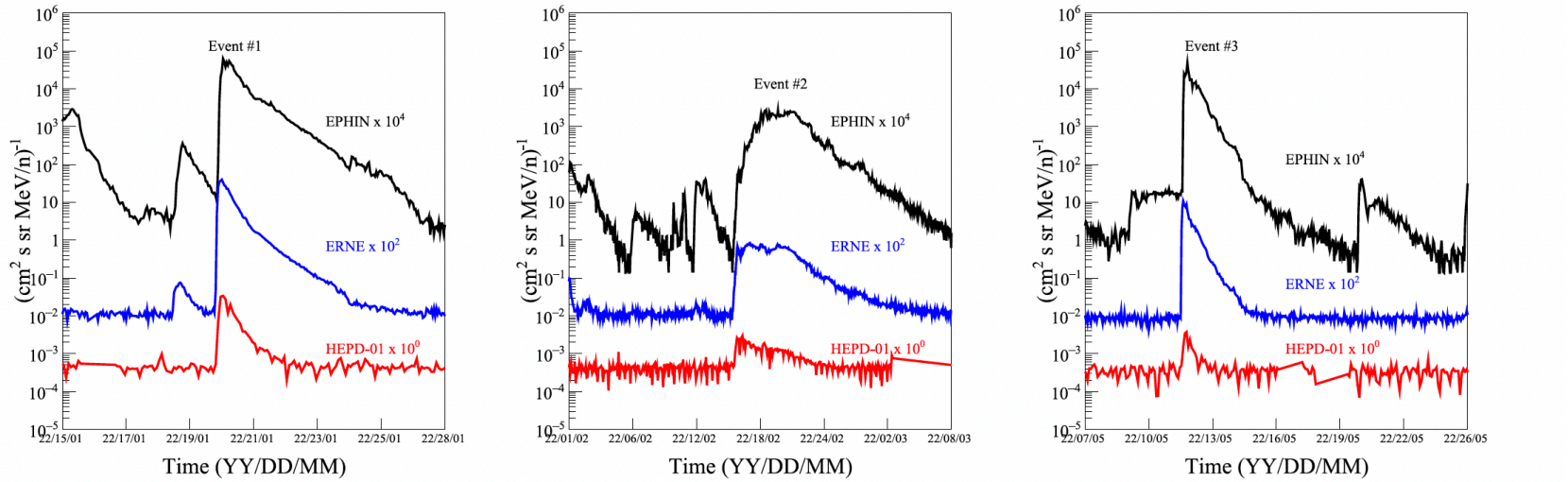

Figure 1. Time profiles of energetic protons of the three SEPs under study. Hourly proton data are a composition of SOHO/EPHIN 4.3–7.8 MeV (black), SOHO/ERNE 40–50 MeV (blue), and HEPD-01 80–90 MeV (red). Note the time extension in the central panel: the time extent of event 2 is larger than the other two.

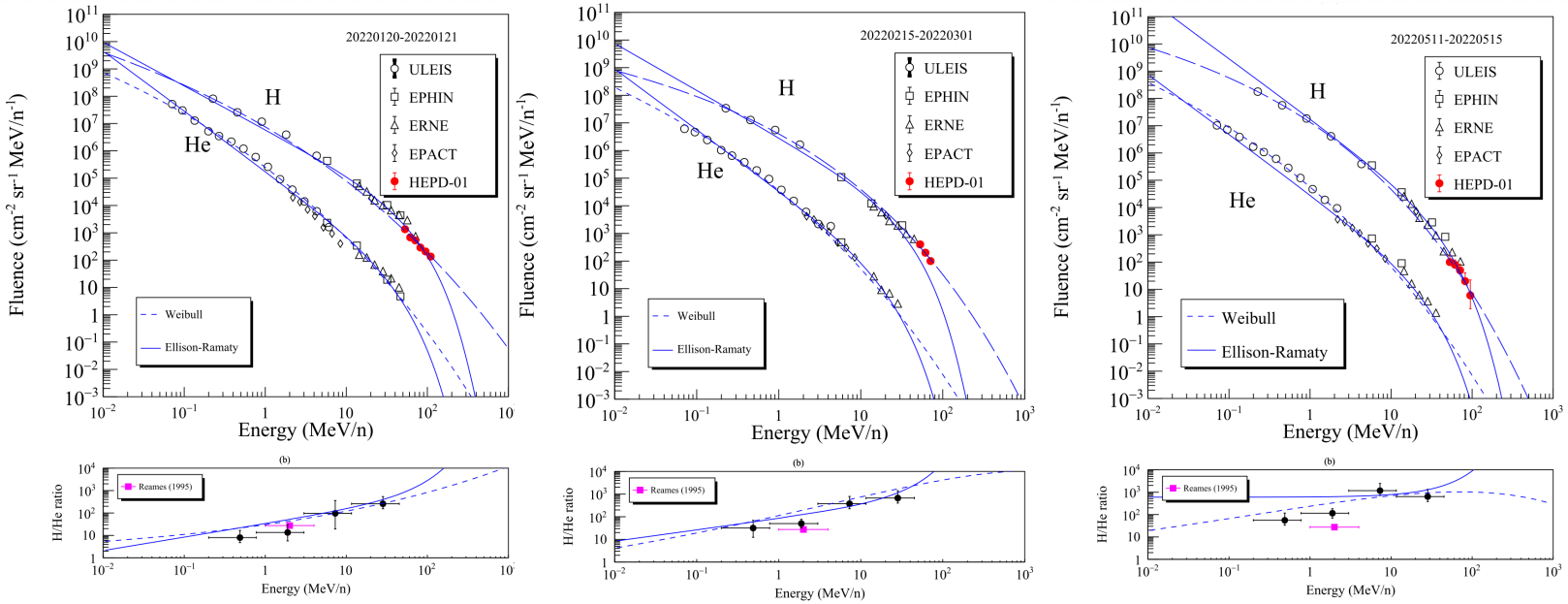

Each SEP spectrum was fitted with Ellison–Ramaty (solid blue line) and Weibull (dashed blue line) functions.
Although the first one seems to reproduce the spectra reasonably well, the **Weibull distribution presents a slightly better reduced χ^2 for all SEPs**, and it adapts to the break at higher energies and the lower portion of the spectra.

Uncertainties too large to significantly discriminate among parametrizations

Ground level enhancements observed with HEPP-L

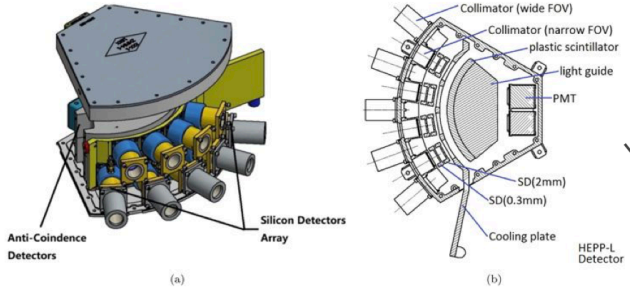

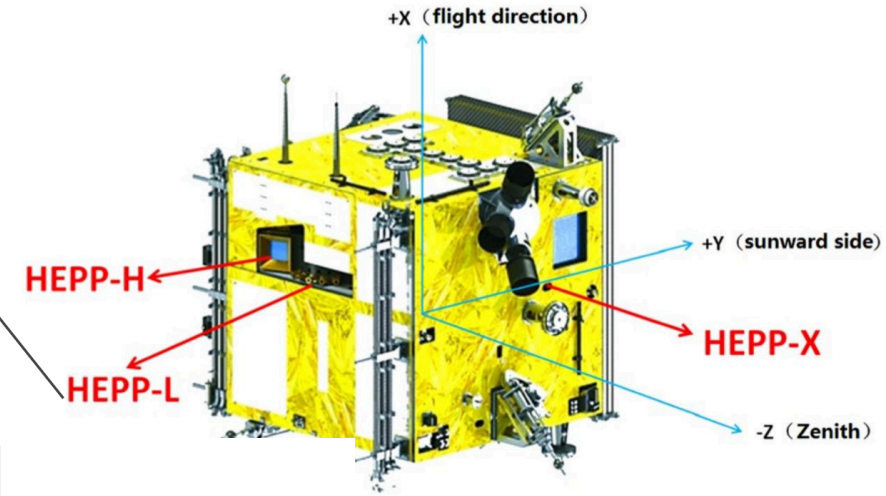

In-depth analysis of selected major solar events with the HEPP-L particle detector onboard CSES-01 in low-Earth orbit

GLE 2021-10-28

in publication

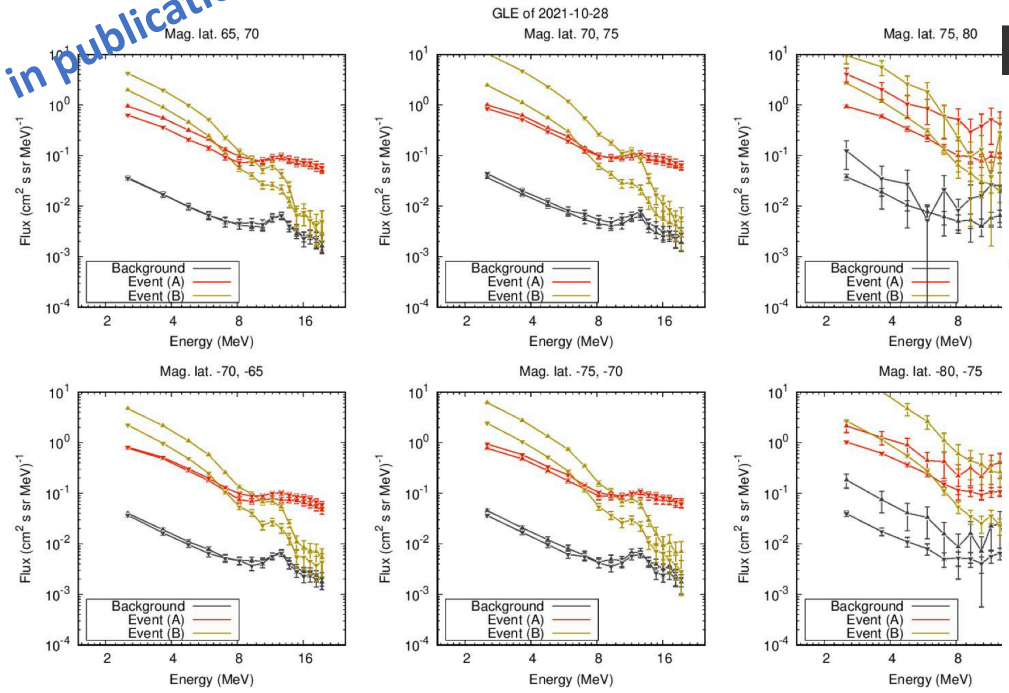

X3.3 flare 2024-02-09

GLE 2024-05-11

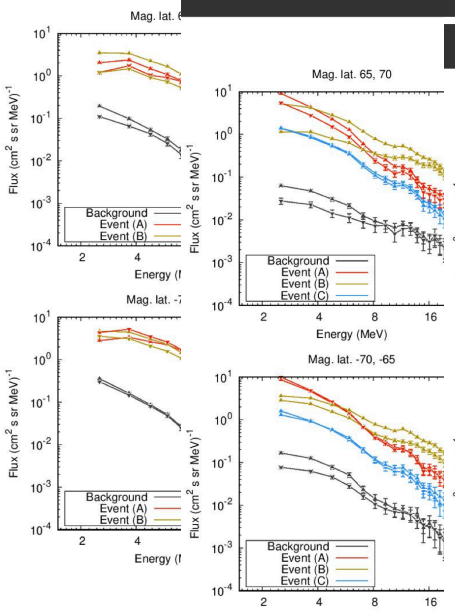

GLE 2024-06-08

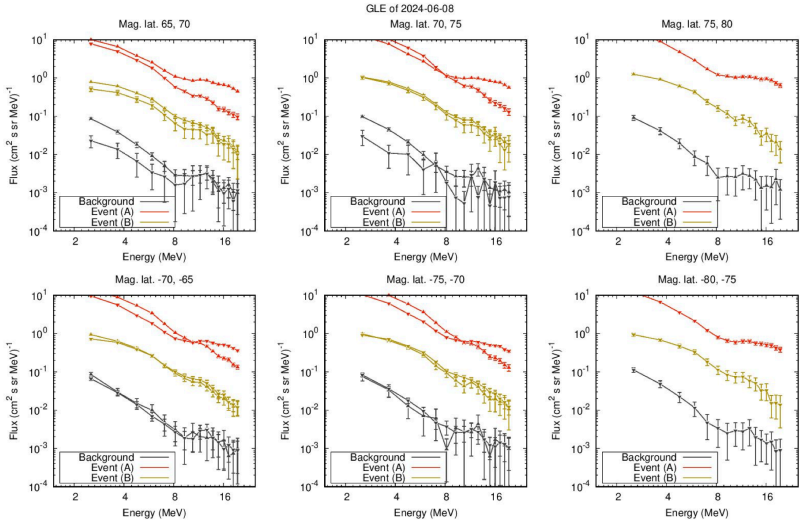

27-day periodicity for GCRs

CSES-HEPD (LEO)

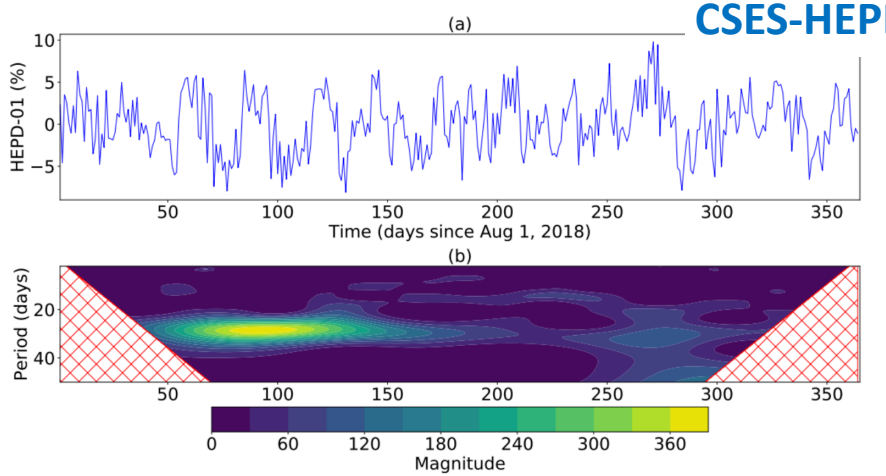

Figure 2. Top: temporal evaluation of the relative (detrended) proton fluxes measured by HEPD-01. Bottom: wavelet analysis of daily HEPD-01 proton flux for the August 2018-August 2019 period; cross-hatched regions on either end indicate the cone of influence where edge effects become important.

SOHO-ERNE (L1)

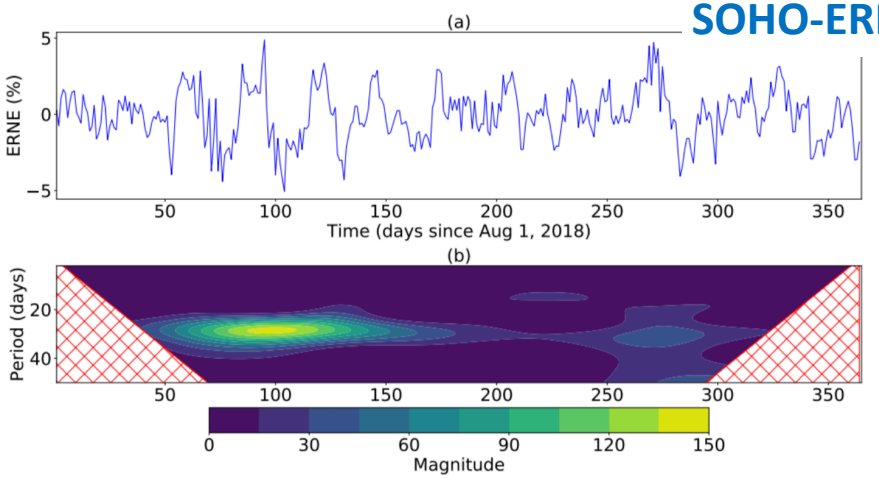

Figure 3. Top: temporal evaluation of the relative (detrended) proton fluxes measured by ERNE. Bottom: wavelet analysis of daily ERNE proton flux for the August 2018-August 2019 period; cross-hatched regions on either end indicate the cone of influence where edge effects become important.

In addition to the long-term solar modulation, Galactic Cosmic-Ray (GCR) intensities exhibit recurrent variations caused by their passage through plasma interaction regions co-rotating with the Sun

CSES-HEPD data combined with measurements of SOHO-ERNE, SOHO-EPHIN and AMS-02

- CSES-HEPD bridging measurements from SOHO (below 0.5 GV) and from AMS-02 (above 1 GV)
- the rigidity dependence of the amplitude of the ~27-day GCR variations cannot be described by a unique power law (spectrum flattening below ~0.8 GV)

The Electric Field Detector 02

The EFD-02 payload

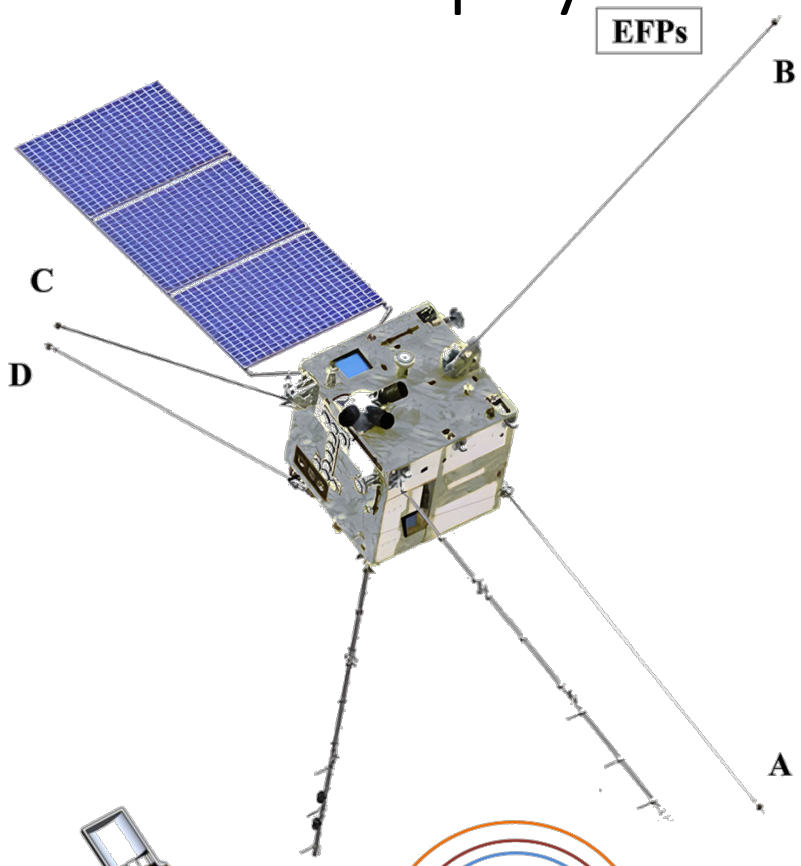

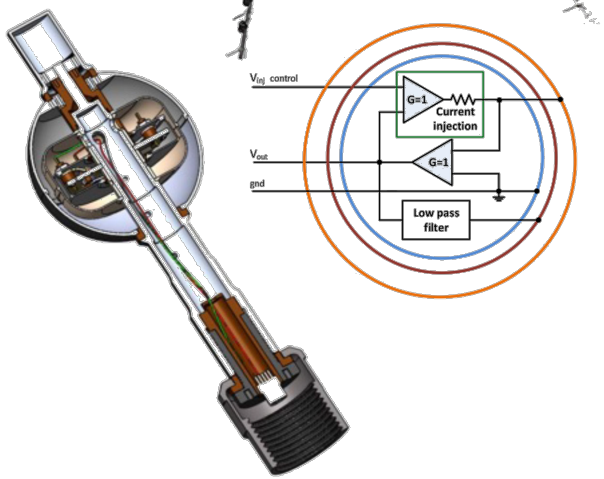

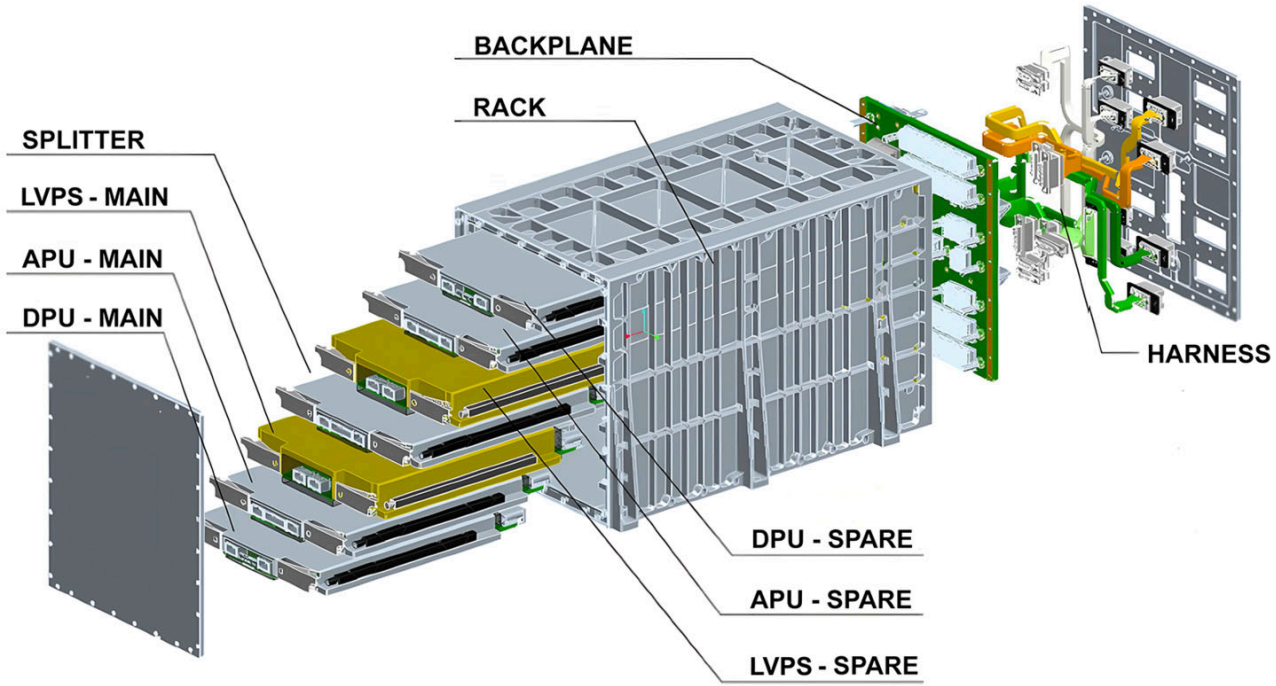

Home > Space Science Reviews > Article

Electric Field Detector on Board the CSES-02 Satellite for Characterization of Ionospheric Plasma Dynamics

Special Communication | Open access | Published: 15 April 2025

Volume 221, article number 39, (2025) Cite this article

Ionospheric current systems – Expected to observe

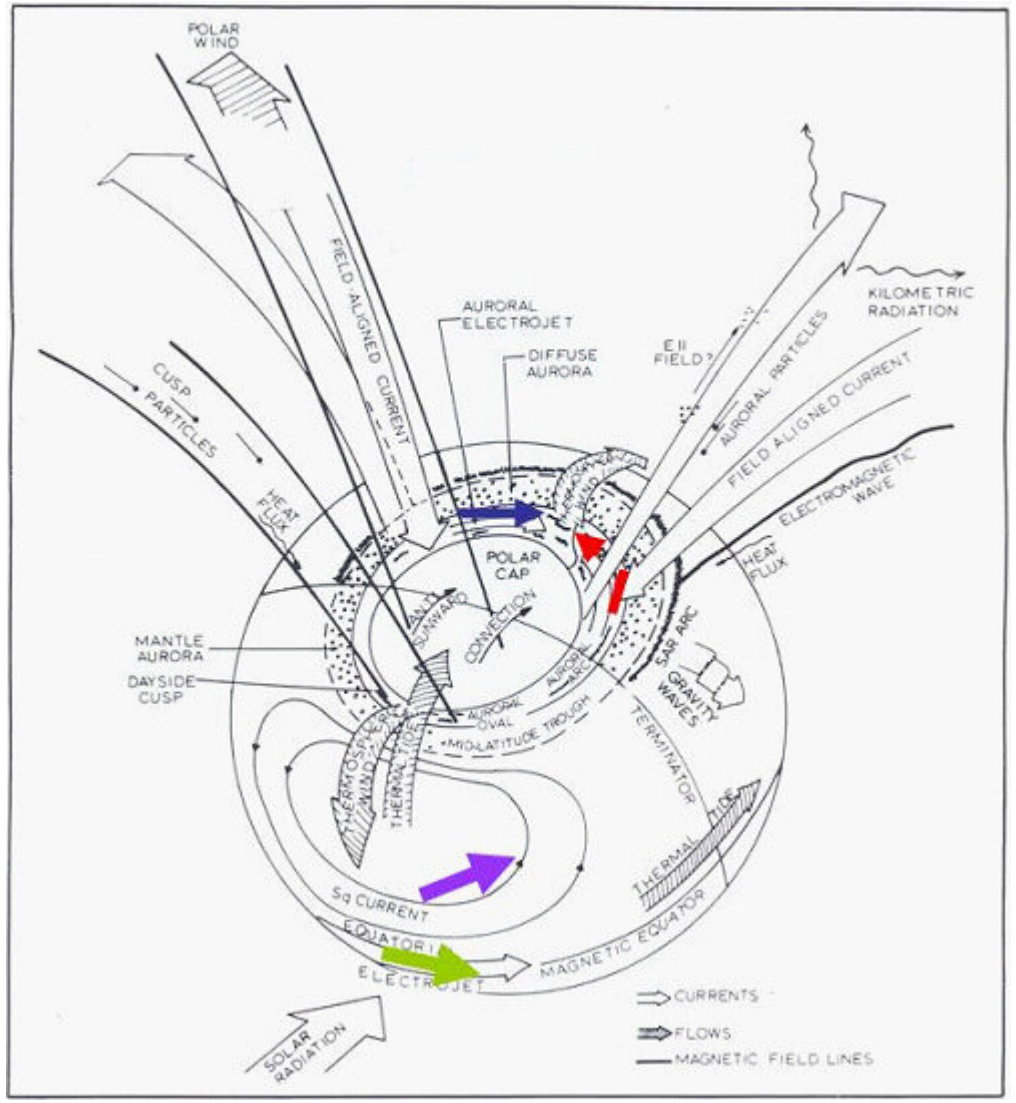

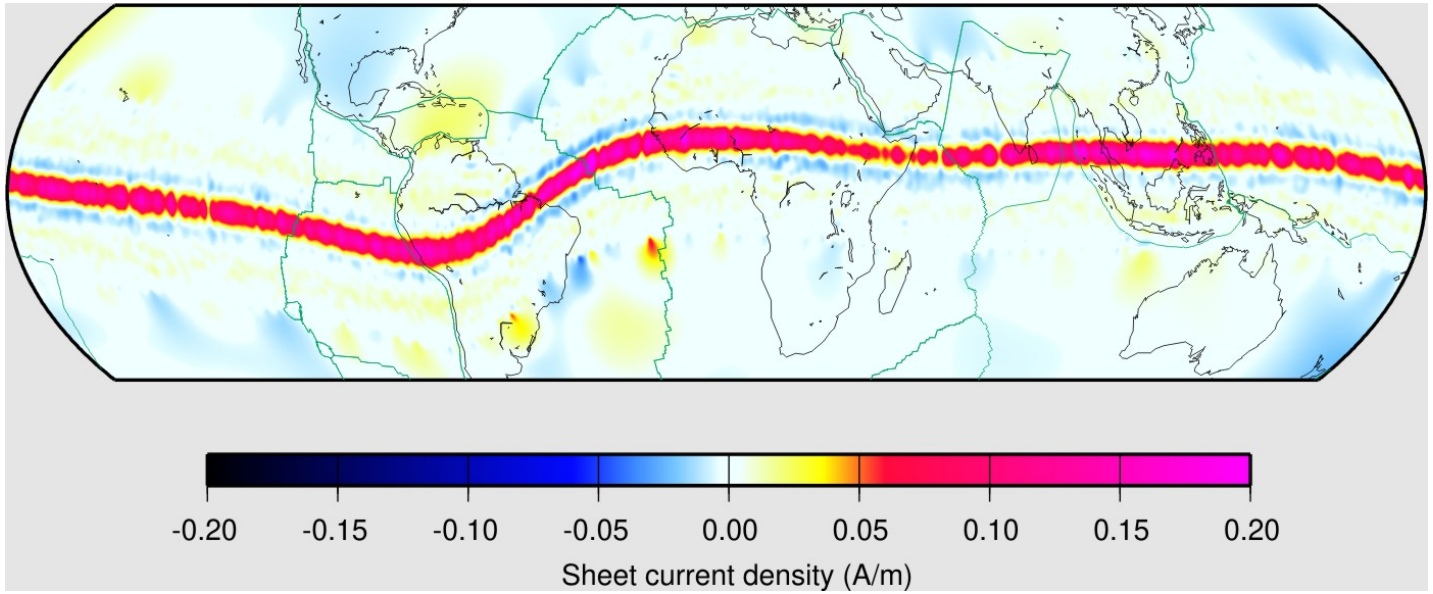

E-ULF and vxB subtraction

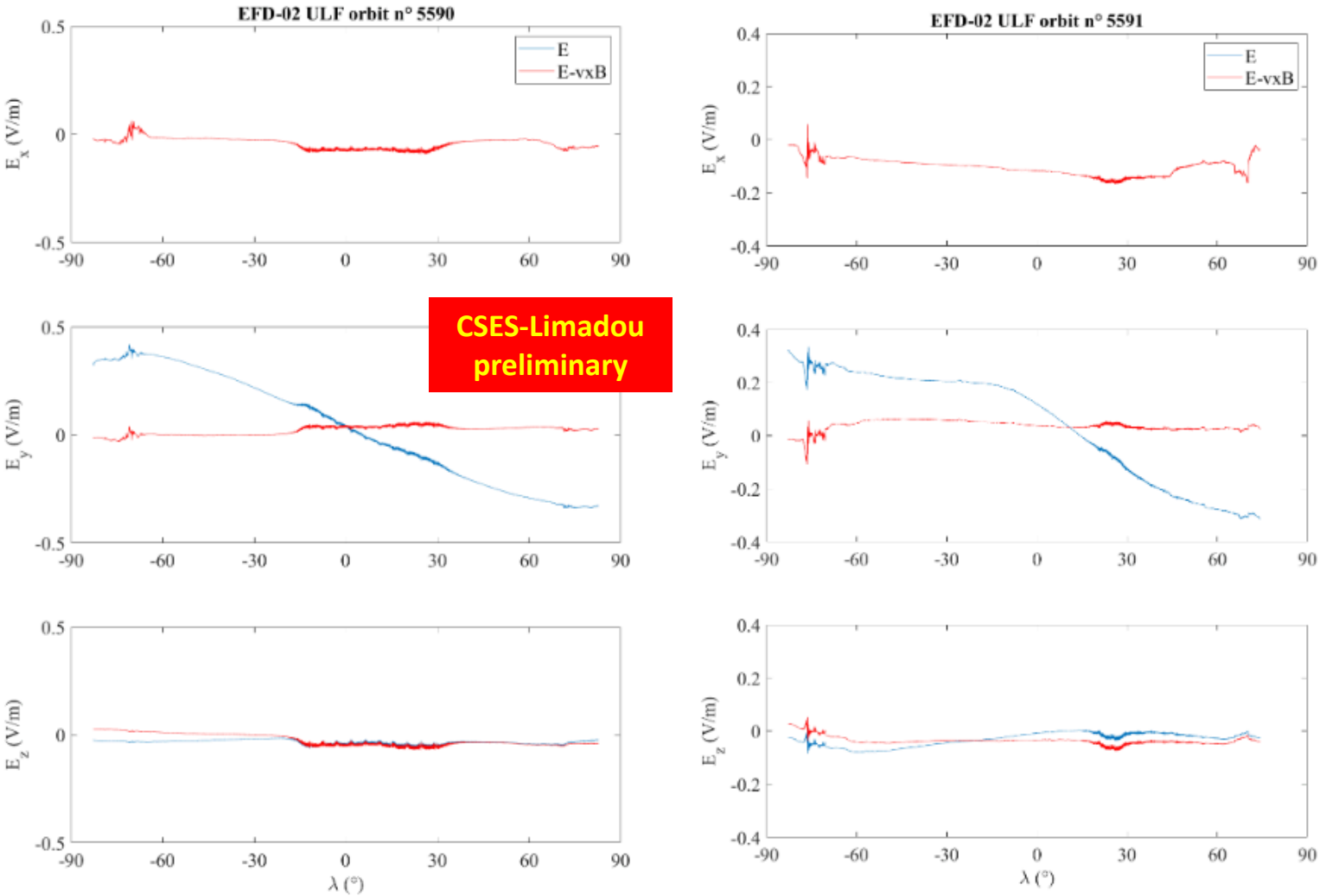

E - ULF

- Electric field resulting from the potentials (blue line) shows latitudinal variations between -0.5 V/m and 0.5 V/m, as expected, generated by vxB;
- Electric field along the ram direction is free from vxB, as expected;
- In polar regions, presence of both positive and negative variations of E is observed, as expected during CSES crossings through R1 and R2 field-aligned currents (FACs);
- In equatorial regions, variations in E are due to the equatorial electrojet.

ELF –Whistlers

- Whistlers* are extremely clean and visually discernible;
- Clean spectrum in which the background signal is evident.

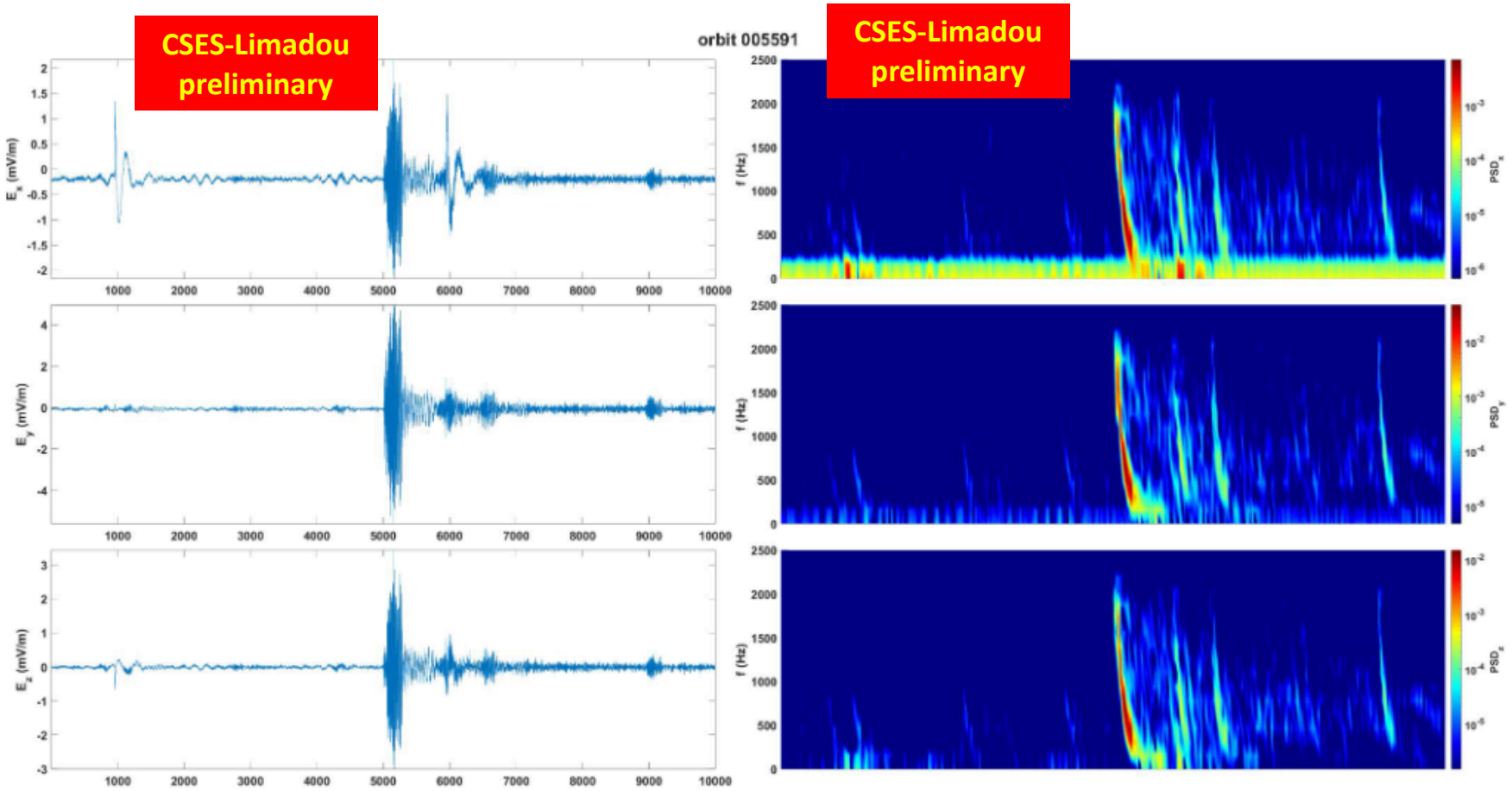

(*) Very-Low-Frequency (VLF) electromagnetic waves generated by lightning that propagate through the ionosphere

EFD02 Response to Geomagnetic Storm

GS of January 19, 2026:
Clear Detection of both Sudden Impulse over Northern America and strong auroral activity during the Main Phase of the storm

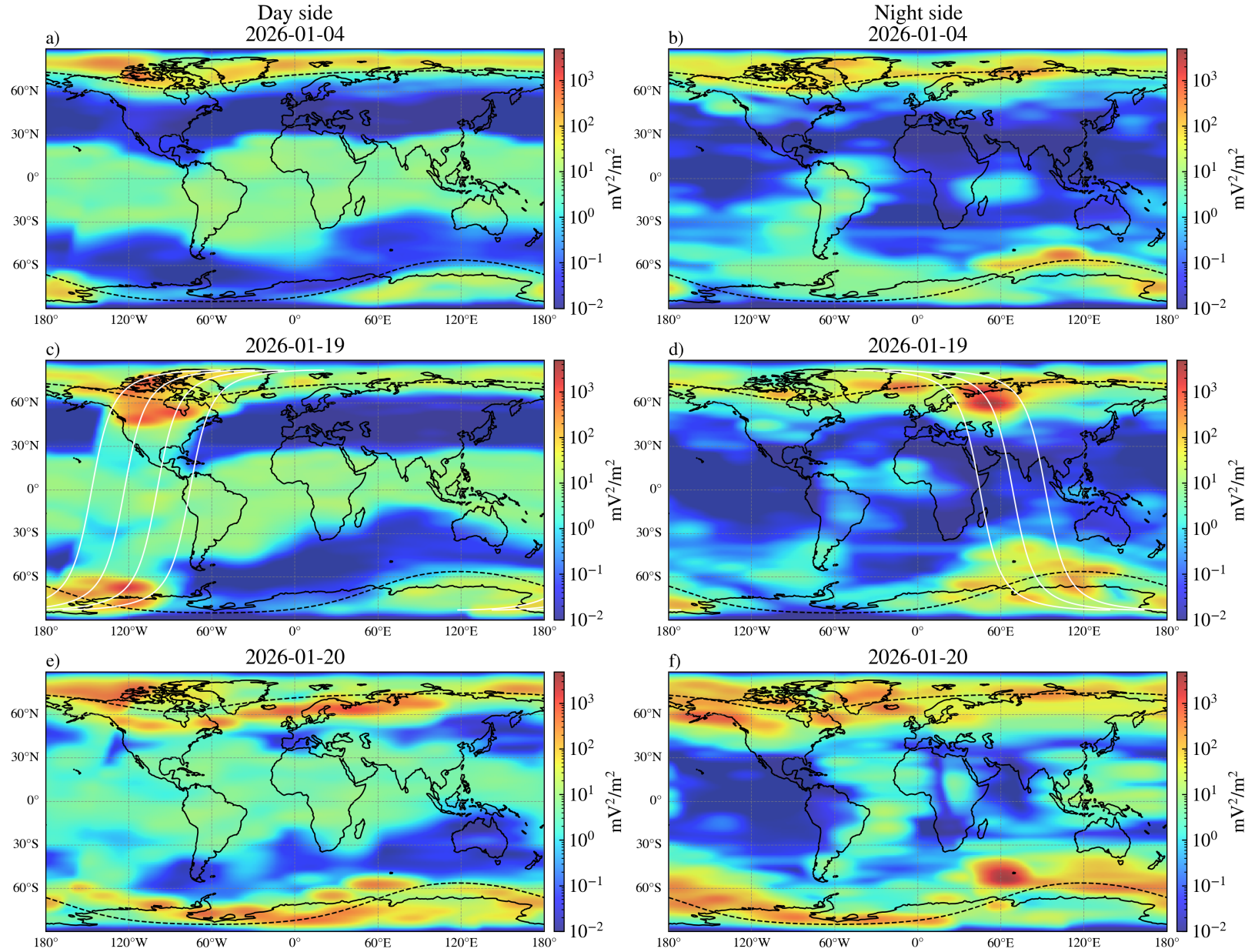

Why it matters for CSES and ionospheric physics

In spaceborne EM data, lightning is a real, strong, and physically informative background.

- Low-altitude E/B measurements must separate meteorological sources, sferics, whistlers, hiss/chorus, and possible geophysical signals from below.

- Lightning also provides a natural tracer of trans-ionospheric wave transport.

- For CSES this is a conceptual calibration slide: what a known, repeatable, strong EM source looks like.

What we measure in E and B

In the topside ionosphere the observation becomes simultaneously electromagnetic, optical, and contextual.

- CSES-01/02 measure wave packets and sferics associated with lightning, with independent confirmation from optical flashes and global lightning networks.

- The useful signature may appear as an electric-field transient, a magnetic perturbation, or a whistler-mode packet in rarefied plasma.

- Timing with lightning occurrence, orbit, altitude, and ionospheric state is crucial for interpretation.

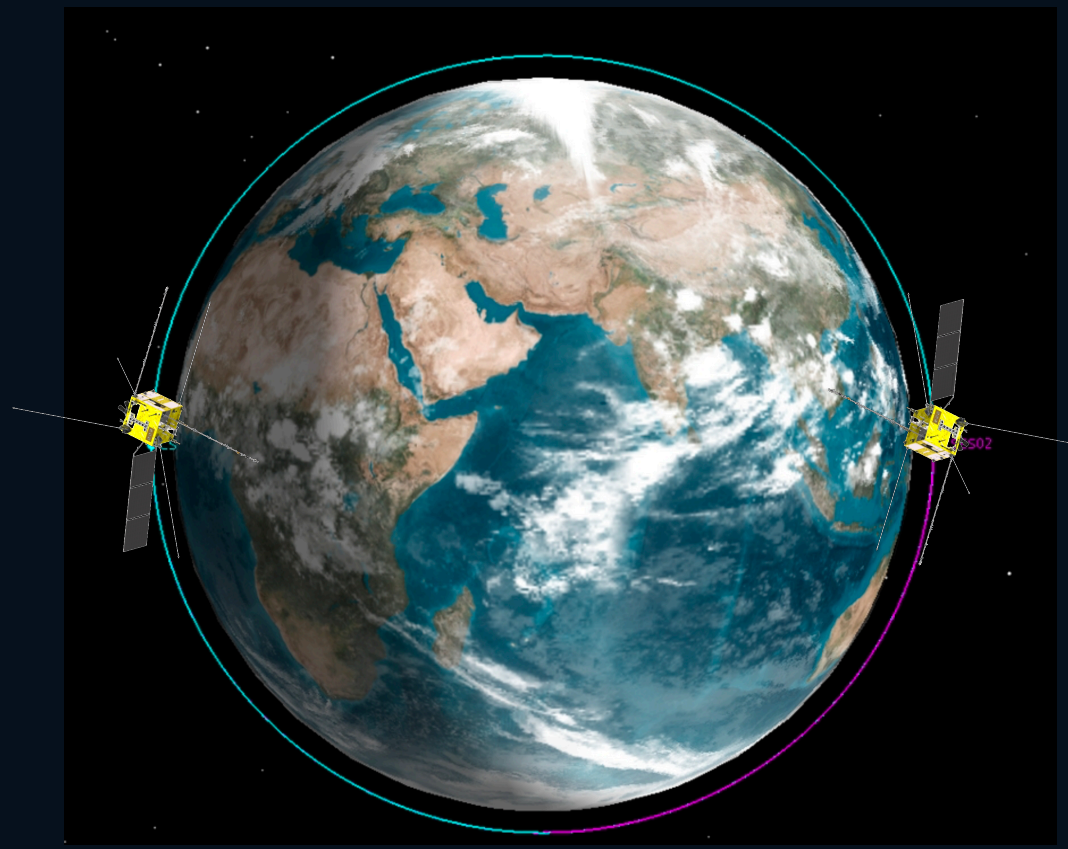

From sferic to whistler

The descending “whistle” is born from plasma dispersion: higher frequencies arrive first.

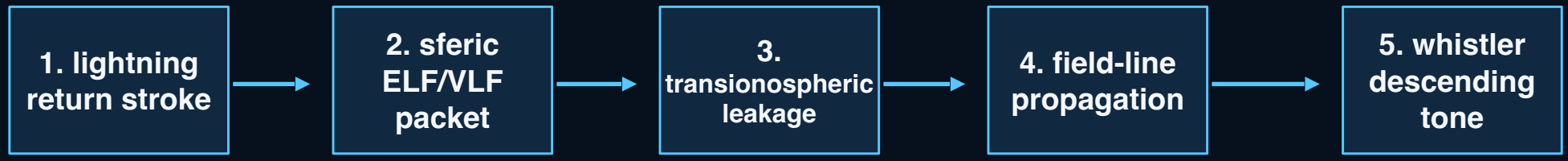

Plasma dispersion orders the frequencies in time: a broadband impulse is reshaped into a falling-pitch whistler.

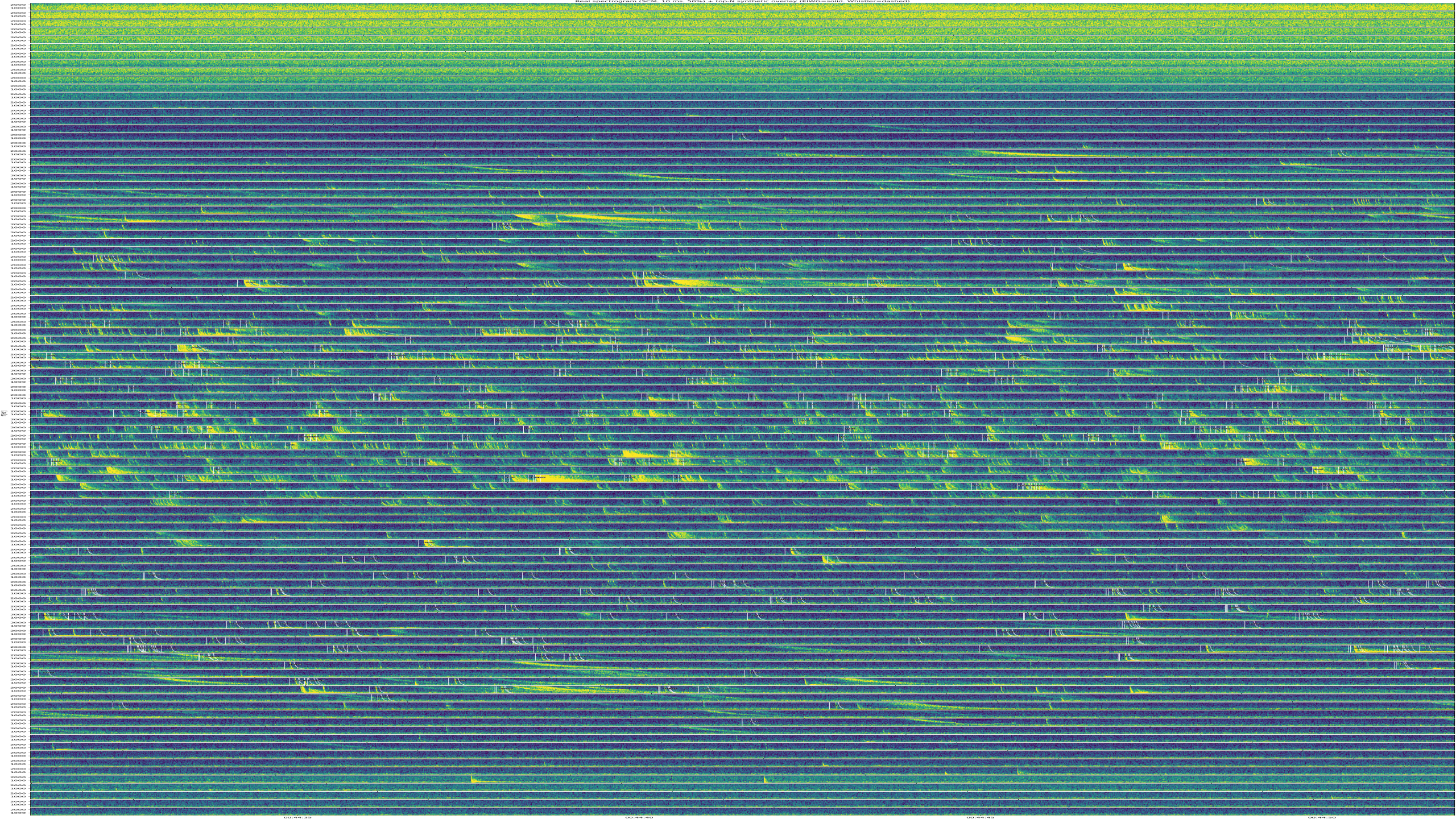
Real spectrogram (SCM, 10 ms, 50%) + top-N synthetic overlay (EIWG=solid, Whistler=dashed)
Hz
00:44:35
00:44:40
00:44:45
00:44:50

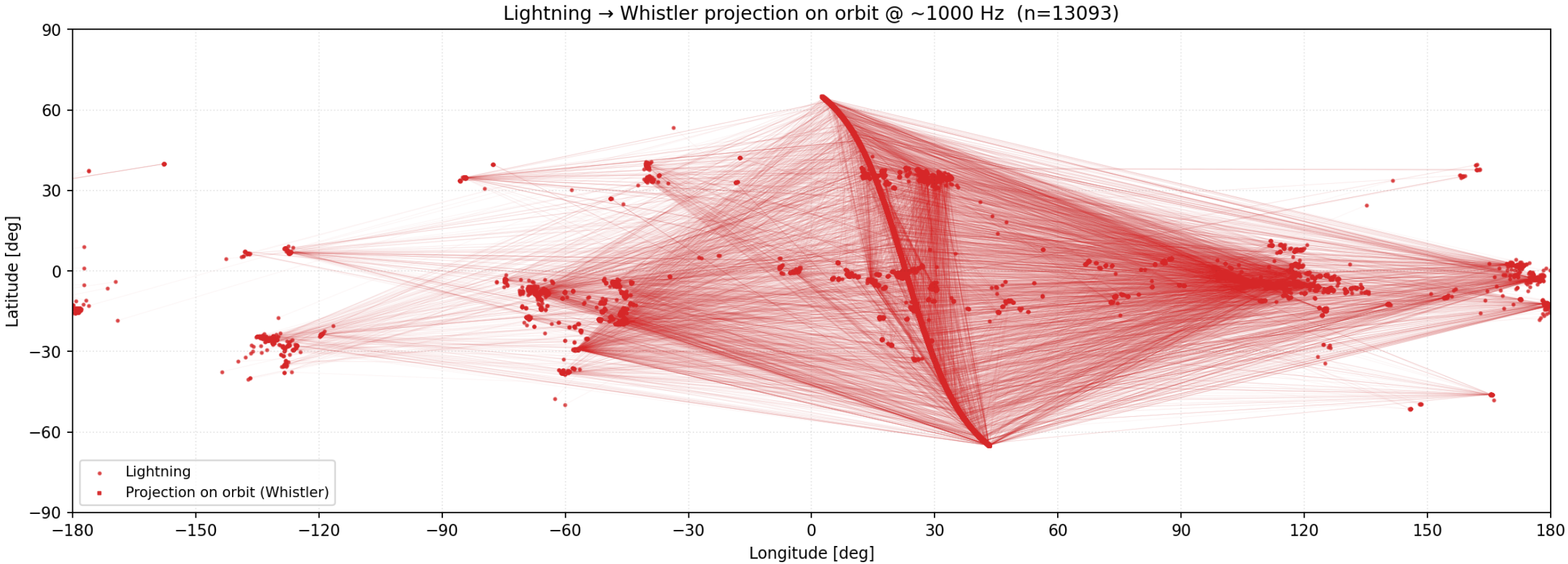
Lightning → Whistler projection on orbit @ ~1000 Hz (n=13093)
Latitude [deg]
Longitude [deg]
90
60
30
0
−30
−60
−90
−180
−150
−120
−90
−60
−30
0
30
60
90
120
150
180
Lightning
Projection on orbit (Whistler)

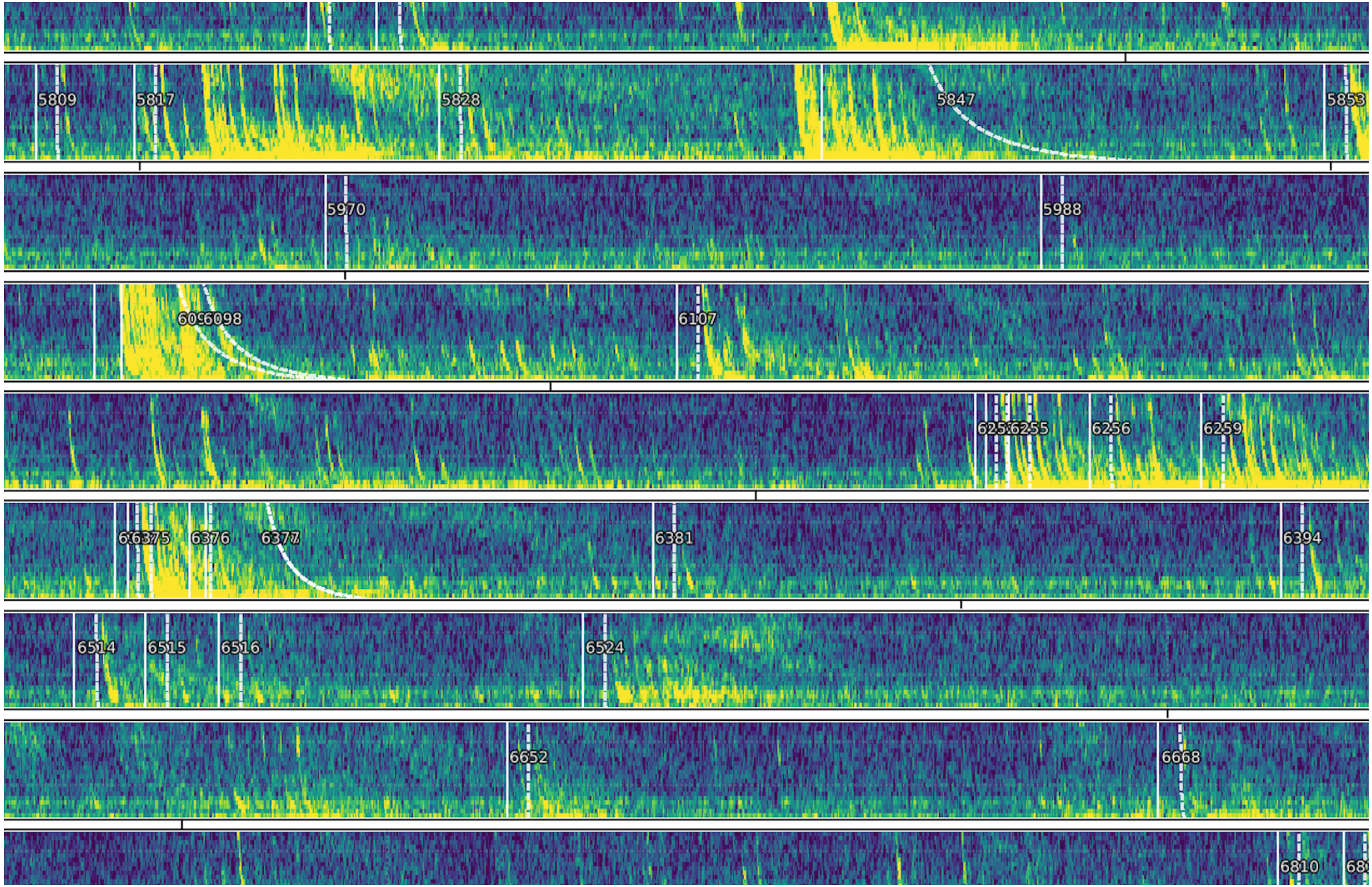
5809
5817
5828
5847
5853
5970
5988
6098
6107
6255
6256
6259
6375
6376
6377
6381
6394
6514
6515
6516
6524
6652
6668
6810

Whistler-mode in Earth's ionosphere and plasmasphere

The emphasis here is the terrestrial plasma environment

- Inside the plasmasphere, whistler-mode waves behave differently than in more tenuous plasma outside it.
- Local density, wave-normal angle, and field-aligned geometry control whether we hear hiss, chorus-like activity, or lightning-born whistlers.
- So hearing a whistler is not enough: we must also ask in which part of Earth's ionosphere–plasmasphere system it propagated.

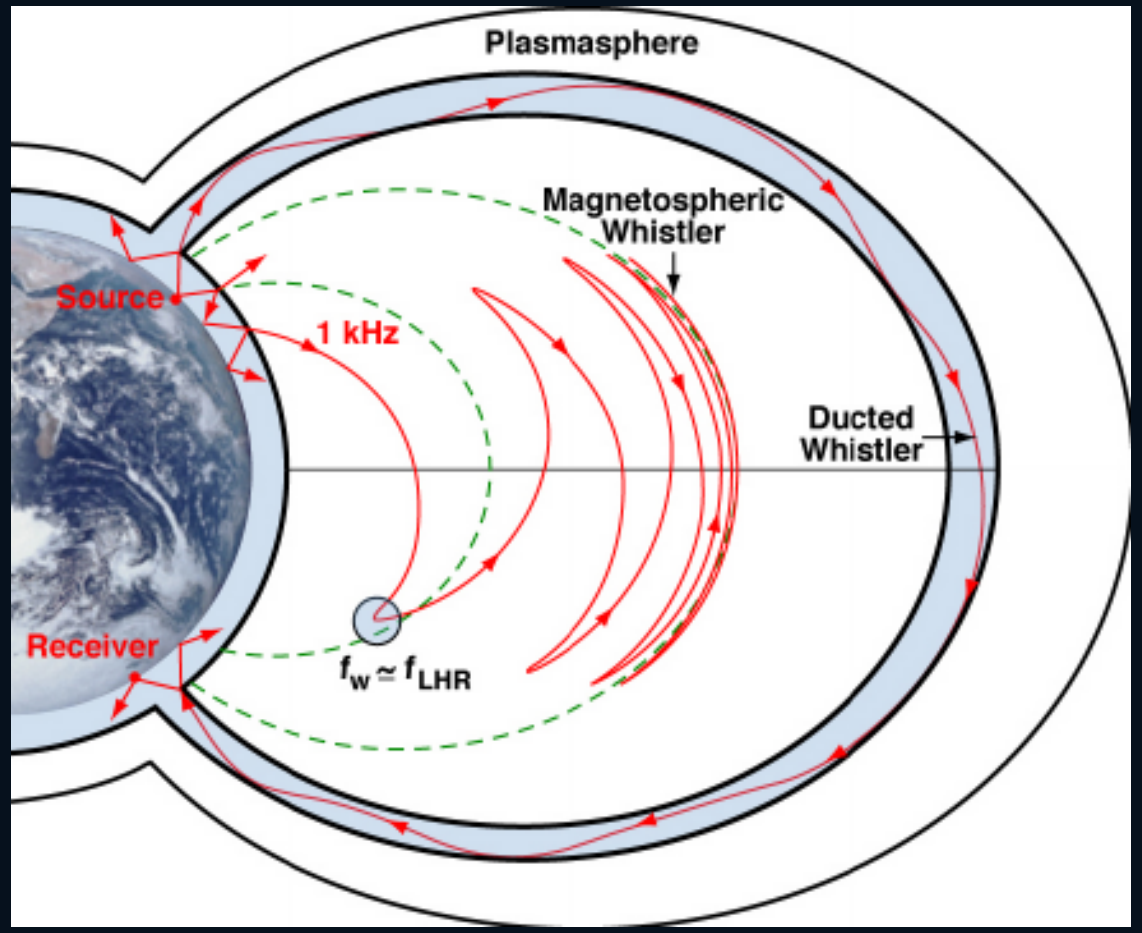

Example of a good event #2: EFD EIWG_ok, fuzzy follow up

```
[EFD-FIT 04:37:41] [PNG] salvato: burst_00054_SCM_EFD.png
```

SCM vs EFD — auto_id=54 Δt_macro=398.2 ms | Δt_fine(curva)=12.00 ms | Δt_fit=nan ms | Δt_total_final=386.16 ms | t0_EFD=1546302736.849s

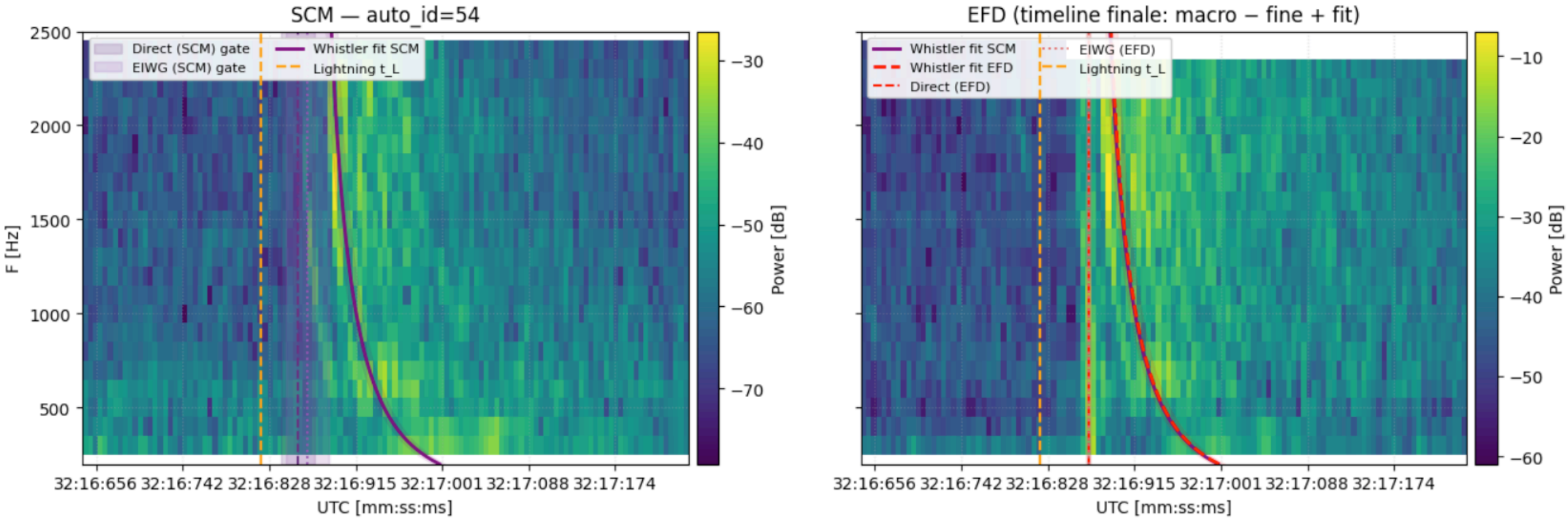

How to tell them apart in data

The difference is not cosmetic: it changes how we infer source, L-shell, and energy transport.

DUCTED

- arrival angles closer to B
- tighter footprint
- often stronger focusing / amplitude
- sensitivity to ducts / irregularities

NON-DUCTED

- more oblique ray paths
- interpretation depends more strongly on refraction model
- broader footprint
- easier source–path ambiguity

useful observables:
WNA · dispersion · polarization · timing · multi-station direction finding

Why the distinction matters ?

Without propagation physics, an E/B measurement remains ambiguous: it can say “there is a wave,” but not yet “where it came from.”

- Propagation geometry determines the source → satellite → magnetic-footprint mapping.
- It affects how we interpret whistlers, chorus, hiss, and lightning- or transmitter-induced backgrounds.
- It is essential if we want to move from anomaly hunting to quantitative EM transport physics in near-Earth plasma.

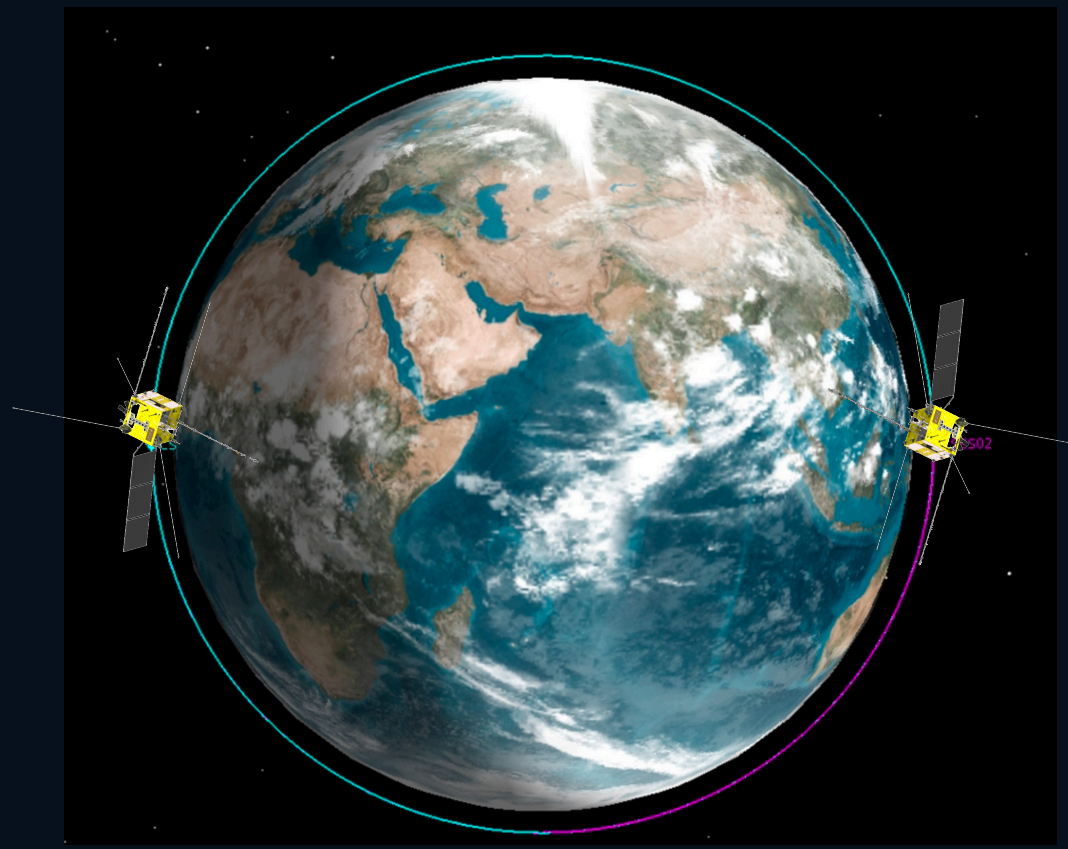

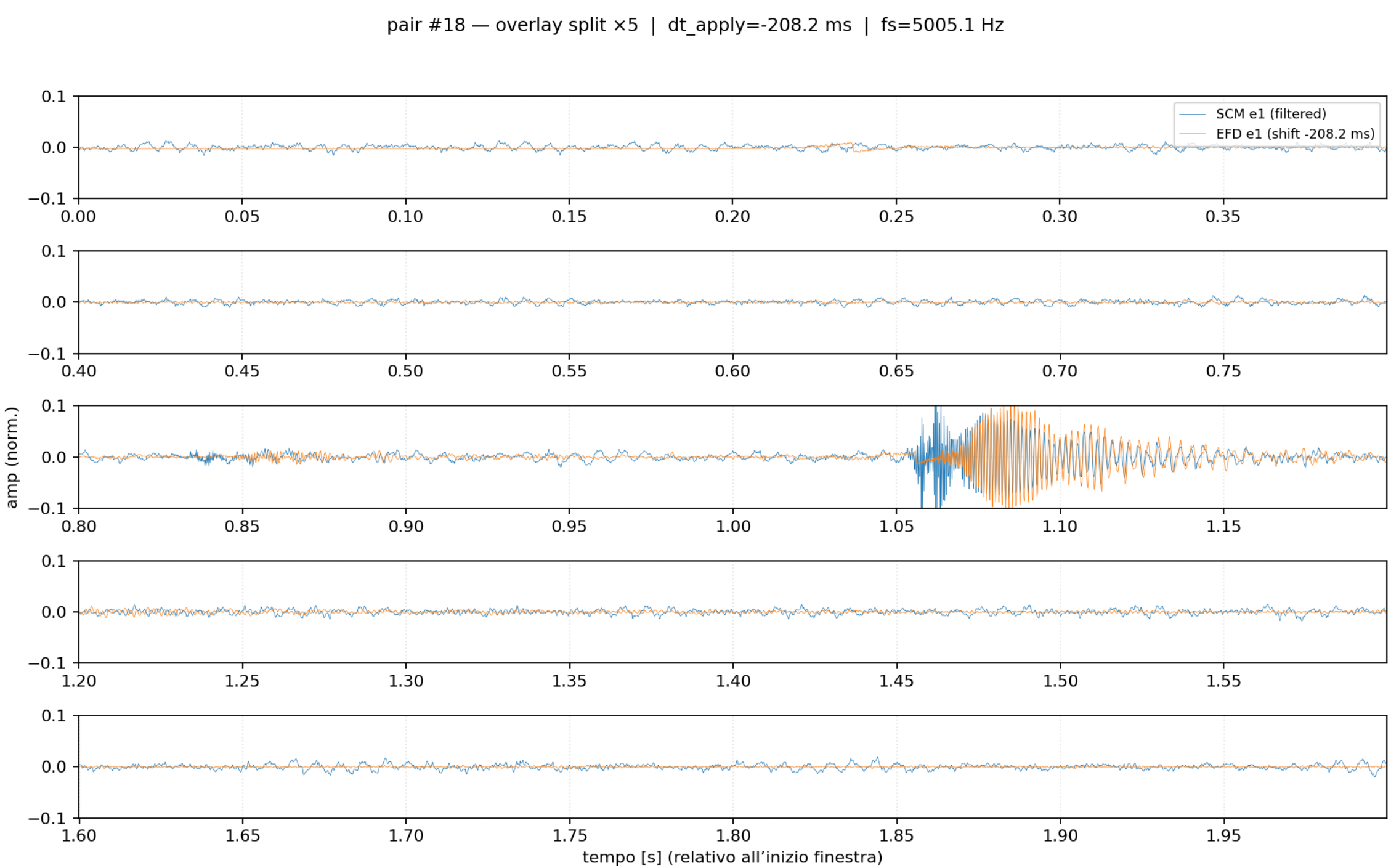
pair #18 — overlay split ×5 | dt_apply=-208.2 ms | fs=5005.1 Hz
SCM e1 (filtered)
EFD e1 (shift -208.2 ms)
amp (norm.)
tempo [s] (relativo all’inizio finestra)

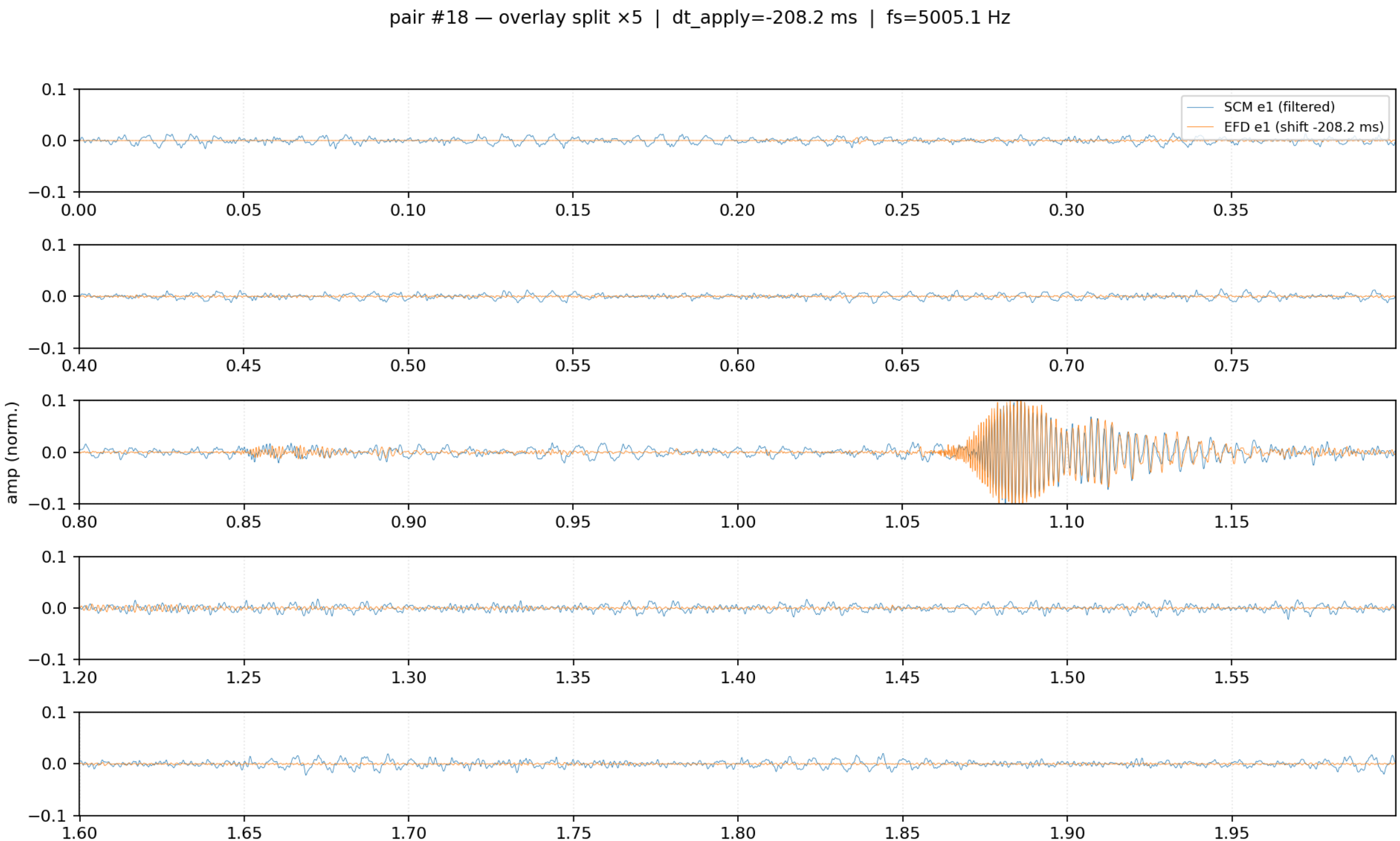
pair #18 — overlay split ×5 | dt_apply=-208.2 ms | fs=5005.1 Hz
SCM e1 (filtered)
EFD e1 (shift -208.2 ms)
amp (norm.)
0.1
0.0
−0.1
0.00
0.05
0.10
0.15
0.20
0.25
0.30
0.35
0.40
0.45
0.50
0.55
0.60
0.65
0.70
0.75
0.80
0.85
0.90
0.95
1.00
1.05
1.10
1.15
1.20
1.25
1.30
1.35
1.40
1.45
1.50
1.55
1.60
1.65
1.70
1.75
1.80
1.85
1.90
1.95

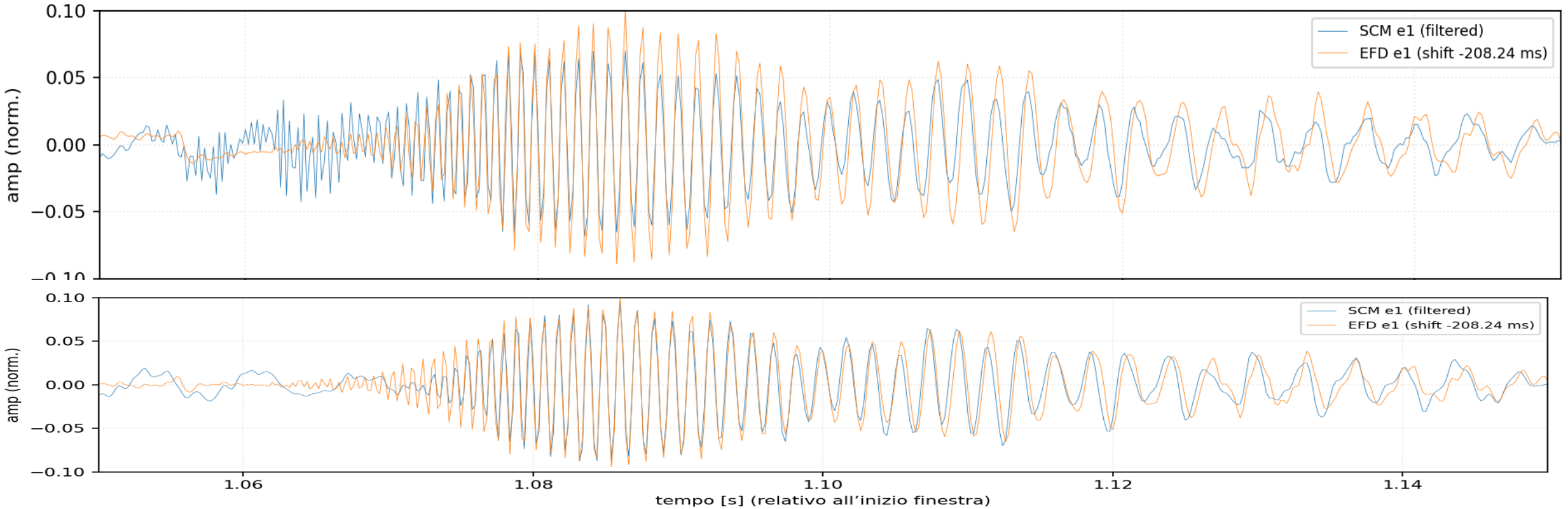
SCM e1 (filtered)
EFD e1 (shift -208.24 ms)
amp (norm.)
0.10
0.05
0.00
−0.05
−0.10
1.06
1.08
1.10
1.12
1.14
tempo [s] (relativo all'inizio finestra)

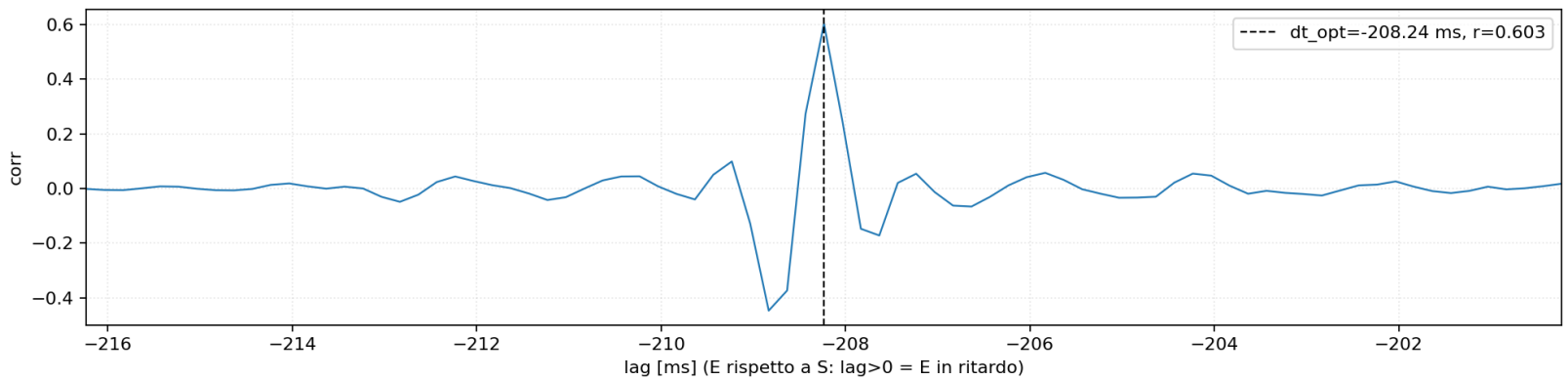
dt_opt=-208.24 ms, r=0.603
corr
0.6
0.4
0.2
0.0
−0.2
−0.4
−216
−214
−212
−210
−208
−206
−204
−202
lag [ms] (E rispetto a S: lag>0 = E in ritardo)

Photons as you have never seen them !

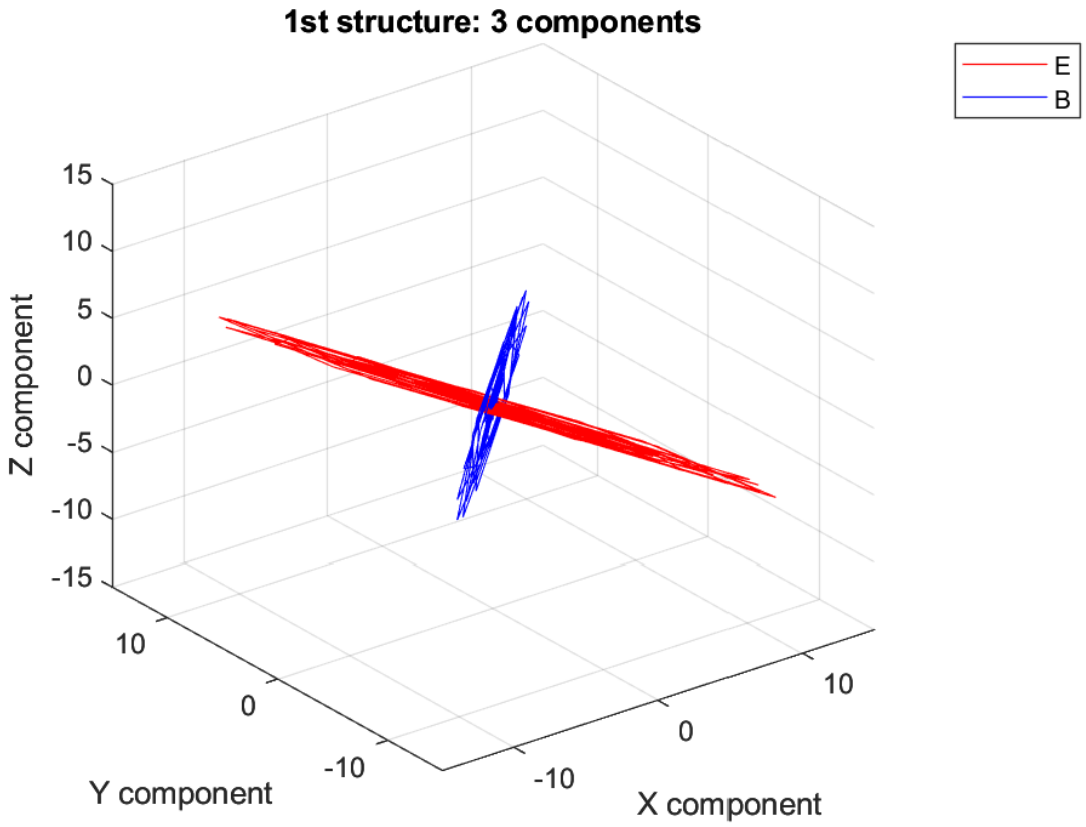

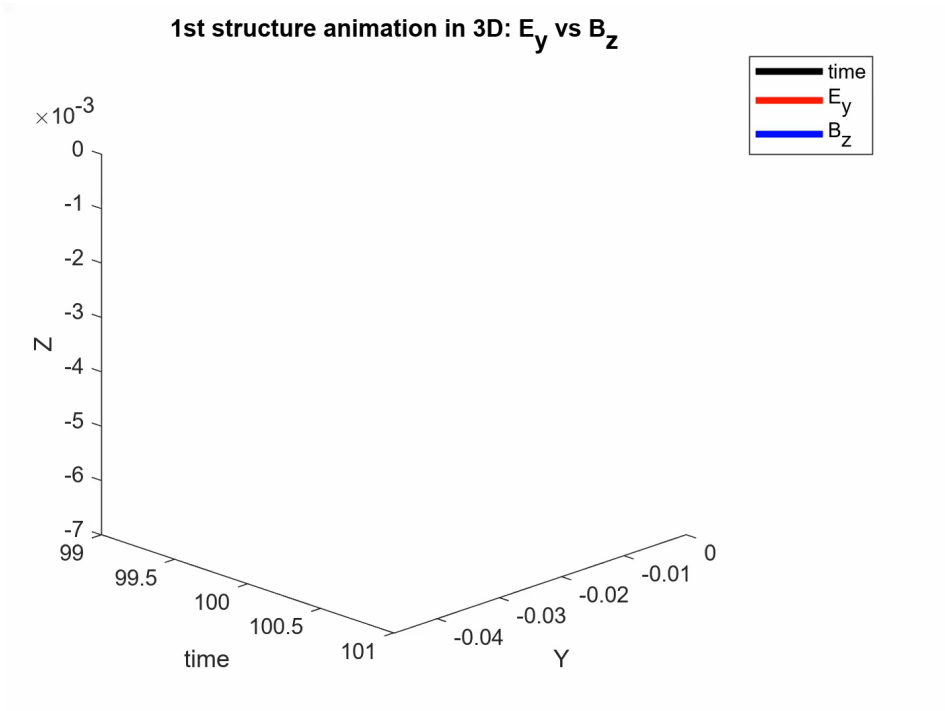

TGF, ligthning and associated particle precipitation

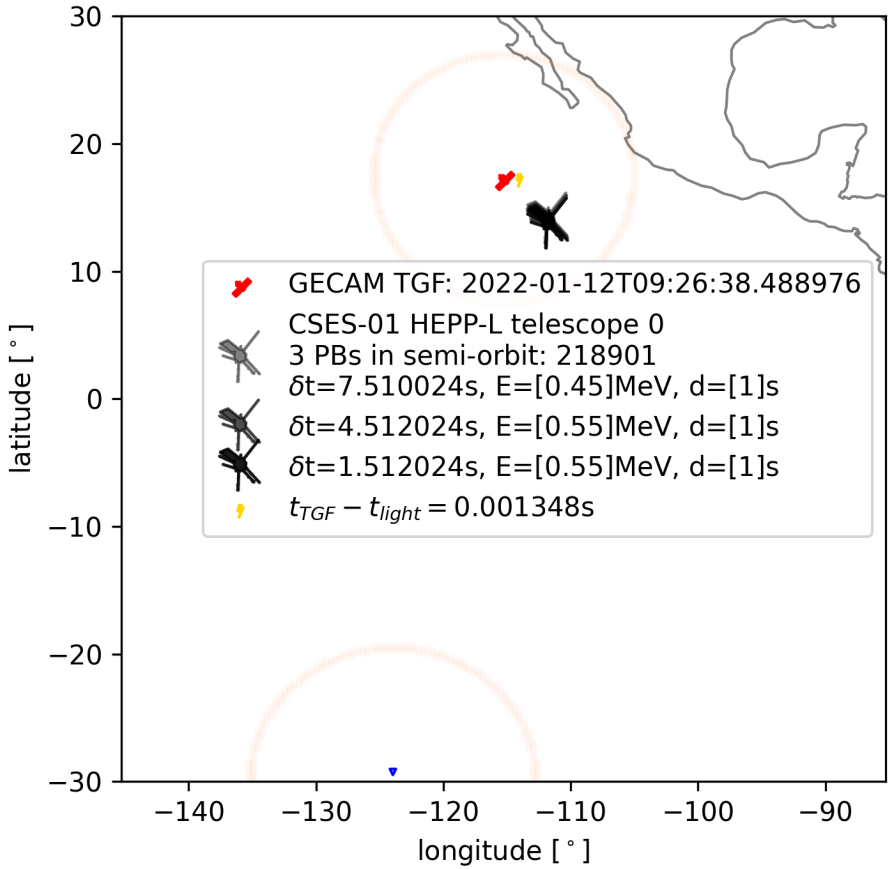

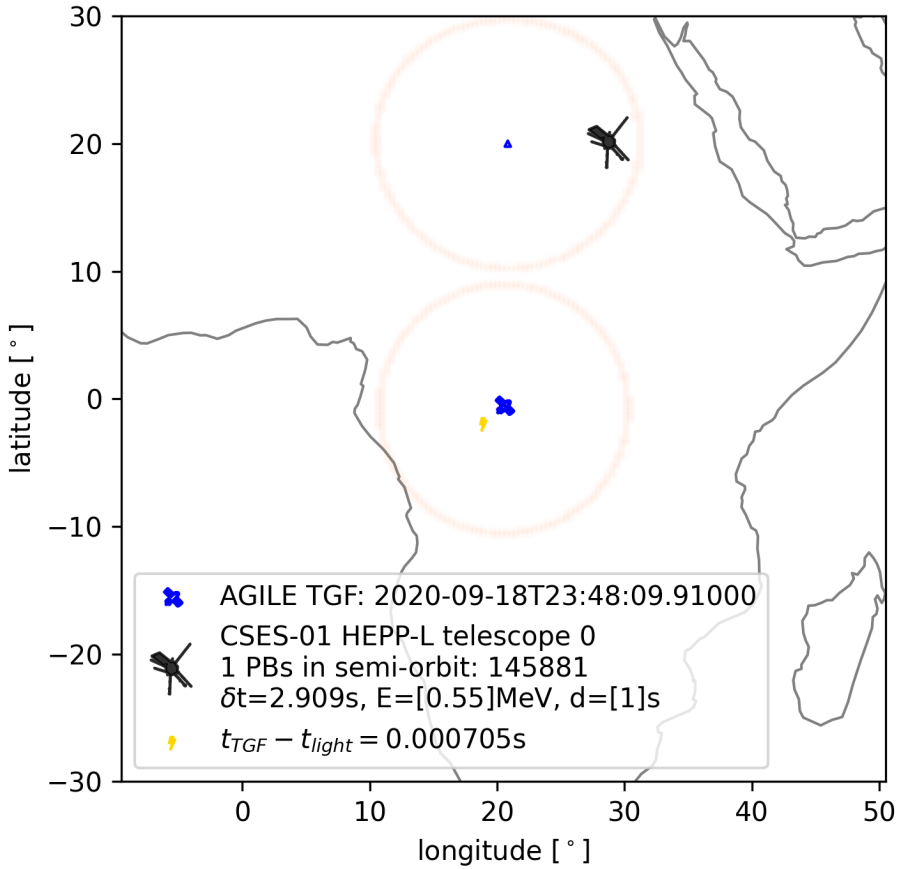

LITHOSPHERE

Lithosphere: the rigid shell that hosts many sources

Earthquakes and volcanoes share the same geodynamic stage, but not the same kind of forcing upward.

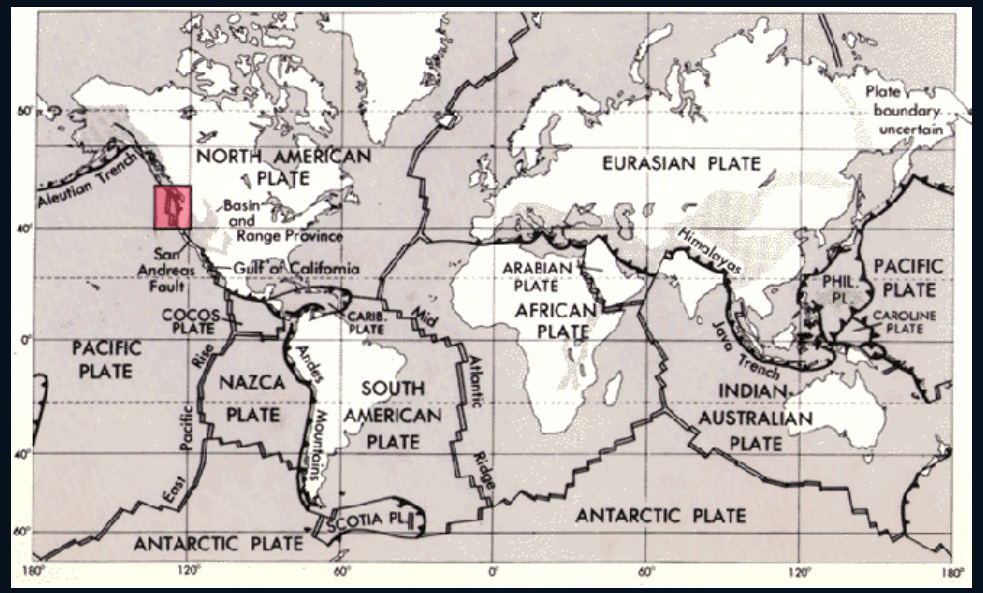

- The lithosphere is crust plus cold upper mantle, organized into tectonic plates moving relative to one another.
- Plate interactions concentrate elastic stress, deformation, partial melting, degassing, and volcanism.
- For space geophysics, what matters most is how these processes imprint observable signatures on the fluid envelopes above them.

Earthquakes: stress, faults, rupture

An earthquake is impulsive mechanical release; its primary signature is seismic waves plus surface deformation.

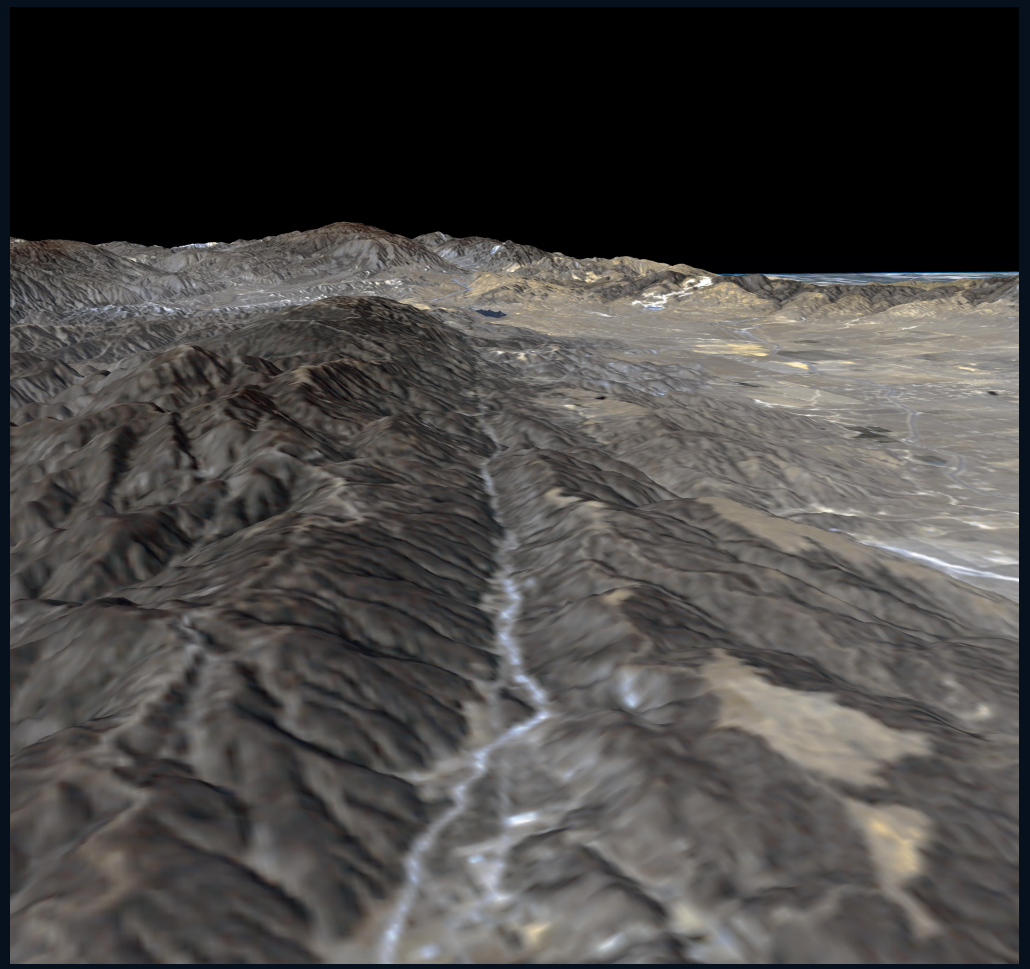

NASA/JPL · San Andreas Fault

- Plates accumulate stress until failure on a fault releases elastic energy over seconds to minutes.
- Seismic waves, ground motion, and deformation provide the first step in coupling toward atmosphere and ocean.
- If rupture occurs beneath the sea, the next step may be a tsunami.

Volcanoes: magma, gas, plume, aerosol

Volcanic forcing is less impulsive than an earthquake, but much richer: thermal, mechanical, chemical, and electrical.

NASA · Sarychev eruption image

- Magma ascent changes pressure, temperature, degassing, and stress state in the crust.
- An eruption can produce deep plumes, stratospheric aerosols, acoustic–gravity waves, and in extreme cases regional or global climatic effects.
- For satellites, volcanism is a multi-parameter source: deformation, heat, gas, ash, and atmospheric response.

LITHOSPHERE

Volcanic lightning: when lithosphere charges the sky

This is the moment when a geological source produces a directly electromagnetic atmospheric signature.

APOD / NASA · volcanic lightning

- Within an eruptive plume, fragmentation, ash collisions, and charge separation can generate intense lightning.
- This is a direct EM pathway from geology to atmosphere, distinct from — but complementary to — acoustic–gravity-wave coupling.
- For a CSES audience, it is a powerful example of a known natural EM source that can both enrich and contaminate observations.

From lithosphere upward: signatures and observational limits

The methodological rule is simple: the satellite does not “see” the tsunamis or earthquake; it sees the coupling chain.

Correct method: every step must have compatible timing, spatial scale, and observables.

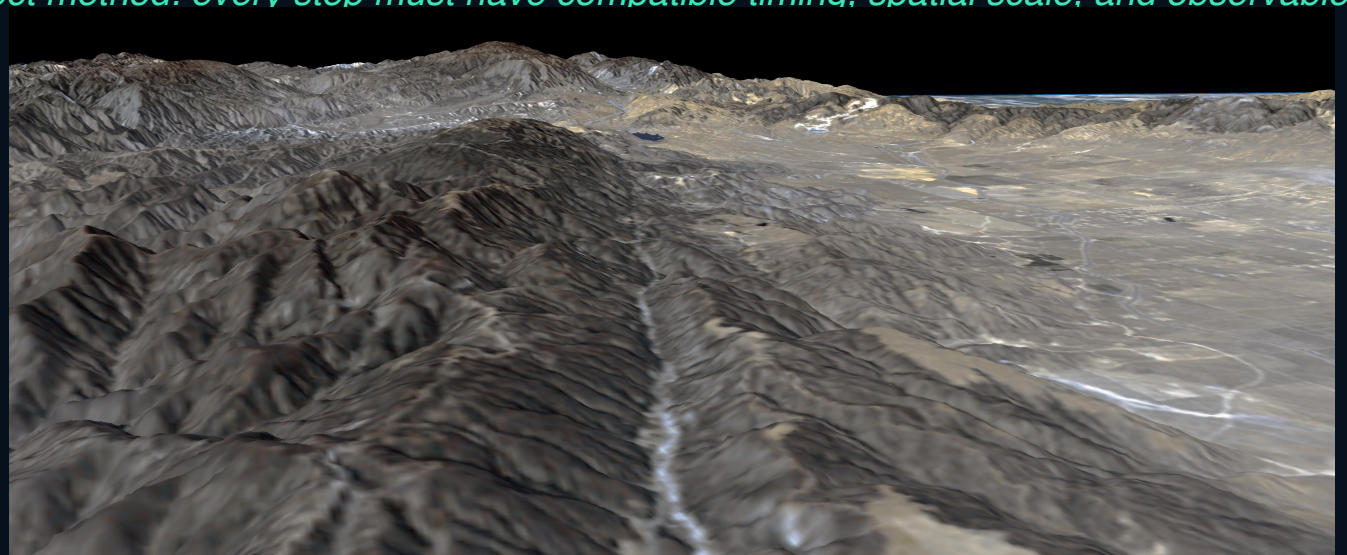

Physical chain: sea → atmosphere → ionosphere

The tsunami version of bottom-up coupling.

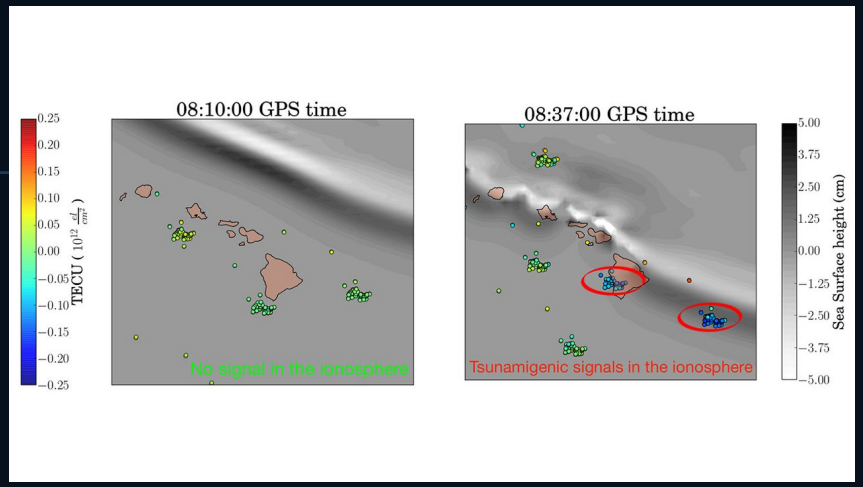

sea-surface displacement → gravity waves → upper-atm propagation → TEC / GNSS perturbation → hazard interpretation

The strength of the method is that the tsunami does not need to be seen in the ocean to be inferred from its ionospheric echo.

Tohoku 2011: travel time, speed, wave separation

The elegance of GNSS is that the same plot separates Rayleigh, acoustic, and tsunami-related gravity waves.

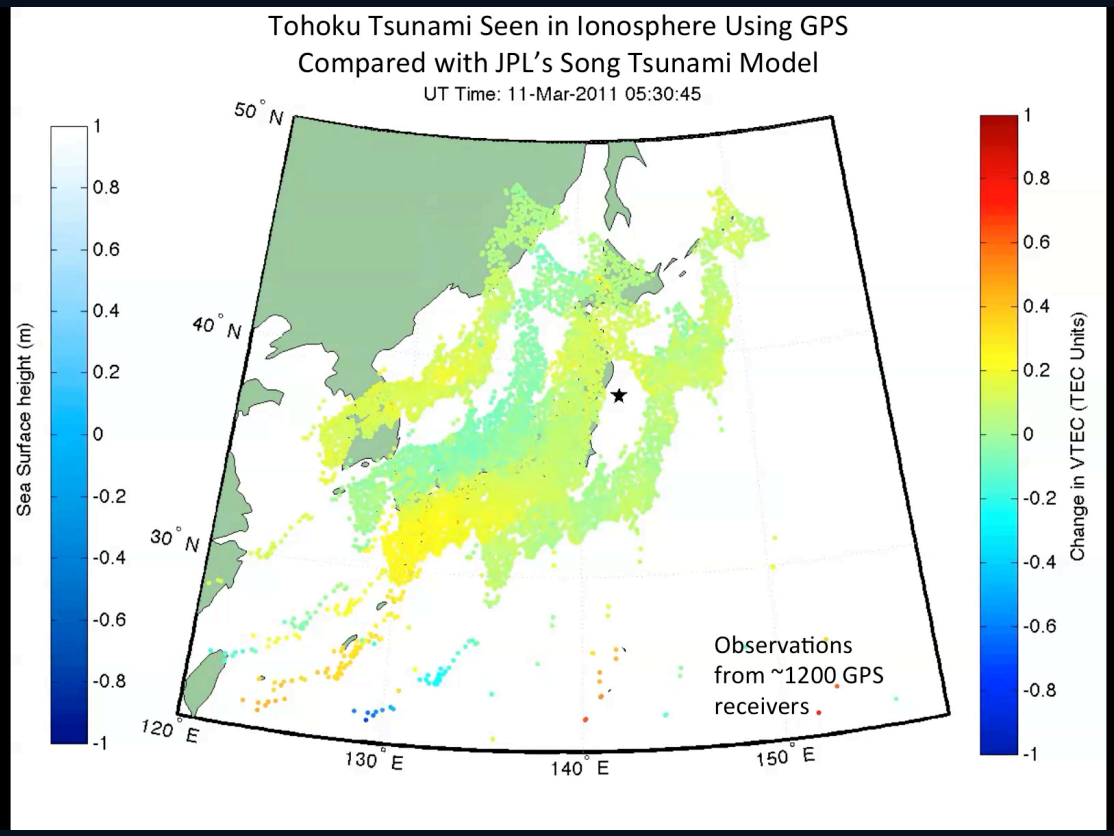

- The plot shows slopes compatible with Rayleigh waves (~3400 m/s), acoustic waves (~1000 m/s), and gravity waves (~200–300 m/s).
- A reference line near ~240 m/s represents the average tsunami speed in the modeled region.
- This cleanly separates seismic source, atmospheric response, and oceanic tsunami signature.

NASA/JPL · observed ionospheric perturbations vs modeled tsunami

From Pacific events to near-real-time support: VARION, GDGPS, GUARDIAN

The key recent change is the move from case study to an operational support framework.

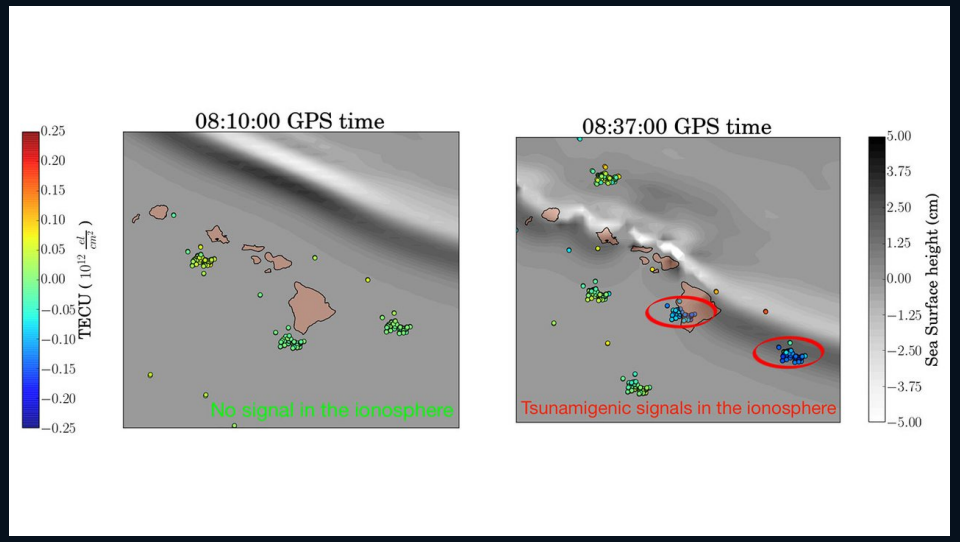

- Queen Charlotte, Tohoku, Tonga, and more recent events show that ionospheric perturbations can be tracked close to real time.
- GUARDIAN uses near-real-time multi-GNSS TEC series to explore perturbations from tsunamis, earthquakes, and eruptions.
- It does not replace classic ocean warning systems: it complements them, especially where buoy coverage is sparse.

JPL / Sapienza real-time example

“Today there are two ways to know if a tsunami was generated ... DART buoys and GNSS-ionosphere observations.”

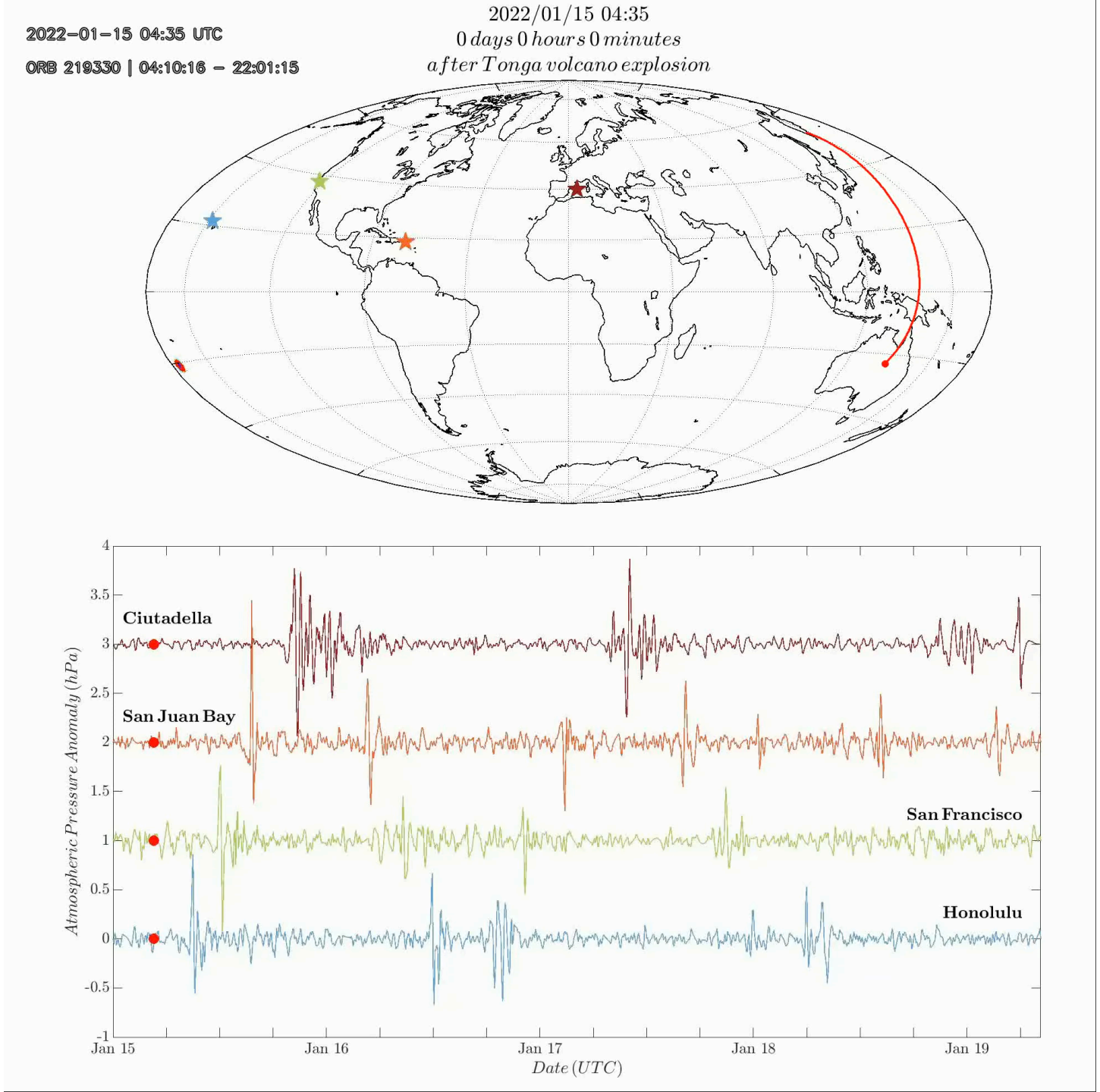
2022-01-15 04:35 UTC
ORB 219330 | 04:10:16 – 22:01:15
2022/01/15 04:35
0 days 0 hours 0 minutes
after Tonga volcano explosion
Ciutadella
San Juan Bay
San Francisco
Honolulu
Atmospheric Pressure Anomaly (hPa)
4
3.5
3
2.5
2
1.5
1
0.5
0
-0.5
-1
Jan 15
Jan 16
Jan 17
Jan 18
Jan 19
Date (UTC)

What about CSES ? (preliminary). (1)

CSES Langmuir probe provides the measurement of T_e and N_e *every 1 s.*

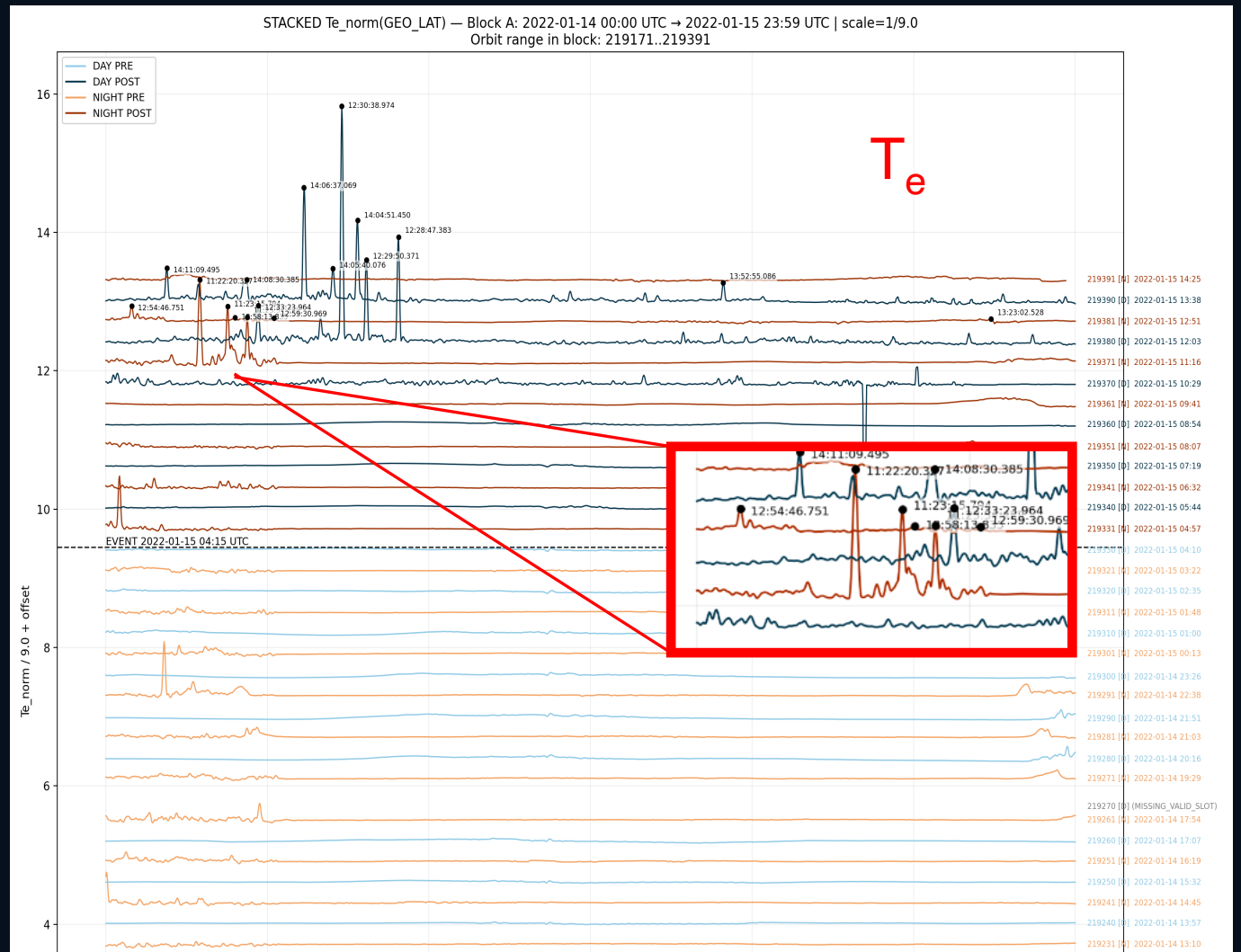

- **Orbit 219371** is indeed a **candidate tsunami-ionospheric signature:** a simple triangulation **gives** apparent velocities relative to the source of approximately **197, 188, and 182 m/s,** which is exactly the right scale for a tsunami front in the deep ocean (180–200 m/s)**.**

- **Lamb wave velocities** from the literature a much higher, ~308–319 m/s, **TID/near shock waves** ~450–750 m/s, **Lamb-related TID** ~300–370 m/s, and ~250 m/s

- The **group of 3–4 peaks** peaks observed between 11:22 and 11:24 UTC, i.e., approximately 7.1 hours after the explosion, if translated into wave period, gives about **24–35 min** for a **190 m/s** front.

- multiple trains of shorter disturbances have been reported, so the **multiple-peak structure** would be consistent with a real wavefront.

15-jan-2022
UT 04:00

elapsed time:
00h00m

Coupled atmosphere-ocean model & observed runup

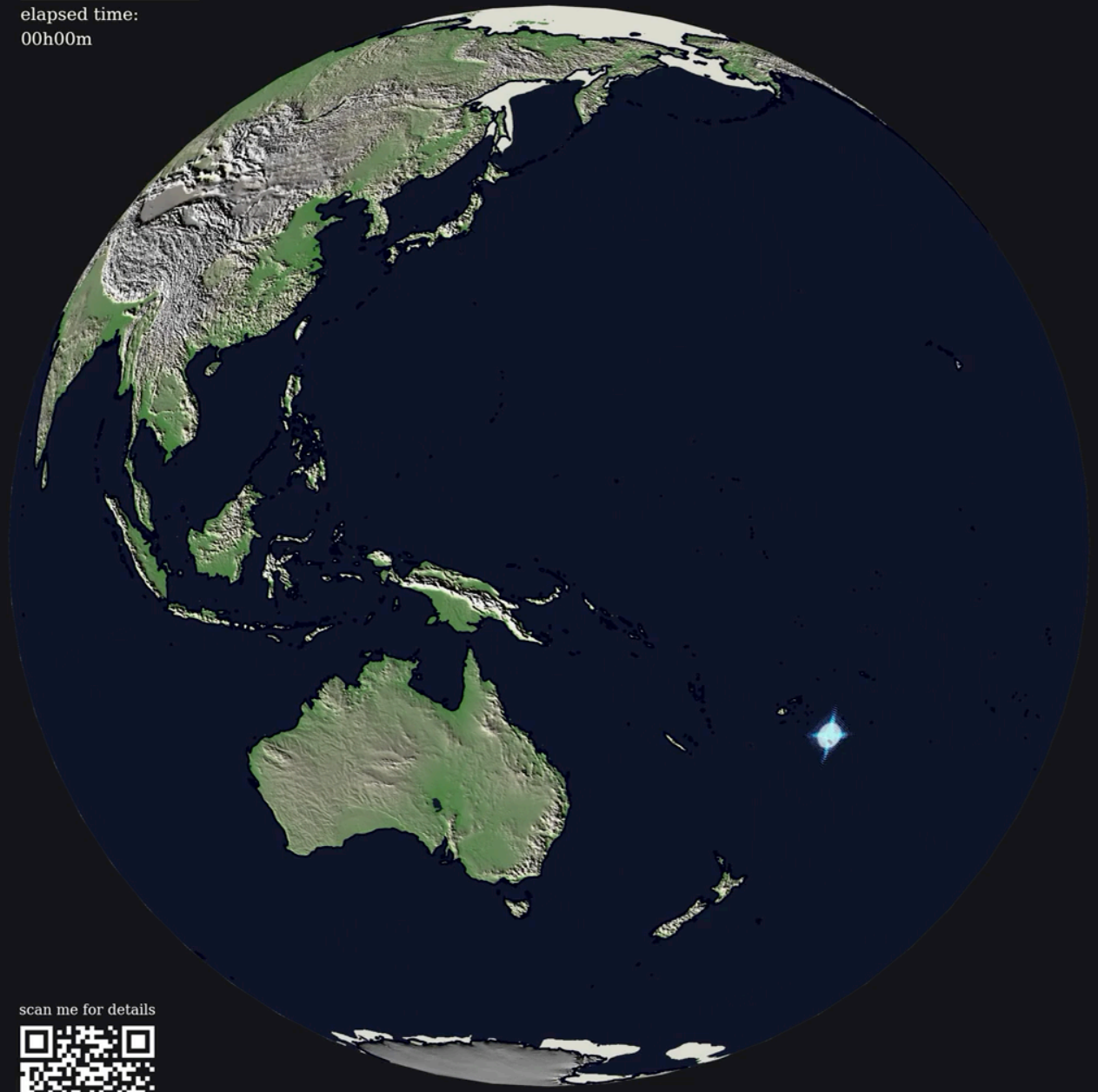

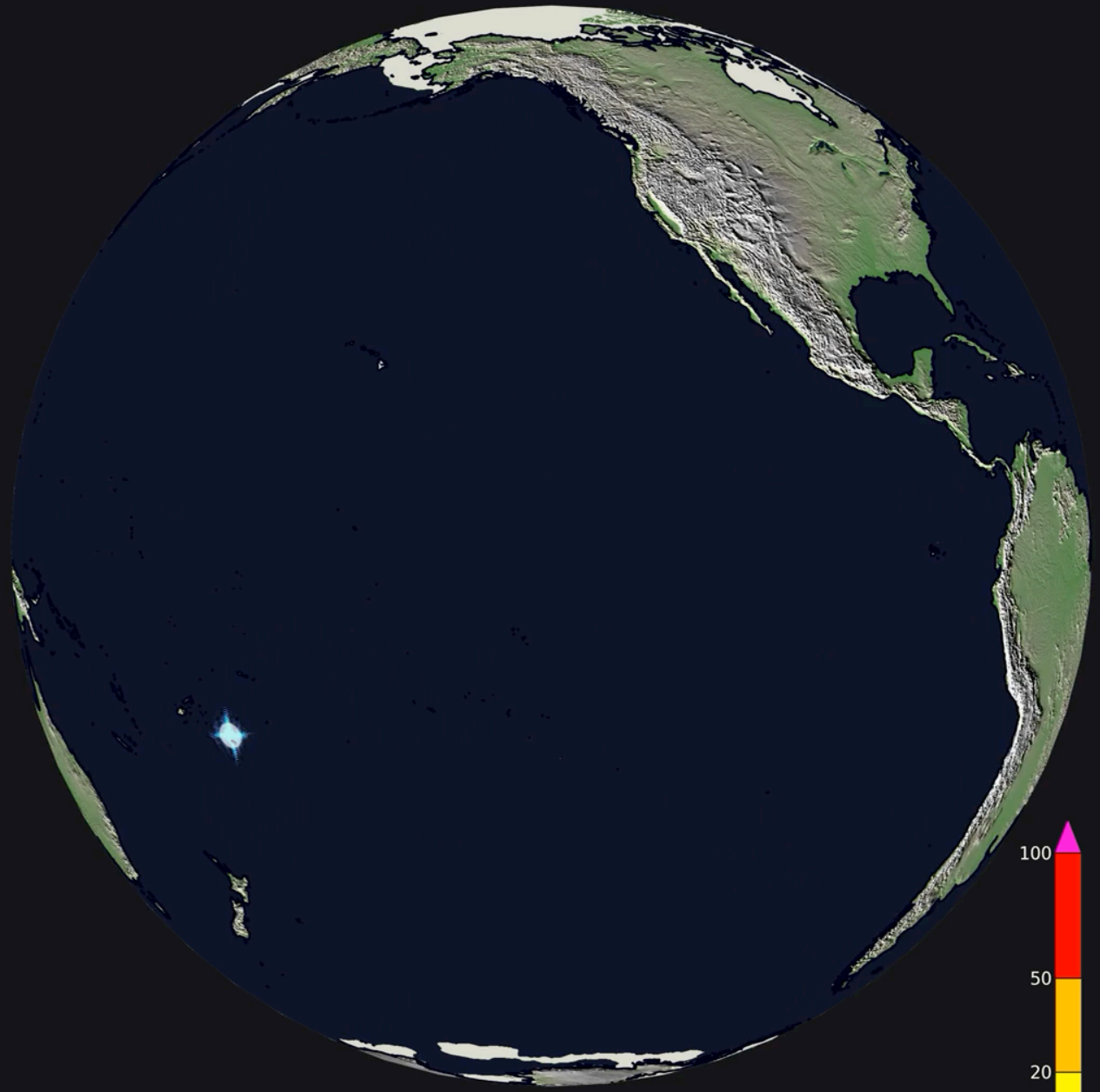

100
50
20
10
5
[cm]

runup data from NOAA

scan me for details

Take-home: the ionosphere as an ocean sensor

This is one of the clearest examples of geophysics from space: the measurement does not touch the ocean, yet reads its signature in plasma.

strengths

- global coverage at low marginal cost
- clean physics through sea–atmosphere–ionosphere coupling
- useful to confirm that a tsunami actually exists

limits

- depends on GNSS geometry and station density
- requires filtering of geomagnetic and meteorological noise
- not every ionospheric perturbation is a tsunami

This is the tsunami version of precision physics in the ionosphere: timing, pattern, and multi-sensor consistency.

Now the most difficult questions

1. Is there any Litho-Atmo-Ionosphere Coupling (LAIC) before large Earthquakes?

2. If yes, can the LAIC effects be detected from space?

Let us start from an “easier” task: co-seismic coupling

- In 2020 Piersanti, R.B. et al. developed:

1. a global Magnetospheric – Ionospheric – Lithospheric coupling (MILC) model for EQ able to explain possible signals detected during EQ occurrence;
2. a robust approach able to disentagle between internal and external sources of such signal, respectively.

The MILC model : a rigorous mathematical analysis of earthquake coupling with Earth surrounding layers based on oscillating phenomena

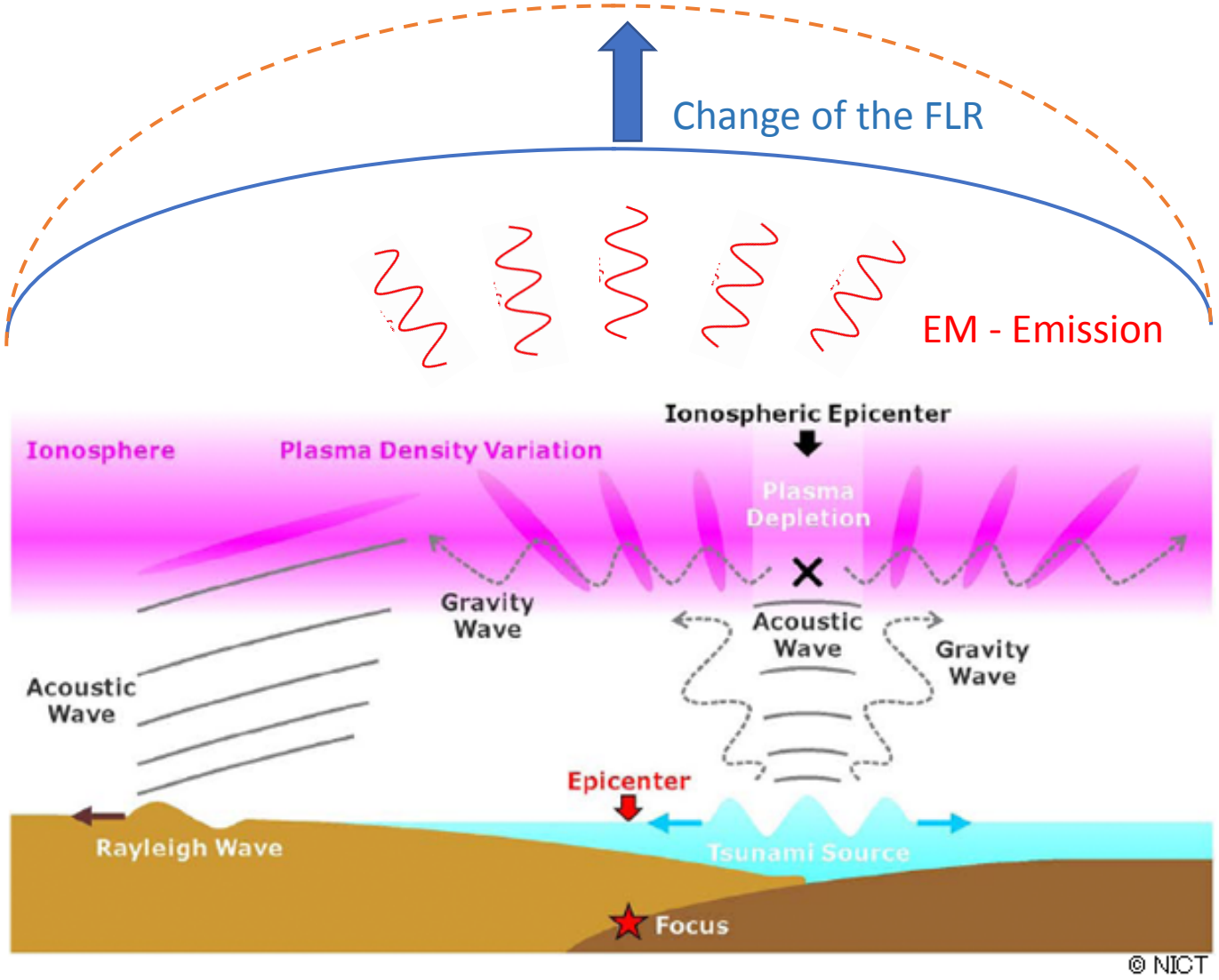

3)

2)

1)

The model is based on three steps:

1) The earthquake generates an AGW, propagating through the atmosphere;
2) The AGW interacts with the ionosphere generating local instability in the plasma distribution through a pressure gradient
3) The ionospheric plasma variation generates EM waves propagating through the magnetosphere that interact with the magnetospheric field
4) The interaction causes a FL eigen-frequency change.
5) Since the FL is stretched, its eigen-frequency has to lower.

Coupling of the lithosphere to the magnetosphere

MILC MODEL (2020-2023)

1- Piersanti M., Materassi, M., Battiston, R., Carbone, V., Cicone, A., D'Angelo, G., Ionospheric–Lithospheric Coupling Model. 1: Observations during the 5 August 2018 Bayan Earthquake, Remote Sensing 12 (20), 3299 (2020).

2 - Carbone, V., Piersanti, M., Materassi, M. , Battiston, R. , Lepreti F., Ubertini, P., A mathematical model of lithosphere–atmosphere coupling for seismic events, Nature Sci Rep. 2021, 11, 8682.

3- Piersanti M., William Jerome Burger W.J., Carbone V. , Battiston r., Iuppa R. and Ubertini P. , On the Geomagnetic Field Line Resonance Eigenfrequency Variations during Seismic Event, Remote Sens. 2021, 13, 2839.

4 –D'Angelo G., Cicone A., Plainaki,C., Piersanti M, Battiston R, Bertello I., Carbone V., Diego P., Papini E., Parmentier A., Picozza P., Recchiuti D., Sparvoli R. and Ubertini P. ,Haiti Earthquake (Mw 7.2): Magnetospheric–Ionospheric– Lithospheric Coupling during and after the Main Shock on 14 August 2021, Remote Sens. 2022, 14, 5340

5- Carbone F., Piersanti M., Lepreti F., Primavera L., N. Gencarelli C.N., Pirrone N. and Battiston R., A nonlinear Shallow Water investigation of atmospheric disturbances generated by strong seismic events,, Physical Review E, Vol. 108, No. 3. (2023)

The Bayan Earthquake
CSES&other satellite/ground data

- On August 5, 2018 an earthquake stroked Indonesia.
- Mw= 6.8;
- λ=-8.3 °N - ϕ=116.5 °E;
- UT=11:46,34.

Orbit CSES #2797: 2018/08/05 - 05:20 - - 06:00 UT

Terremoto di magnitudo **Mwp 6.8** del 05-08-2018 ore 13:46:34 (Italia) in zona: **Indonesia [Land]**

Dati Evento | Sismicità e Pericolosità | Impatto | Localizzazioni e Magnitudo | Meccanismo focale | Download

Un terremoto di magnitudo **Mwp 6.8** è avvenuto nella zona: **Indonesia [Land]**, il

- 05-08-2018 11:46:34 (UTC) 7 mesi fa
- **05-08-2018 13:46:34 (UTC +02:00) ora italiana**
- 05-08-2018 19:46:34 (UTC +08:00) orario locale nella zona del terremoto (Asia/Makassar)

con coordinate geografiche (lat, lon) **-8.3**, **116.5** ad una profondità di **10 km**.

Il terremoto è stato localizzato da: **Sala Sismica INGV-Roma**.

Ricerca terremoti: Qualsiasi nel raggio di 30 km

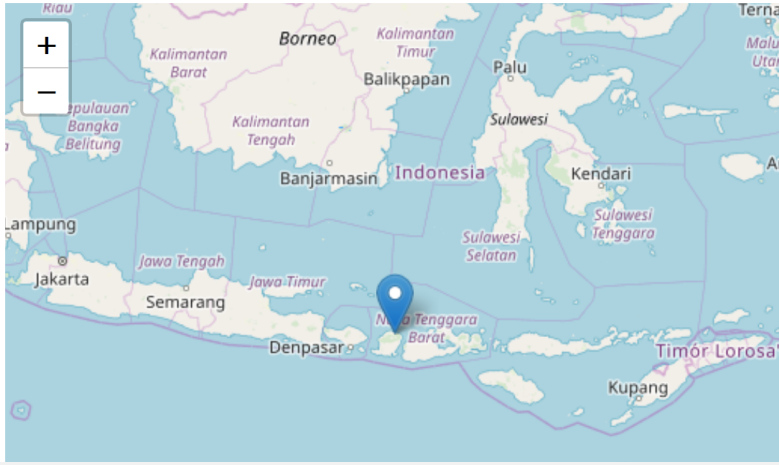

- CSES payloads: what did they observed?

Temperature Profile (ERA data)

- The potential energy density is defined as (VanZandt, 1985; Piersanti et al., 2020):

$$E_P = \frac{1}{2}\left(\frac{g}{N}\right)^2 \overline{\left(\frac{T'}{\overline{T}}\right)^2}$$

Where g is the gravitational acceleration (constant), N is the Brunt-Vaisala frequency defined as:

$$N = \sqrt{\frac{g}{\theta}\frac{d\theta}{dz}}$$

where $\theta = T\left(\frac{P_o}{P}\right)^{\frac{R}{c_p}}$ is the potential temperature, z is the altitude, P_0 is the standard reference pressure (1 hPa), R is the gas constant of air and c_p is the specific heat capacity at a constant pressure. R/c_p = 0.286 for air (Piersanti et al., 2020).

T' is the perturbation deviated from the background temperature $\overline{T}$ that are all function of the altitude. The variance term $\left(\frac{T'}{\overline{T}}\right)^2$ is calculated within a layer of 2 km thikness as:

$$\overline{\left(\frac{T'}{\overline{T}}\right)^2} = \frac{1}{z^{max} - z^{min}} \int_{z^{min}}^{z^{max}} \left(\frac{T'}{\overline{T}}\right)^2 dz$$

AGW evaluation – results

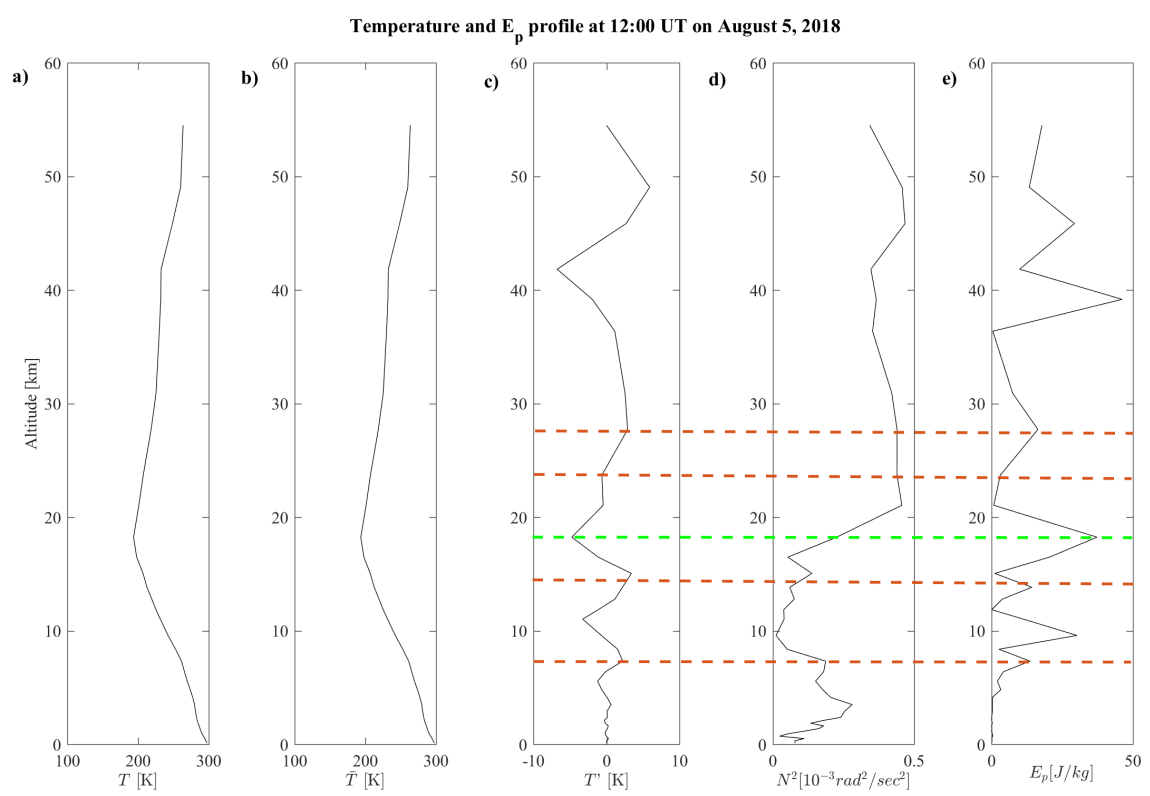

- The vertical wavelength of stratospheric AGW is about 2–10 km (Tsuda et al., 1994).
- The vertical temperature profile (left) at the EQ epicenter retrieved from ERA5 is hence filtered by a moving average (2 km), to obtain the background temperature profile (second panel from left);
- Then the temperature deviation (third panel) is computed by subtracting the background from the original temperature profile.
- Besides, the squared term of the Brunt-Väisälä frequency (Figure forth panel) can also be derived from the temperature profile. Finally, all the variables are substituted into equation (1),
- and the potential energy is calculated (right panel).
- The E_P value is absolutely maximum around the altitude of 17 km (the tropopause). The temperature inversion around this altitude is filtered out by the moving average. The similar increase can also be found in Brunt-Vaisala frequency.

- **Gravity waves disturb the temperature profile, and their influence is revealed in the temperature deviation profile (third panel).**
- **The wavelength is thus defined by a full period in the sinusoidal variation in the temperature deviation but not in the EP profile.**

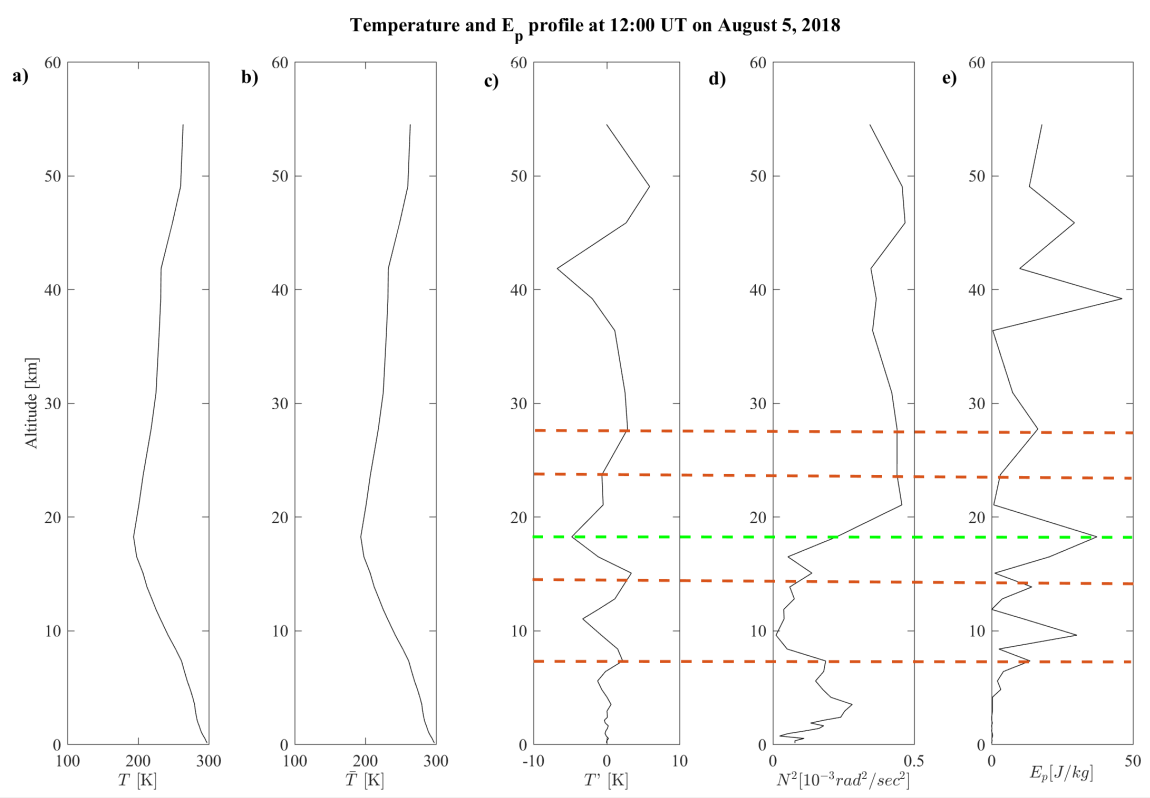

- Four wave crests are found in the temperature deviation profile at the altitudes of 17.8, 27.6, 36.6, and 44.8 km. There exist two sinusoidal periods, and the corresponding vertical wavelengths are 9.8 and 7.2 km, respectively.
- On the other hand, the *E*P profile maximizes only for the first wavelength.

So, there is a AGW of 9.8 km wavelength propagating in the atmosphere .

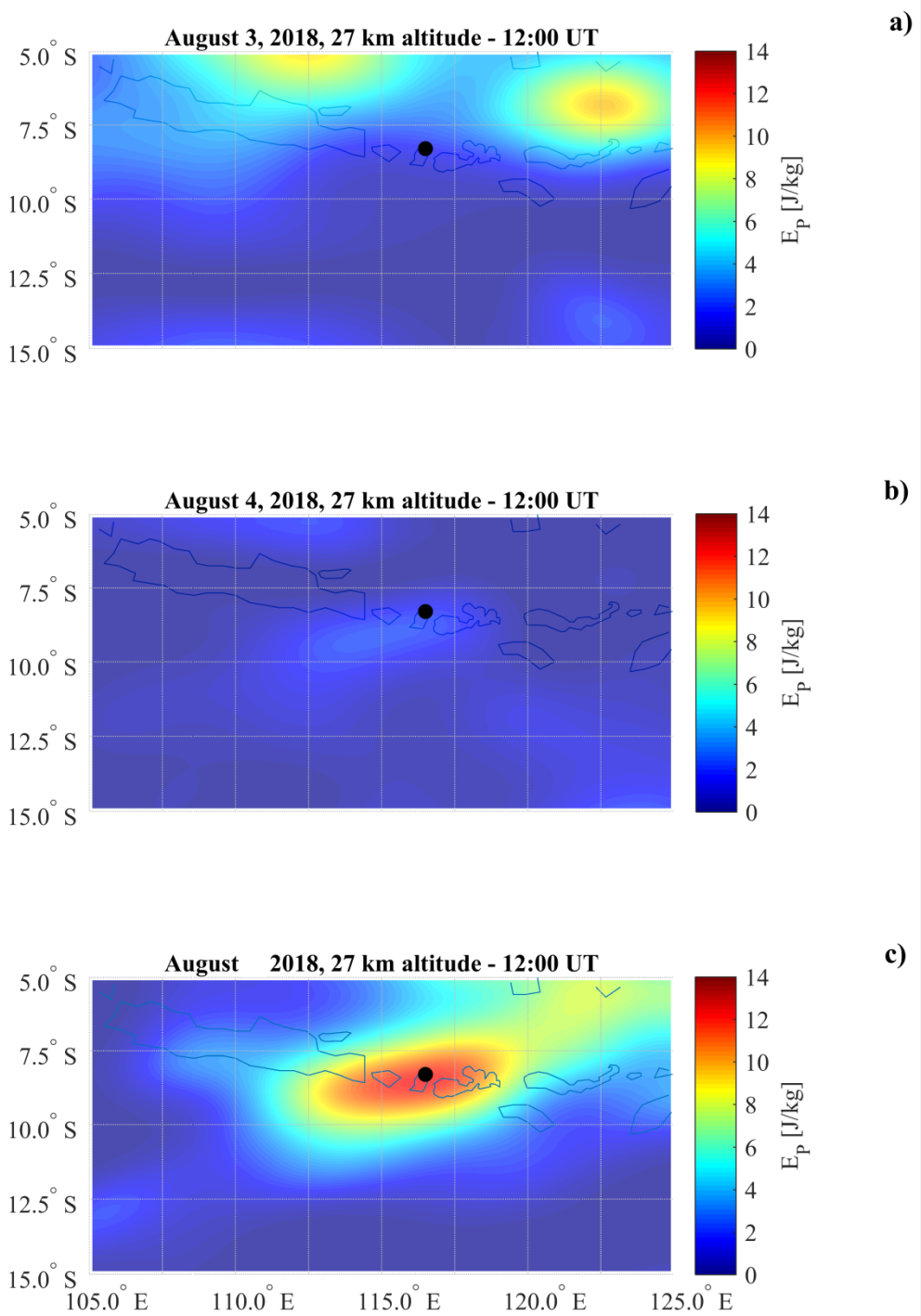

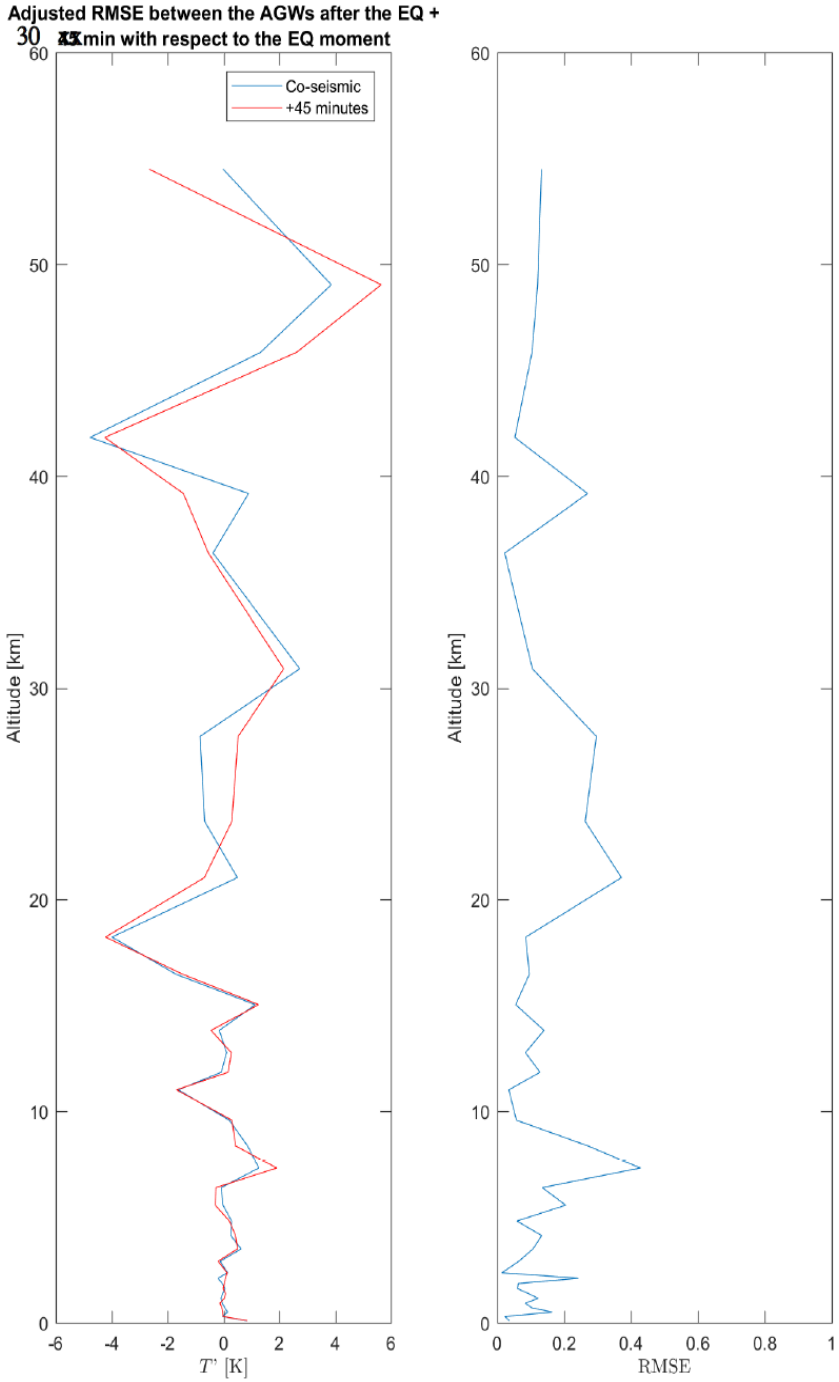
Adjusted RMSE between the AGWs after the EQ +
30 min with respect to the EQ moment
Co-seismic
+45 minutes
Altitude [km]
T' [K]

Altitude [km]
RMSE

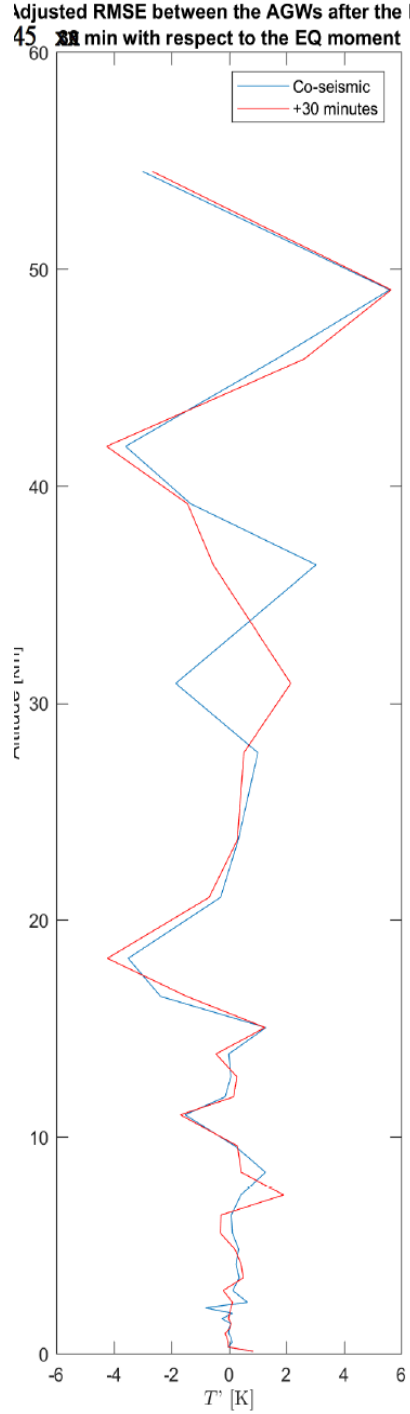
Adjusted RMSE between the AGWs after the EQ +
45 min with respect to the EQ moment
Co-seismic
+30 minutes
T' [K]

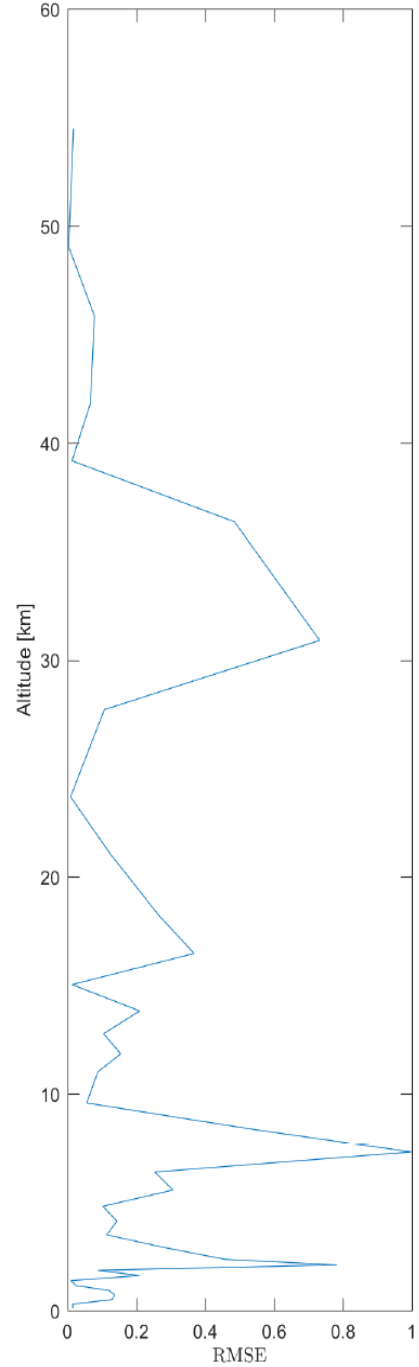
Altitude [km]
RMSE

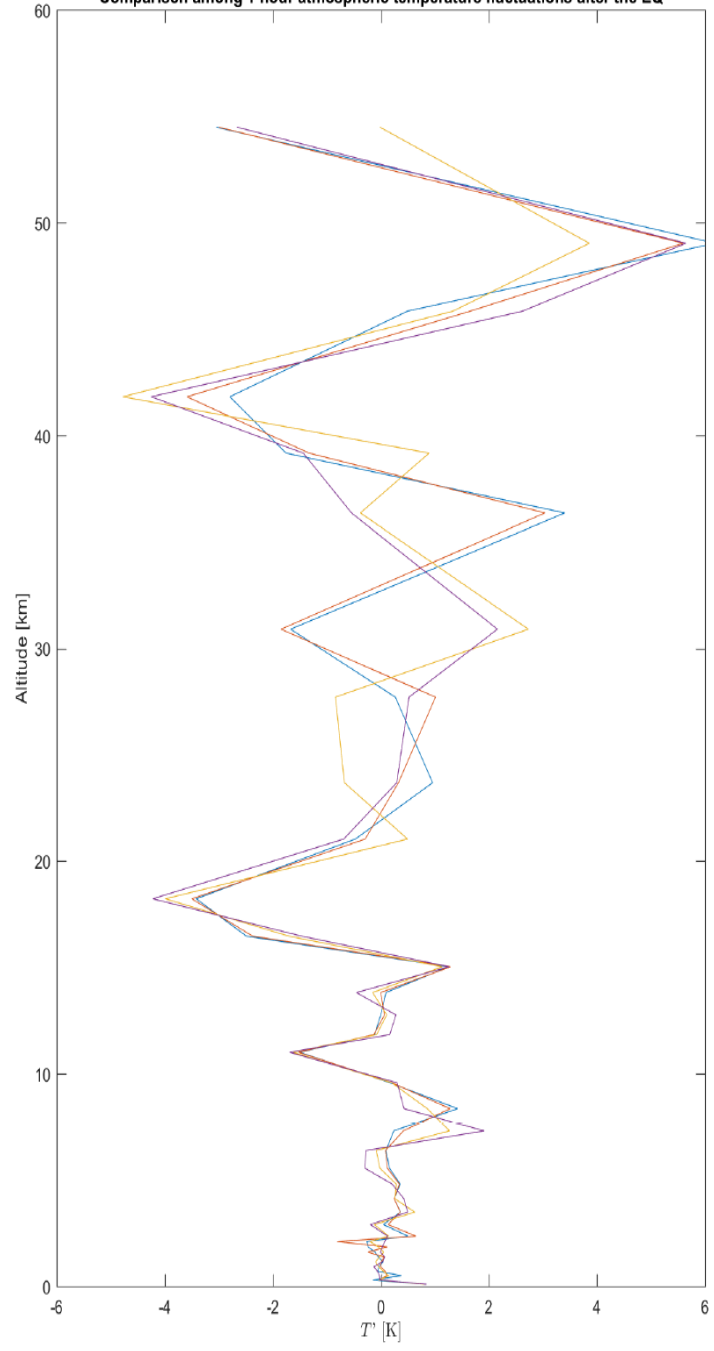
Comparison among 1 hour atmospheric temperature fluctuations after the EQ
Altitude [km]
T' [K]

August , 2018 – vTEC GPS-Ground

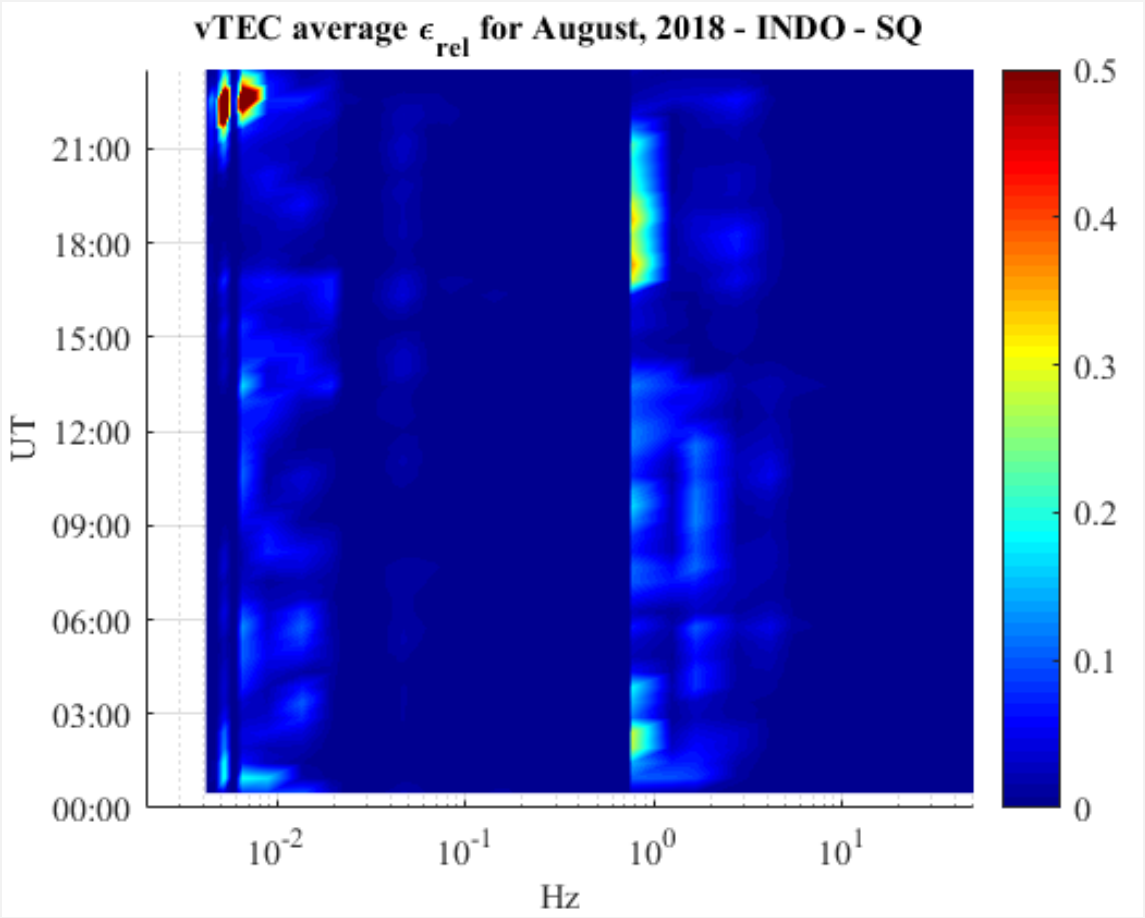

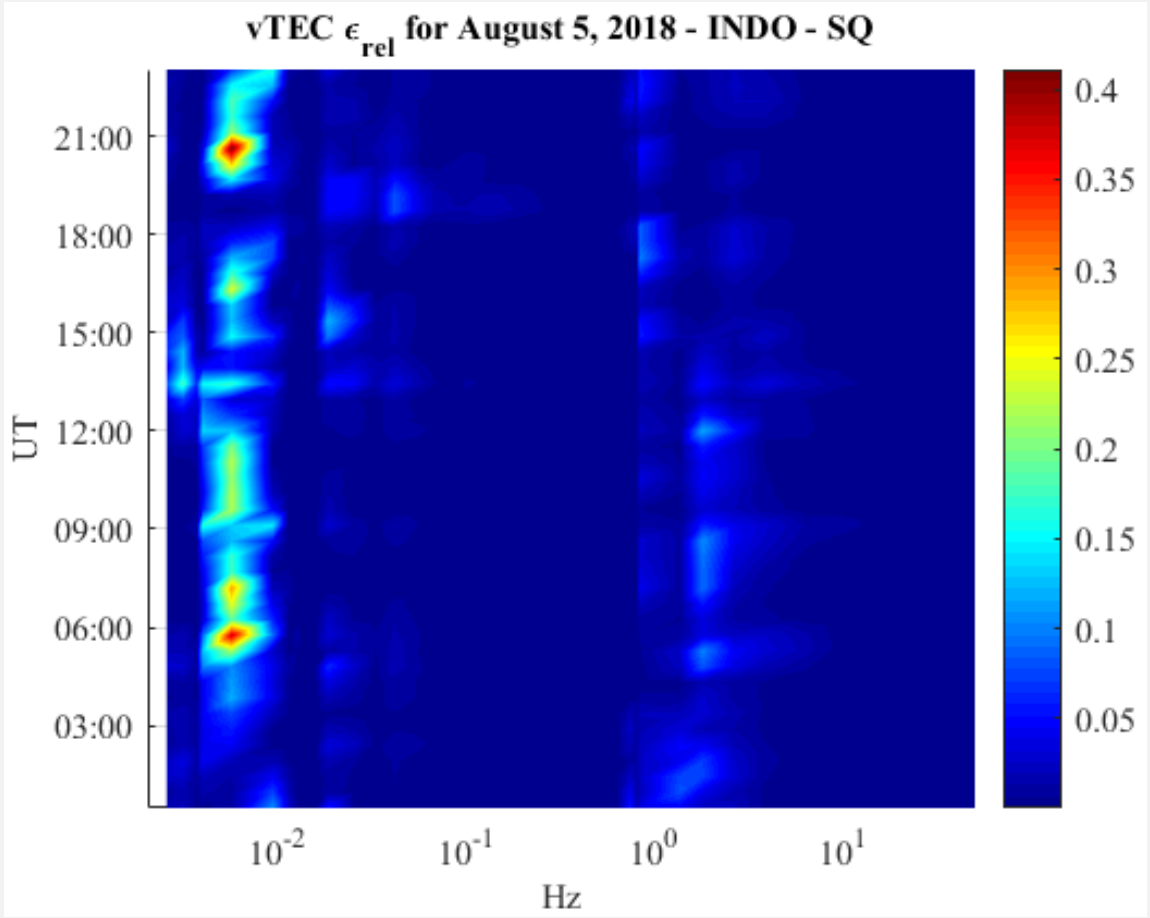

- **Clear anomaly of vTEC with respect to monthly average.**
- **The first anomaly starts around 5:45 UT.**
- **The second anomaly starts around 09:00 UT with its peak at the EQ.**
- **Possible clear relation with EQ.**

August , 2018 – vTEC

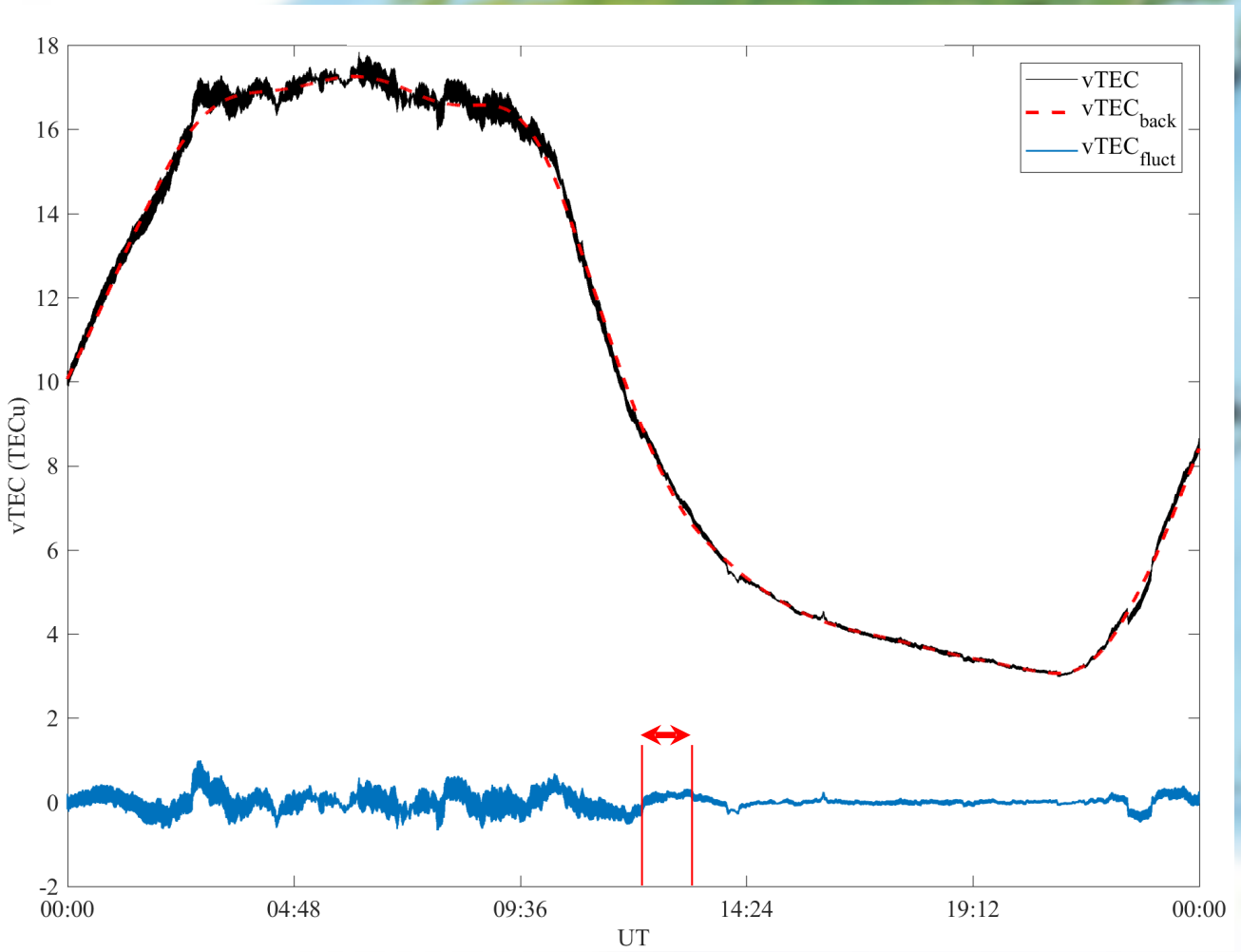

- To derive the vTEC fluctuation we used a new data-analysis technique called **FIF**.
- A posteriori decomposition method useful for nonlinear and non-stationary datasets [Piersanti et al. 2017];

$$\mathrm{vTEC}(t) = \sum_{j=1}^{m} c_j(t) + r(t)$$

- $c_j(t)$ is called Intrinsic Mode Component (IMC) and $r(t)$ is the residue of the decomposition;
- For each IMC, we can obtain a characteristic mean period as:

$$T_j = \frac{2\pi}{\langle \omega_j(t) \rangle};$$

- Specifically, starting from real vTEC observation (black):

1. we first calculate the trend (red);
2. We substract the trend to obtain flactuations (blue) which correspond to the sum of all IMCs.

Finally, we selected all the IMCs having a characteristic mean period between 5 and 9 minutes

TID – MILC model results

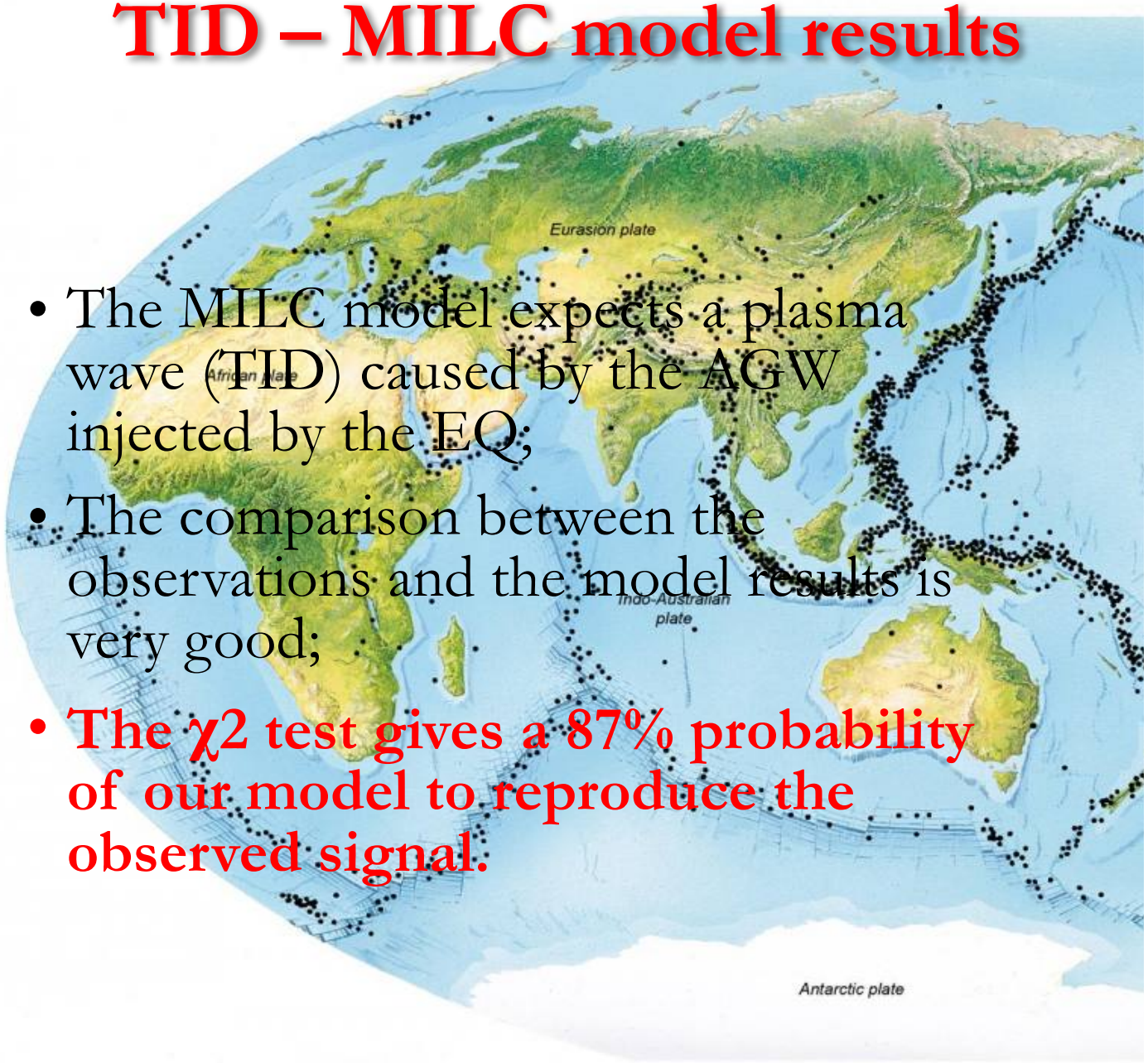

- The MILC model expects a plasma wave (TID) caused by the AGW injected by the EQ;
- The comparison between the observations and the model results is very good;
- **The χ2 test gives a 87% probability of our model to reproduce the observed signal.**

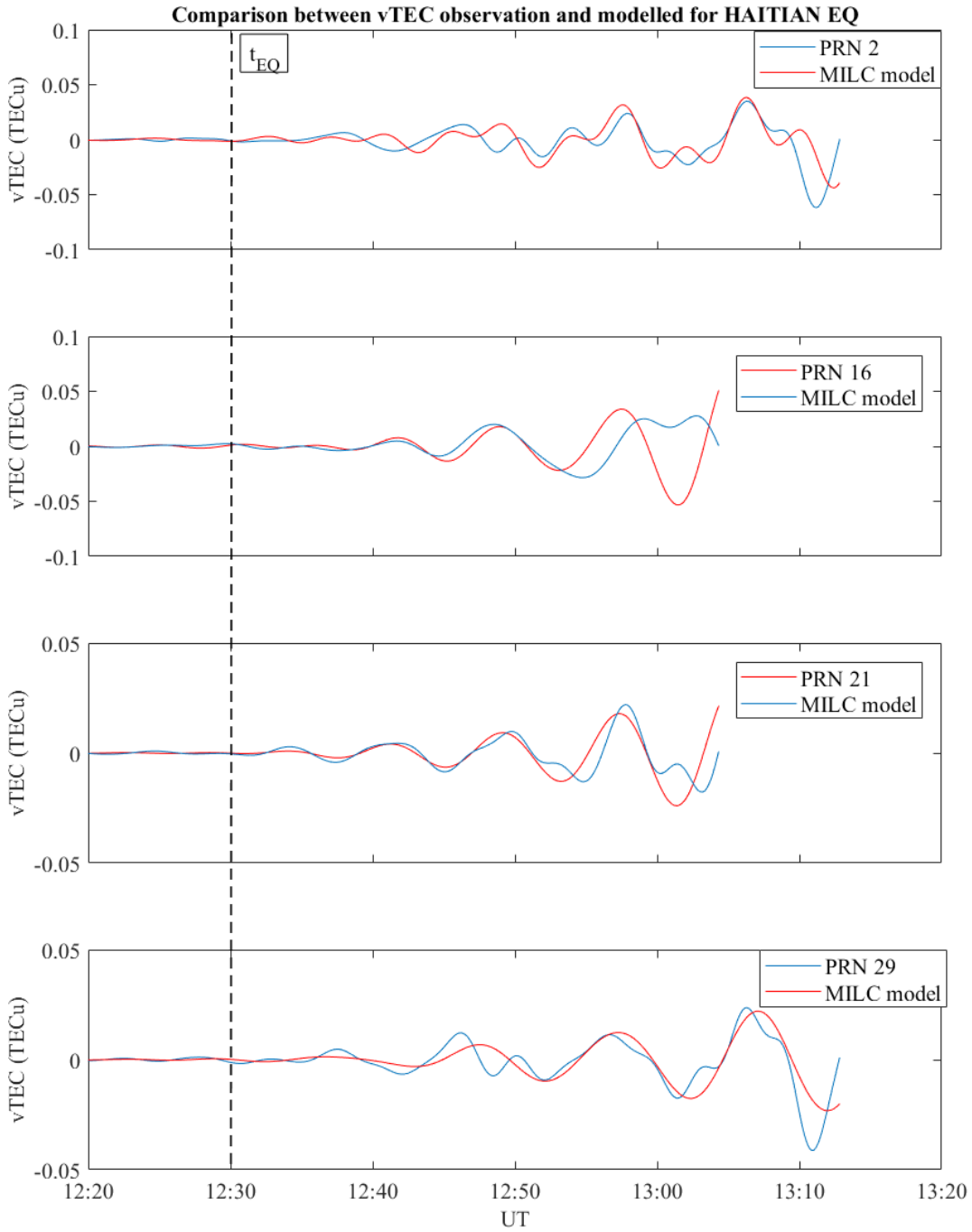

Ionospheric Plasma Waves - TID

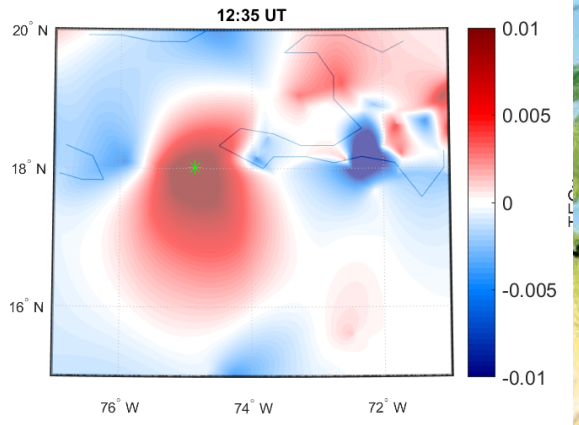

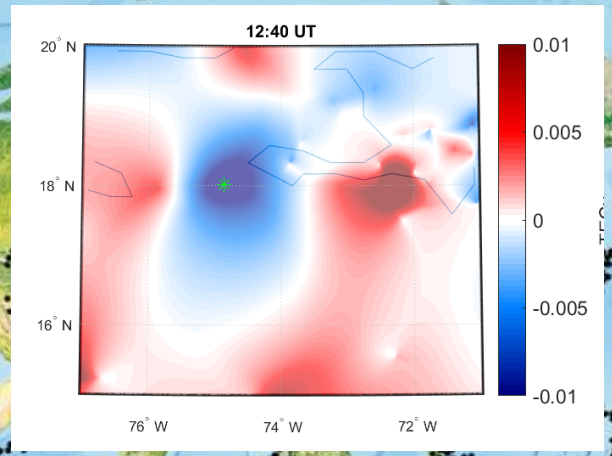

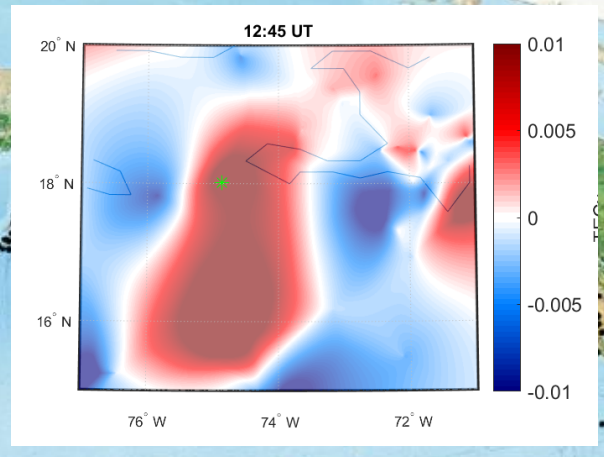

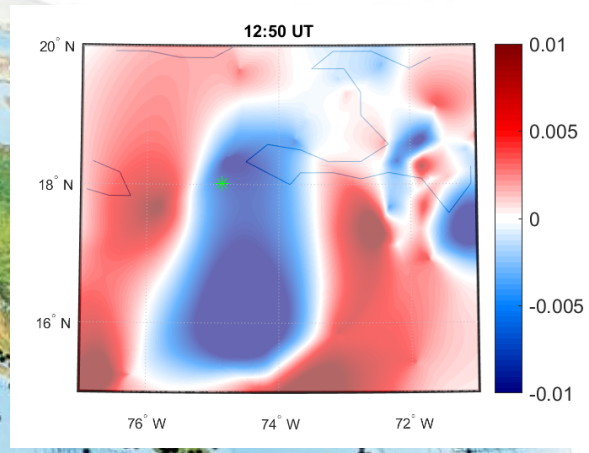

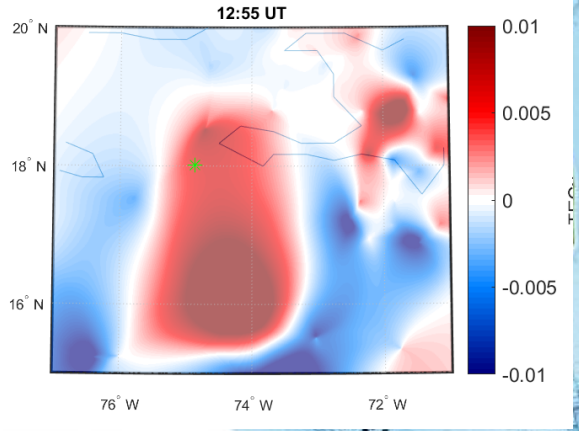

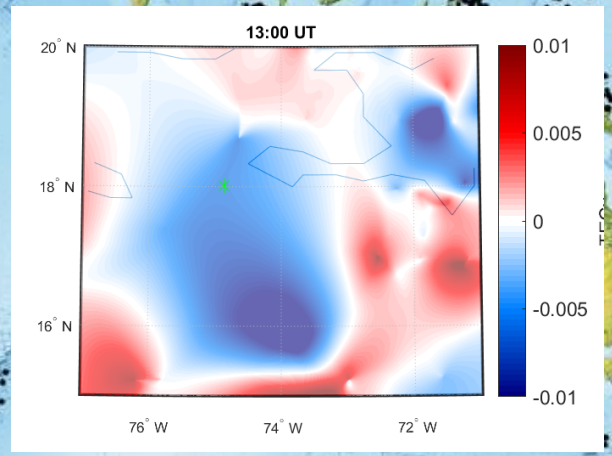

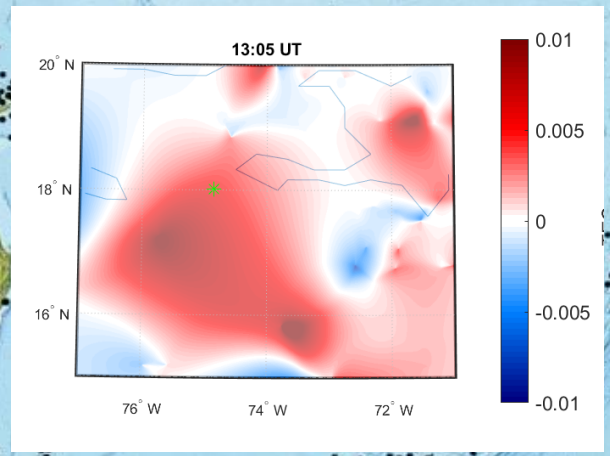

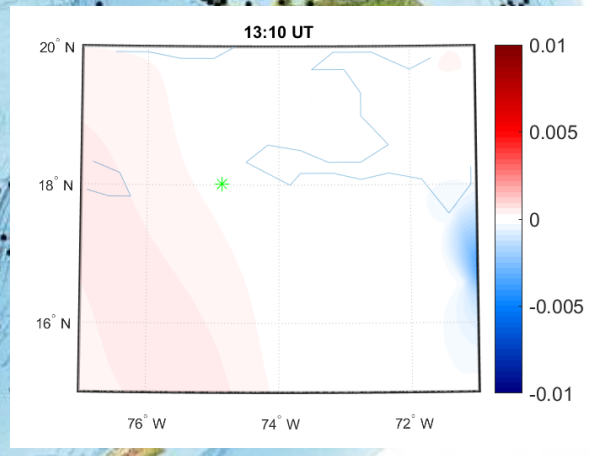

Pacific plate

Antarctic plate

- Clear TID injection at the moment of the EQ occurrence.
- It has a period of about 7 minutes and lasts for 30 minutes.

Gradient method for detecting field line resonances from ground-based ULF measurements

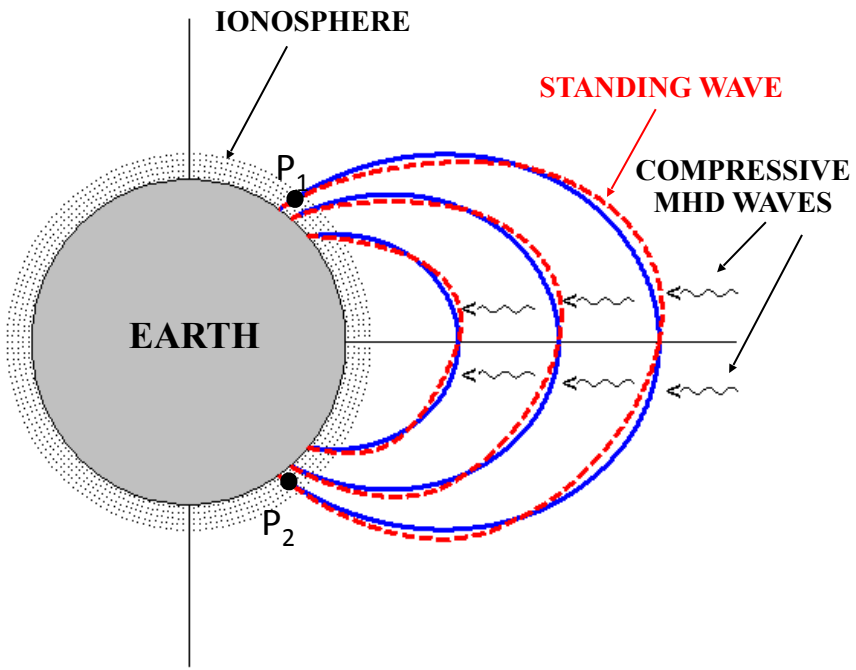

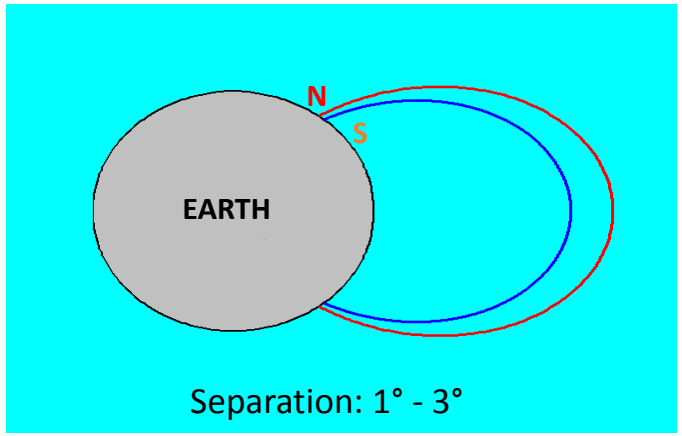

— Higher latitude field line → Lower resonance frequency (f_N)

— Lower latitude field line → Higher resonance frequency (f_S)

V_A: Alfvén velocity

FREQUENCY RESPONSE OF TWO OSCILLATORS

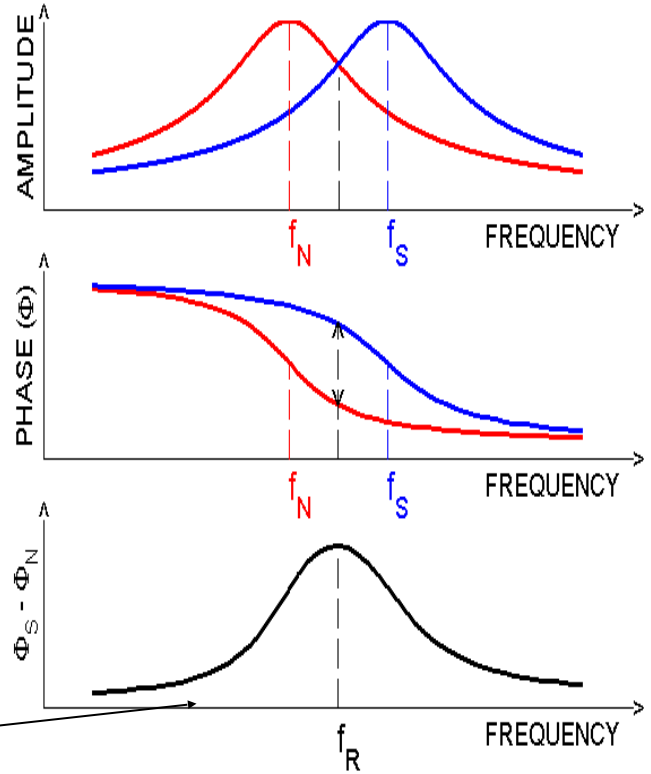

CROSS-PHASE TECHNIQUE

Resonance frequency at the middle point.

Identified by a maximum in the phase difference

FLR	Date	UTC Time	K_p	M	Latitude	Longitude	Region
X	17/07/2001	14.50.57	0	6.3	3.061◦ S	148.180◦ E	Bismarck Sea
X	27/11/2002	00.17.20	1	5.4	12.279◦ N	120.753◦ E	Philippines
X	12/12/2003	08.07.30	1	5.2	0.110◦ S	123.991◦ E	Indonesia
X	28/01/2004	07.41.04	1	5.7	4.931◦ S	153.584◦ E	New Guinea
-	09/02/2006	05.44.30	2	6.2	4.810◦ S	133.063◦ E	Indonesia
X	17/05/2006	01.21.26	1	6.0	3.743◦ S	144.305◦ E	New Guinea
X	24/06/2006	00.03.07	1	6.3	3.071◦ S	127.183◦ E	Indonesia
X	16/09/2007	01.20.38	2	6.4	2.763◦ S	101.106◦ E	Indonesia
-	26/10/2007	16.34.47	0	6.0	3.271◦ S	143.763◦ E	New Guinea
X	14/11/2007	17.44.04	2	5.7	23.215◦ S	70.526◦ W	Chile
-	25/07/2008	20.11.07	1	6.5	5.808◦ S	146.658◦ E	New Guinea
X	11/09/2008	00.00.02	1	6.6	1.885◦ N	127.363◦ E	Indonesia
-	19/12/2008	00.34.58	2	6.8	20.372◦ N	146.339◦ E	Mariana Islands
X	06/01/2009	19.56.25	2	6.0	0.566◦ S	132.784◦ E	Indonesia
X	16/02/2009	00.33.36	2	6.1	3.664◦ S	149.608◦ E	Bismarck Sea
X	02/03/2009	00.03.39	1	6.5	1.105◦ S	119.868◦ E	Indonesia
X	25/07/2009	18.41.58	2	5.8	1.869◦ N	97.020◦ E	Indonesia
X	15/10/2009	03.34.28	1	6.0	1.111◦ N	85.322◦ W	Ecuador
-	24/02/2008	04.36.29	2	6.5	3.741◦ S	101.986◦ E	Indonesia
NA	07/06/2008	19.10.48	2	5.0	3.552◦ S	140.851◦ E	Indonesia
-	02/07/2008	00.08.31	2	5.2	12.451◦ N	44.202◦ W	Mid-Atlantic
X	07/02/2008	23.16.41	1	5.3	17.558◦ N	144.922◦ E	Mariana Islands
-	19/12/2006	12.48.16	2	6.0	2.458◦ N	98.000◦ E	Idonesia
X	16/11/2009	18.34.24	0	5.2	19.556◦ S	70.365◦ W	Chile
NA	11/01/2009	14.03.49	1	5.6	6.388◦ S	147.423◦ E	New Guinea
NA	11/01/2009	14.15.54	1	5.0	0.769◦ S	133.506◦ E	Indonesia
X	16/09/2008	21.47.14	2	5.7	17.438◦ N	73.915◦ E	India
X	24/05/2003	01.46.06	1	5.9	14.428◦ N	53.813◦ E	Owen region
-	14/11/2007	18.55.49	2	5.1	22.670◦ S	70.292◦ W	Chile
NA	26/10/2007	16.34.47	1	5.6	3.271◦ S	143.7630 E	New Guinea
X	22/11/2003	09.30.03	1	5.1	13.281◦ N	57.466◦ E	Arabic Sea
X	12/03/2008	01.32.34	2	6.0	1.934◦ N	132.519◦ E	Indonesia
X	02/02/2013	14.17.33	1	6.9	42.8◦ N	143.27◦ E	Japan
-	25/10/2013	17.10.16	2	7.1	37.194◦ N	144.66◦ E	Japan
X	06/10/2017	07.59.32	1	6.2	37.325◦ N	144.02◦ E	Japan
X	08/01/2019	12.39.31	2	6.3	30.526◦ N	131.113◦ E	Japan
X	18/06/2019	13.22.22	0	6.4	38.563◦ N	139.504◦ E	Japan
X	27/07/2019	18.31.07	1	6.3	33.015◦ N	137.413◦ E	Japan
X	19/04/2020	20.39.08	2	6.3	38.858◦ N	141.99◦ E	Japan
-	21/11/2016	20.58.47	1	6.9	38.296◦ N	141.642◦ E	Japan
X	05/08/2018	11.58.00	0	6.5	8.28◦ S	116.4◦ E	Indonesia
X	25/04/2015	06.45.21	2	6.6	28.18◦ N	84.72◦ E	Nepal

Statistical analysis for the Ionosphere-Magnetosphere coupling during EQ

- We made a statistical analysis of the possible FLR signature associated to EQ in the time span from 2001-07-17 and 2020-08-31.
- We selected 42 case events for which the planetary geomagnetic Kp index [Matzka et al., 2021] is lower than 3 in order to exclude any possible variation of solar origin;
- To evaluate the f^*, we studied the cross-space spectrum [Waters et al., 1994] between the North-South magnetic field components observed at two geomagnetic observatories close enough to the EQ epicentre location

Statistical analysis for the Ionosphere-Magnetosphere coupling during EQ

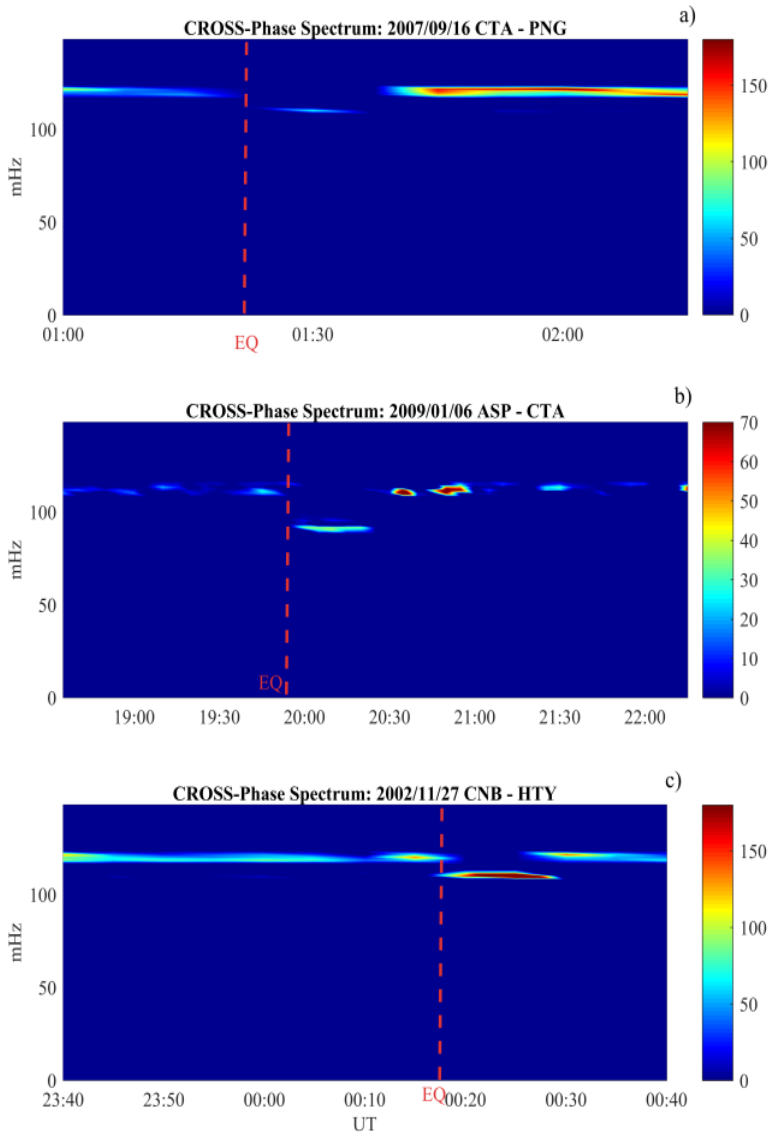

- We found 28 cases out of 42 in which there is a clear variation of the estimated *f** (indicated with the "X").
- In 4 cases it was not possible to correctly evaluate *f** because of the post-sunset occurrence of the EQ (indicated with the "NA").
- Finally, no *f** variations has been detected for 10 case events (indicated with "-").

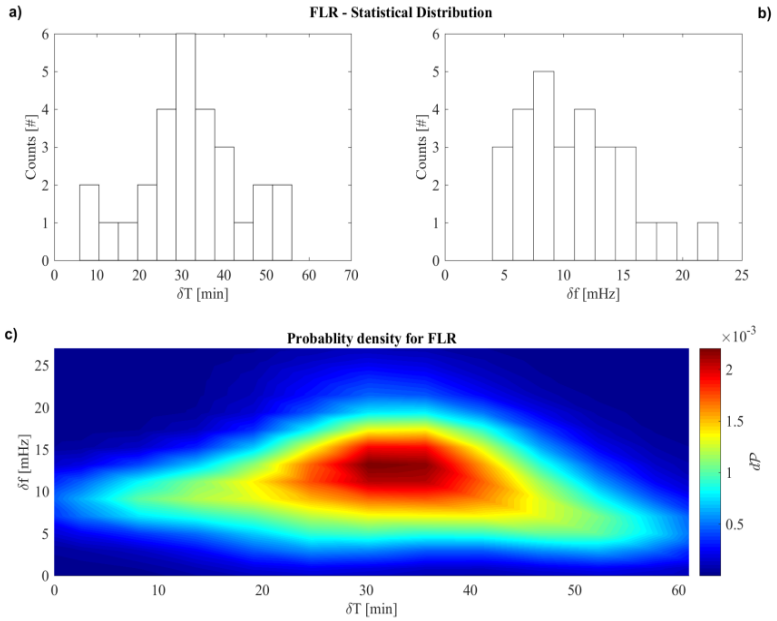

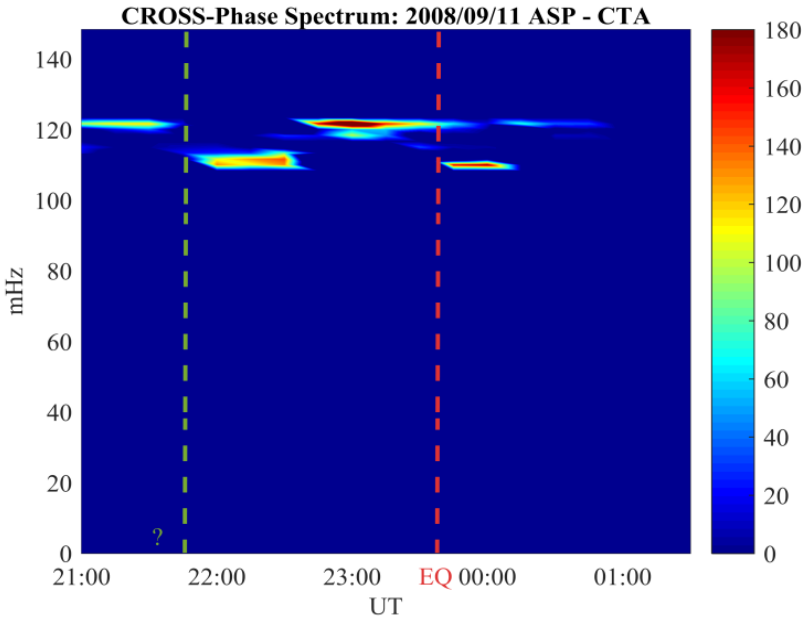

- The co-seismic FLR eigenfrequency variation is characterized by a frequency decrease of 12±3 mHz and a time duration of 36±3 min.

M-Piersanti, R.B., et al. *Remote Sens.* **2021**, *13*, 2839. https://doi.org/10.3390/rs13142839

August 1-31, 2018 – CSES-EFD observation

- On the basis of Piersanti et al. [2020], we first evaluated both the environmental and the instrumental background over Bayan cell [3°x3° - latxlon] for SQ and M<2 conditions.

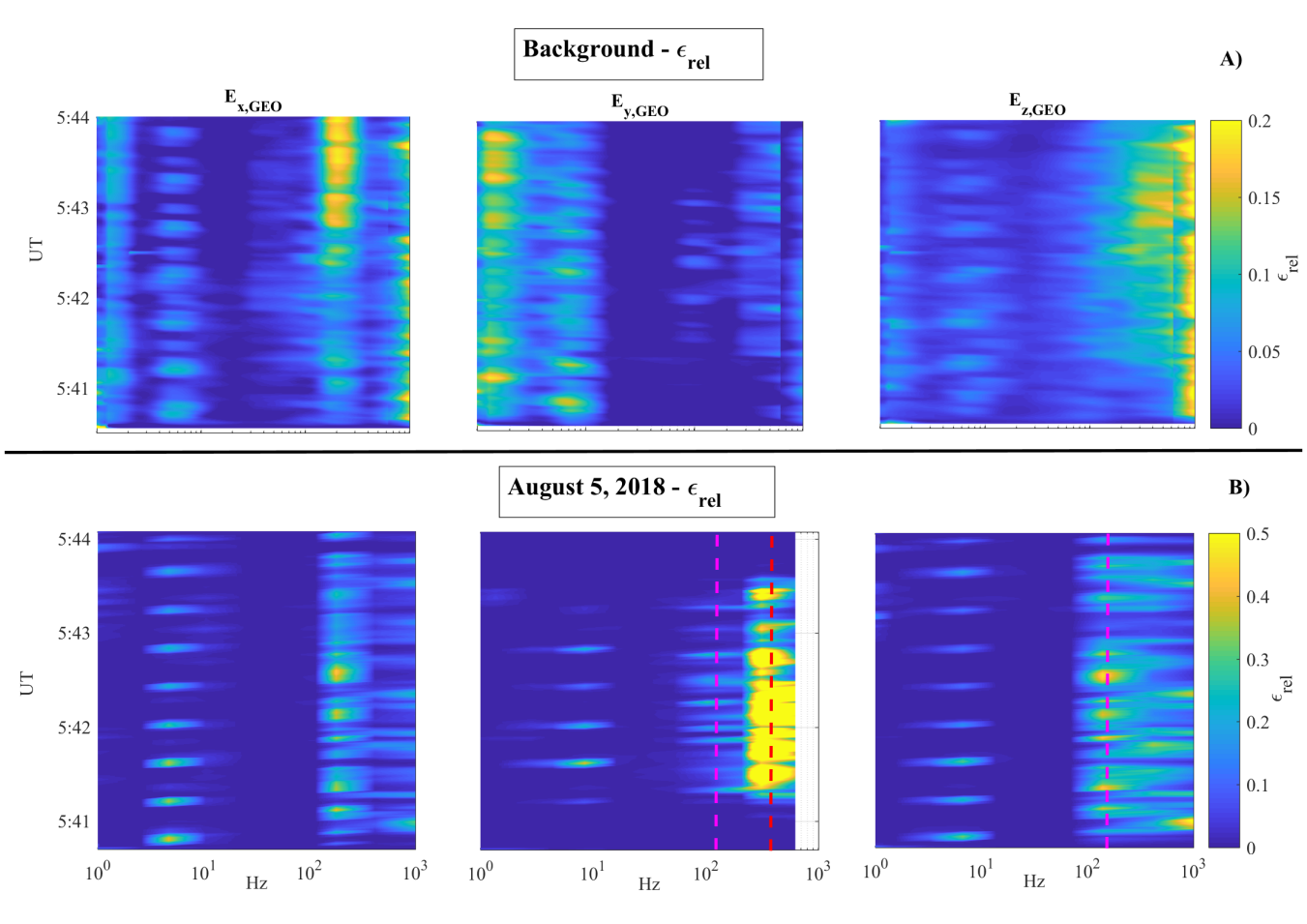

- A signature (pink circle) at ≈8 Hz is visible at all components, related to the Schumann ionospheric resonance at CSES orbit.
- The peaks detected at frequency around 2 Hz are due to the VxB electric field present in the ELF band.
- The peak around 1kHz is the signature of the Plasmaspheric hiss [Balazs, 2008; Vellante et al, 2014; Zhima et al., [2019].
- The peak around 250-300 Hz are a portion of the whistler mode chorus generated around L=5 propagating into the plasmasphere [Li et al. 2009; Zhima et al., 2019].

- Anomalous peaks at 180 Hz (E_y and E_z component, magenta) and at 630 Hz (E_y component, red line) with respect to the background has been detected.

August 1-31, 2018 – CSES-SCM observation

- As for EFD we evaluatd the Background

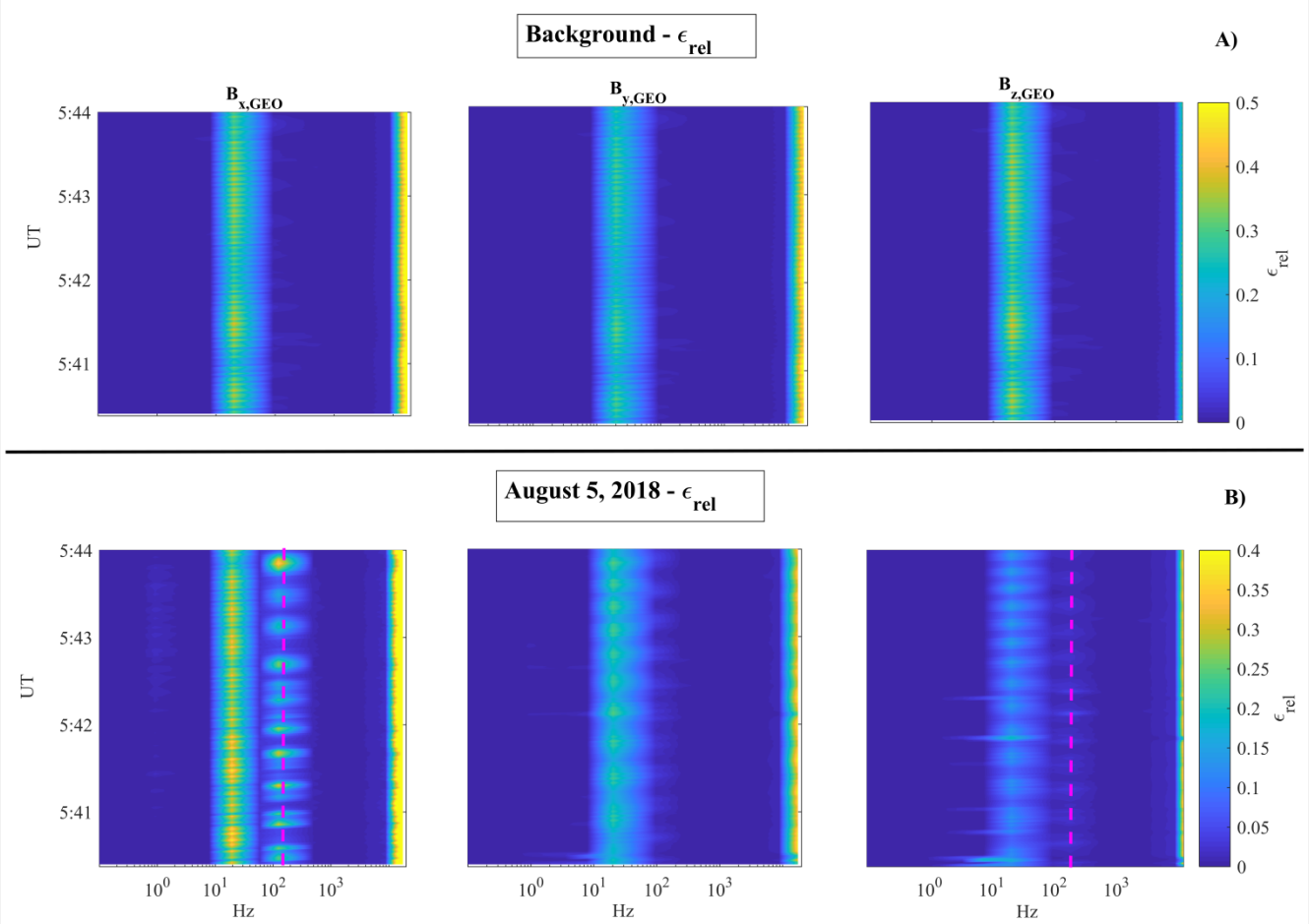

- A signature at ≈20 Hz is visible at all components, related to the Schumann ionospheric resonance at CSES orbit.
- The peak around 12 kHz is the signature of the lower-hybrid resonance of the ionosphere F2 layer.

- Anomalous peak (magenta line) at 180 Hz with respect to the background has been detected along the Bx and Bz component.
- **Interestingly, this oscillation is perpendicular to the one detected to the EFD. It is an EM wave!**

August 5, 2018 – Poynting flux

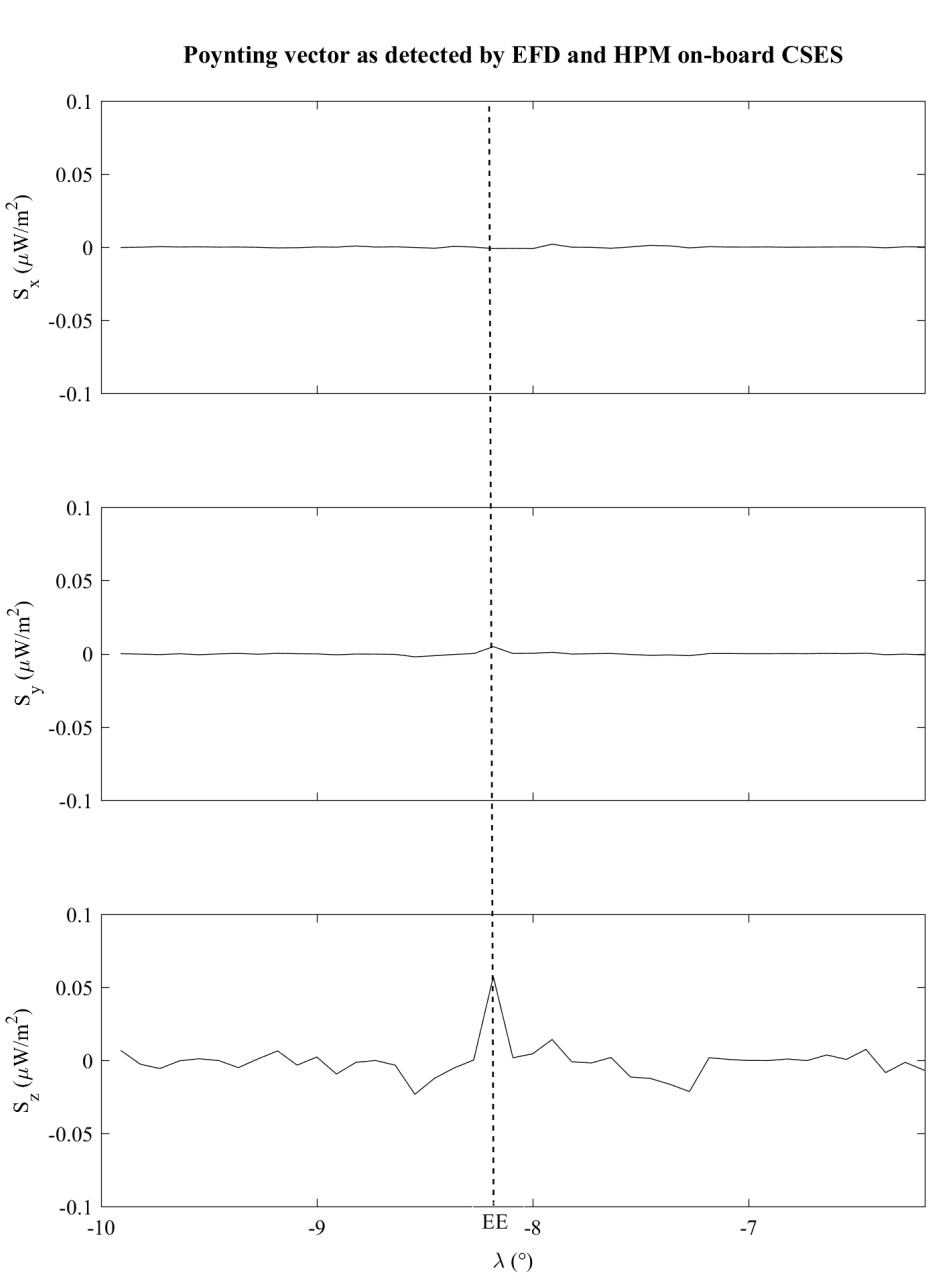

- The Poynting flux analysis confirms the injection of EM wave coming downward.

FLR over the EQ location: indication for additional phenomena ? 30% of cases → thermal precursor ?

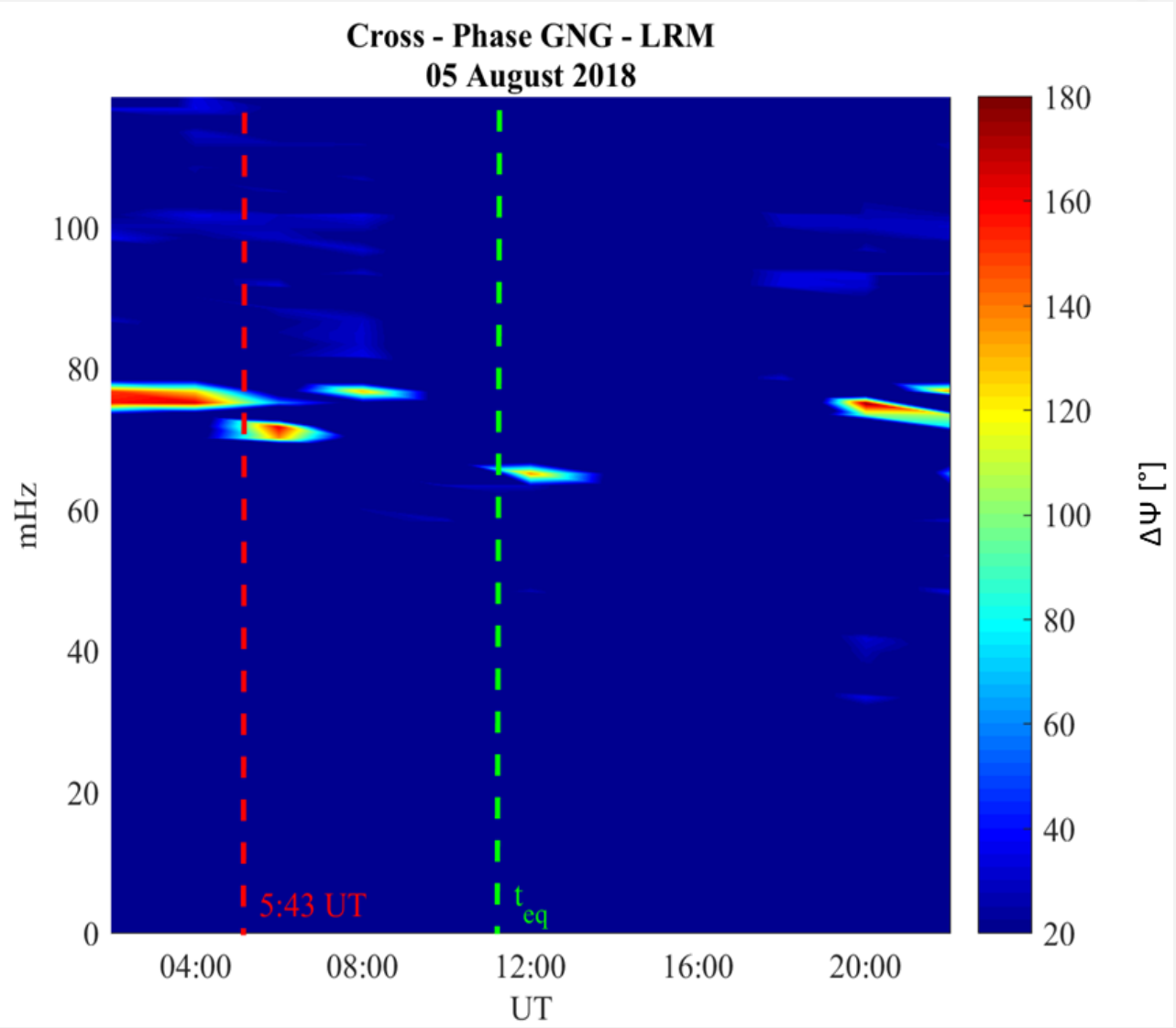

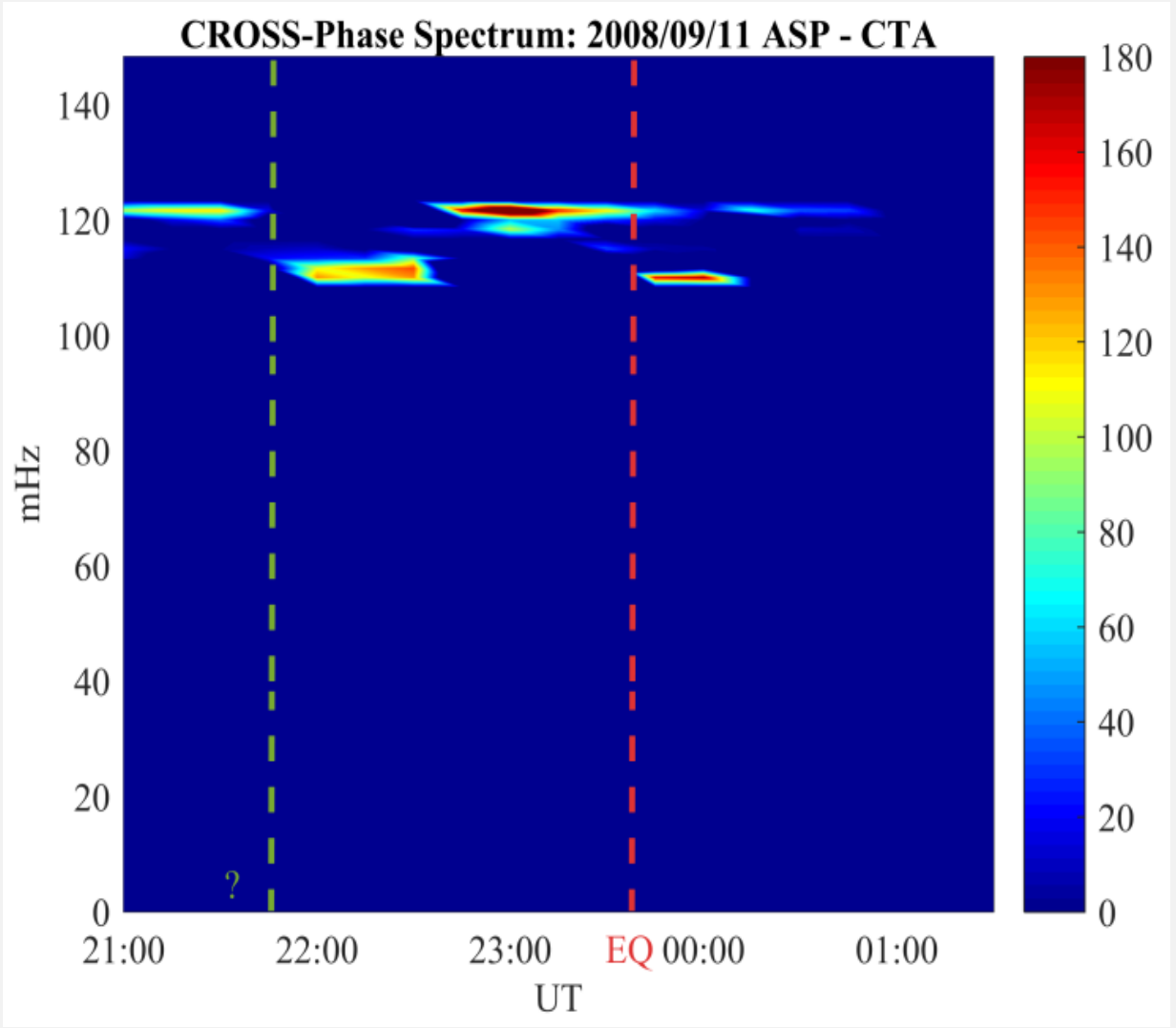

2D MILC extension

We worked on expanding the MILC model in 2D using data from both simulated and observed ground displacements (seismograms). Using ground displacements simulation in a grid of 1°x1° lat/lon, we normalized the response of the AGW temperature profile of each point of the map and reconstructed the Ep. Relative error of about 5%

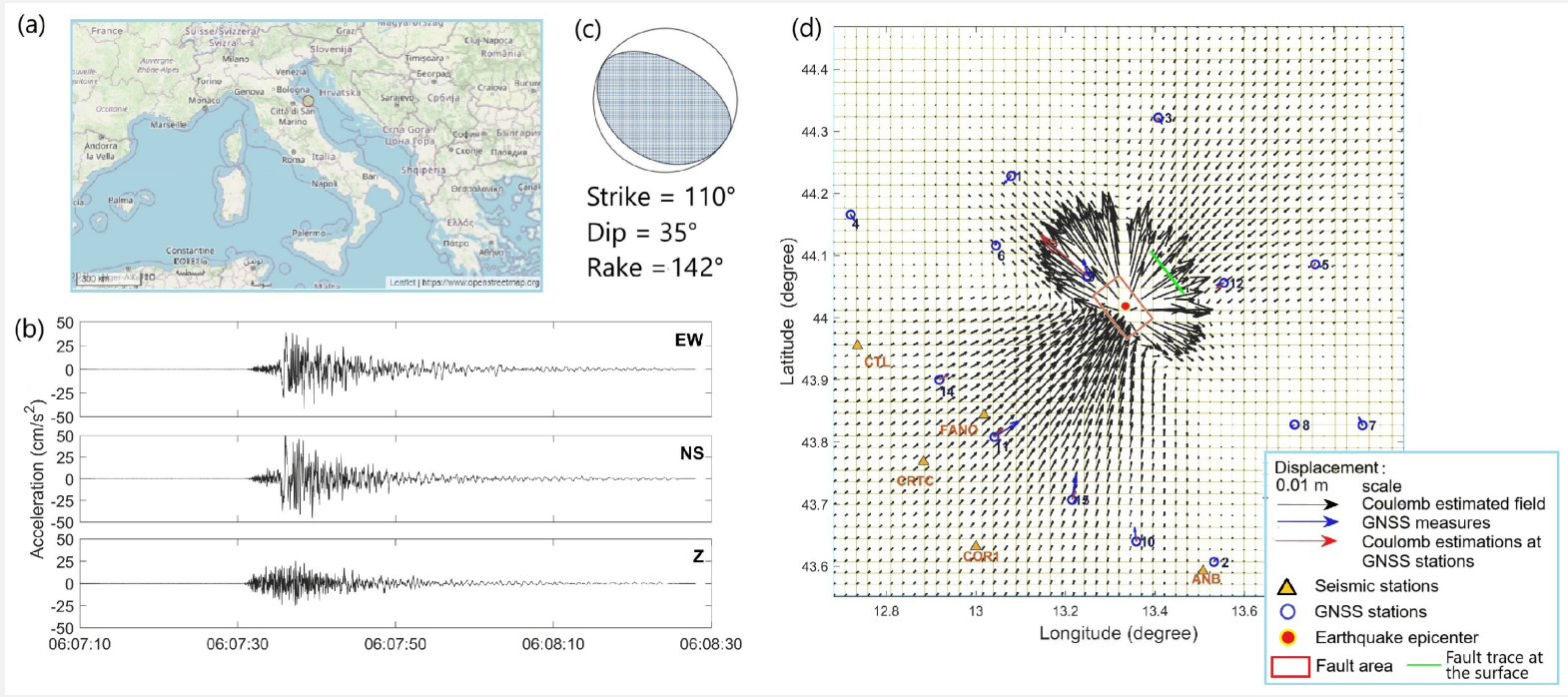

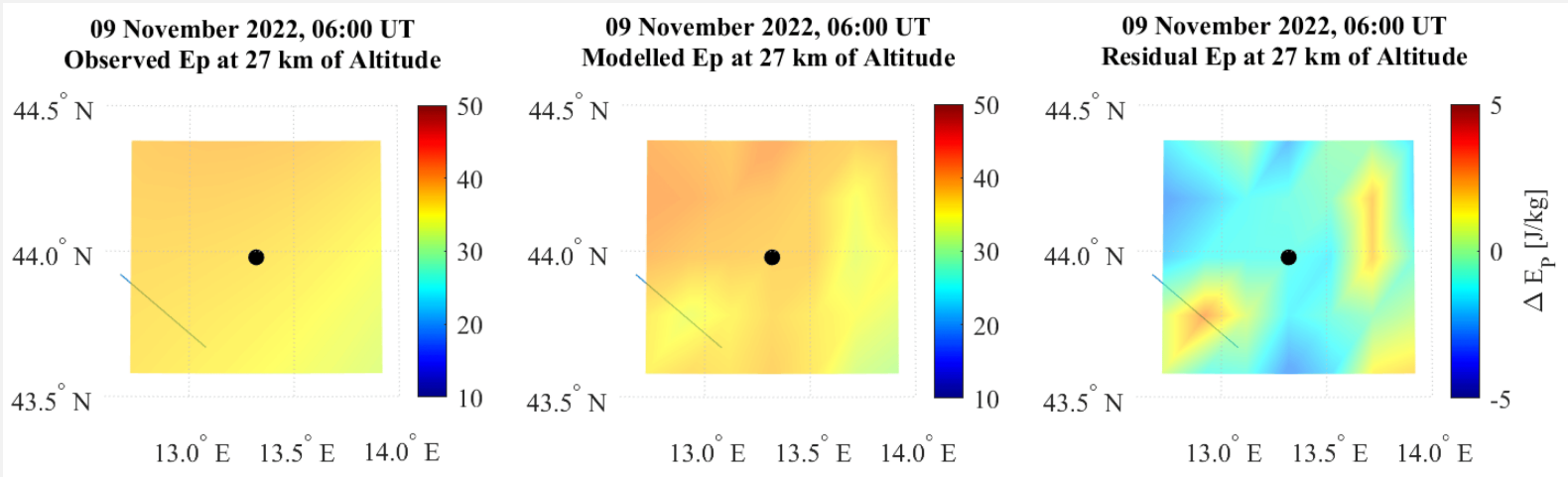

Conclusions on litospheric coupling

1. On co-seismic he observational scenario can be explained in terms of the MILC model

2. The previsions completely agree well with the observed AGWs during the EQ occurrence.

3. MILC model expected to observe a FLR frequency decrease

4. Previsions agrees with the observed FLR frequency behaviour

5. Current work : extend the model to precursor phenomena, “the unknown territory”


ASI
Agenzia Spaziale Italiana


INFN


INAF
ISTITUTO NAZIONALE
DI ASTROFISICA


ISTITUTO NAZIONALE
DI GEOFISICA E VULCANOLOGIA


Consiglio Nazionale
delle Ricerche


UNIVERSITÀ
DI TRENTO


STUDII
TAURINENSIS
1404

THANKS


UNIVERSITÀ
DEGLI STUDI
DELL'AQUILA


ALMA MATER STUDIORUM
UNIVERSITÀ DI BOLOGNA


Università degli Studi di Napoli
FEDERICO II


UNINETTUNO